Titre: Title:	Using Topology Optimization Techniques for Preliminary Design of Stiffened Panels
Auteur: Author:	Mario Capo
Date:	2021
Type:	Mémoire ou thèse / Dissertation or Thesis
Référence: Citation:	Capo, M. (2021). Using Topology Optimization Techniques for Preliminary Design of Stiffened Panels [Master's thesis, Polytechnique Montréal]. PolyPublie. https://publications.polymtl.ca/9173/

URL de PolyPublie: PolyPublie URL:	https://publications.polymtl.ca/9173/
Directeurs de recherche: Advisors:	Aurelian Vadean, & Sofiane Achiche
Programme: Program:	Génie aérospatial

POLYTECHNIQUE MONTRÉAL
affiliée à l'Université de Montréal

Using Topology Optimization Techniques for Preliminary Design of Stiffened Panels

MARIO CAPO
Département de génie mécanique

Mémoire présenté en vue de l'obtention du diplôme de *Maîtrise ès sciences appliquées*
Génie aérospatial

Août 2021

POLYTECHNIQUE MONTRÉAL
affiliée à l'Université de Montréal

Ce mémoire intitulé :

Using Topology Optimization Techniques for Preliminary Design of Stiffened Panels

présenté par **Mario CAPO**
en vue de l'obtention du diplôme de *Maîtrise ès sciences appliquées*
a été dûment accepté par le jury d'examen constitué de :

Maxime RAISON, président
Aurelian VADEAN, membre et directeur de recherche
Sofiane ACHICHE, membre et codirecteur de recherche
Martin LÉVESQUE, membre

DEDICATION

To my parents Giuseppe and Rosetta and my brother Nicola,
for their love, endless support and encouragement...

Ai miei genitori Giuseppe e Rosetta e a mio fratello Nicola,
per il loro amore, l'infinito sostegno e l'incoraggiamento...

ACKNOWLEDGEMENTS

First of all, I would like to express my deep gratitude to my supervisors, Prof. Aurelian Vadean and Prof. Sofiane Achiche, for giving me the opportunity to start this mind-blowing 2-year experience and for offering me their continuous support throughout the whole research project. I would like to thank you not only for the critical and constructive feedback on my work, but also for encouraging me to have the independence needed to carry out a research work, for teaching me how to do it methodically, and even for supporting me during the drops in motivation that have arisen during this long and unusual period. Thank you for constantly making me feel your confidence in my abilities and your respect. I was working under your supervision, but it felt like we were communicating as in a peer-to-peer collaboration. It was a journey that made me grow a lot as a person.

My heartfelt thanks go immediately to my friend and colleague Jean-François, whom I would like to define as the third supervisor of this project. Thank you for always giving me your full attention, a great patience, and so much effort in helping me overcome many difficulties: at the beginning, in the integration in a new environment, and all along the way, in continuing to work hard and thinking creative. It has been an honor to work with you on this interesting topic. Thanks also to Thomas, who has brought so much enthusiasm to the research team with his arrival and has been always available to collaborate. I wish you good luck in pursuing your research.

I would also like to thank Stelia Canada, for the opportunity of an inspiring even if short first experience in the industry that has strengthened my passion for the aviation sector. Thanks to Nicolas for his valuable advice and encouragement.

Grazie ai miei incredibili amici del Team Move-ez, con cui ho vissuto la prima esperienza internazionale che mi ha aperto gli orizzonti e mi incoraggiato ad intraprendere la doppia laurea all'estero. Grazie Tommaso per essere stato un esempio di inspirazione, un mental coach e un compagno di viaggio dal quale per 4 anni non mi sono mai separato. Grazie Vittorio per avermi insegnato l'importanza delle competenze transversali e per aver sempre riposto grande fiducia e stima in me. Grazie Daniela per avermi dimostrato che la forza di volontà e la fiducia in sé portano a raggiungere i propri obiettivi, non importa quanto bisogna insistere.

Grazie a tutti i miei amici del Politecnico che hanno reso indimenticabili gli anni trascorsi a Milano, soprattutto a te Beppe, che sei stato il mio fratello milanese del sud.

Grazie alla ZUM family, per aver reso il soggiorno in Canada uno dei periodi più felici della

mia vita. Soprattutto tu, Carla, che mi hai sostenuto in un modo speciale per questi due anni.

Un ringraziamento particolare va ai miei genitori Giuseppe e Rosetta, e a mio fratello Nicola, senza di loro nulla di tutto questo sarebbe stato possibile. Fin da quando ero bambino, mi avete supportato e incoraggiato in ogni mia scelta. La vostra fiducia e ammirazione mi hanno motivato a dare sempre il massimo per rendervi orgogliosi di me. Infine grazie alla mia seconda famiglia: gli zii Michele ed Anna, Angela, e dulcis in fundo Giuseppe, che è stato il mio riferimento (nonché datore di tetto) quando ho iniziato questo lungo percorso e sono partito dal mio piccolo paesino per scoprire il mio futuro.

RÉSUMÉ

L'optimisation topologique (OT) est un outil numérique puissant pour le design conceptuel, visant à déterminer les dispositions optimales de matériaux pour obtenir des structures rigides et légères. L'intégration complète d'un critère de prévention du flambage dans cette technique ouvrirait de nouvelles perspectives d'application dans l'industrie aérospatiale.

Dans ce travail, les méthodes d'OT implicites et explicites qui considèrent, respectivement, comme variables de conception les propriétés des éléments du maillage ou un ensemble de paramètres contrôlant la géométrie des composants ont été étudiées. Ce travail de recherche vise à améliorer une procédure existante basée sur l'OT pour la conception de panneaux raidis, dans laquelle la position des raidisseurs, les connexions et la courbure de leur axe sont déterminées en utilisant l'OT. Les défis de l'optimisation des configurations de raidisseurs ont été identifiés comme étant l'imposition d'une géométrie appropriée pour obtenir des composants manufacturables et le besoin d'un compromis entre la précision du modèle et la capacité d'explorer de grands espaces de conception.

La méthode Ground Structure (GSM), bien connue pour son efficacité quant à la conception de treillis et de châssis, a été reformulée pour une nouvelle application dans ce contexte en utilisant une structure de base construite avec des éléments de plaques et de poutres. Dans la conception basée sur la souplesse minimale de panneaux pressurisés, la GSM a démontré sa capacité à utiliser des maillages à faible coût de calcul et à fournir des descriptions explicites des composants.Une réduction du poids a été obtenue, mais l'ajout des contraintes de sollicitation dans les critères d'optimisation dans les développements futurs est nécessaire.

La difficulté rencontrée dans l'utilisation de SIMP et GSM pour obtenir des dispositions bien définis lors qu'on considère le flambage nous a conduit à nous concentrer sur l'approche MMC (Moving Morphable Components). Dans cette méthode explicite, toutes les exigences géométriques sont facilement imposées et le nombre de variables peut être réduit pour utiliser des techniques d'optimisation globale. L'identification de la disposition des raidisseurs est formulée comme un problème de disposition de deux propriétés de rigidité équivalentes sur un maillage de plaques fixes. Cette approche avait été conçue pour une optimisation basée sur la rigidité, mais ici un critère de stabilité est considéré et des composants curvilignes sont utilisés pour représenter les parcours des raidisseurs avec une grande flexibilité. Après avoir validé le modèle simplifié pour l'analyse de flambage linéaire, la conception pour le coefficient de charge de flambage maximal est résolue à l'aide de l'algorithme Particle Swarm Optimization. Il a été ansi confirmé que les raidisseurs parallèles et équidistants sont optimaux

pour les panneaux principalement chargés en compression, mais il a également été montré que les configurations curvilignes peuvent conduire à une réduction du poids dans le cas de panneaux avec des raidisseurs ayant une interruption à mi-panneau ou des charges de cisaillement élevées.

Mots clés : Optimisation topologique, panneaux raidis, disposition des raidisseurs, flambage, Ground Structure, Moving Morphable Components

ABSTRACT

Topology Optimization (TO) is a powerful numerical tool for conceptual structural design, aiming at determining stiff and lightweight material layouts. Full integration of a buckling prevention criterion into this technique would open up new applications perspectives in the aerospace industry.

This work studied implicit and explicit TO methods, which respectively consider as design variables the properties of the mesh elements or a set of parameters controlling the components' geometry. This research aimed at improving an existing TO-based procedure for stiffened panels design, in which stiffeners' position, connections, and axis path are determined by using TO. The challenges in stiffeners layout optimization were identified as being the need for imposing the appropriate geometry to obtain manufacturable components and the need for a balance between model accuracy and the ability to explore large design spaces.

The Ground Structure Method (GSM), well known for truss and frame design, has been reformulated for a new application in this context by using a ground structure built with plate and beam elements. In minimum compliance design of pressurized stiffened panels, GSM has demonstrated the ability to use low-cost meshes and provide explicit component descriptions. In the example of a rectangular bulkhead, weight reduction was achieved, but the addition of stress constraints in future developments is further needed.

The difficulty presented by SIMP and GSM in obtaining clear layouts when considering buckling shifted the focus to the Moving Morphable Components (MMC) approach. Within this explicit method any geometric requirement is easily imposed, and the number of variables can be reduced to use global optimization techniques. The stiffeners' layout identification is formulated as a problem of arranging two equivalent stiffness properties on a fixed plate mesh. This approach was designed for stiffness-based optimization, but here a stability criterion is considered and curvilinear components are used to represent general patterns with great flexibility. After validating the simplified model for linear buckling analysis, the design for maximum buckling load factor is solved using the Particle Swarm Optimization algorithm. It was confirmed that parallel and equidistant stiffeners are optimal for panel mainly loaded in compression, but it was also shown that curvilinear configurations can lead to weight reduction in case of panels with run-out stiffeners or high shear loads.

Keywords: Topology Optimization, Stiffened Panels, Stiffeners layout, Buckling, Ground Structure, Moving Morphable Components

TABLE OF CONTENTS

LIST OF TABLES

LIST OF FIGURES

LIST OF SYMBOLS AND ACRONYMS

TO	Topology Optimization
FE	Finite Element
FEM	Finite Element Model
FEA	Finite Element Analysis
CAD	Computer Assisted Design
DOE	Design of Experiment
SIMP	Solid Isotropic Material with Penalization
ESO	Evolutionary Structural Optimization
LSM	Level-set Method
MMC	Moving Morphable Components
TDF	Topology Description function
NURBS	Non Uniform Rational Basis-Splines
GS	Ground Structure
GSM	Ground Structure Method
CLPT	Classical Laminated Plate Theory
FSDT	First-order Shear Deformation laminated plate Theory
LSA	Linear Static Analysis
DOFs	Degrees of freedom
BCs	Boundary conditions
LBA	Linear Buckling Analysis
BLF	Buckling Load factor
ICAO	International Civil Aviation Organization
FAR	Federal Aviation Regulations
NGTO	Non-Gradient Based Topology Optimization
PSO	Particle Swarm Optimization
SQP	Sequential Quadratic Programming
IPM	Interior Point Method
MMA	Method of moving asymptotes - Svanberg
ESM	Equivalent Stiffness method
ICTAM	International Congress of Theoretical and Applied Mechanics

LIST OF APPENDICES

CHAPTER 1 INTRODUCTION

1.1 Context and motivations

Nature clearly shows that one of the main characteristics of bird bone structure is lightness, as this minimizes energy consumption [1]. Similarly, in the aerospace industry, it is considered that the best design is the one that guarantees the required performance at the minimum weight. This philosophy has always been one of the aviation industry core beliefs, as aircraft fuel is the most significant and variable component of direct operating costs in aircraft lifecycle.

In 2008, Airbus reported that fuel accounted for approximately 28% of the total operating cost for a typical A320 family operator [2]. Moreover, in the current context of global warming concerns, reducing greenhouse gas emissions, proportional to fuel consumption, is a compelling societal challenge.

ICAO estimated in 2016 that the aviation sector accounts for about two percent of the world's annual CO2 emissions [3]. In addition, due to its pivotal role in the world contemporary economy, the growth of the aviation sector is expected to experience a three-fold increase between 2000 and 2050 in terms of passengers [4].

In this context, manufacturing more sustainable aircraft is a highly valuable goal and multidisciplinary subject, ranging from new forms of electric propulsion to trade-offs between structural weight minimization and drag minimization.

This research work is aligned to this trend and focuses on the structural weight minimization problem. It started from the interest of the GAOSYM (Groupe d'Analyse et Optimisation de Systèmes Mécaniques) research group of Polytechnique Montréal and its industrial partner Stelia North America to develop new design processes that can reduce the design cycle time and improve the performance of stiffened panels assemblies. Finally, as a continuation of a previously traced research path, the main objective and methodological choices are sketched out from the beginning and built upon the experience gained by the research team [5, 6].

1.2 Definitions and basic concepts

The conventional design process of a structural component starts from an initial concept, based on industrial knowledge and experience, which goes through several iterations of improvements and validation until requirements are met and target performances reached. Such a procedure generates systems regardless of whether they are optima.

But in the last decades, a revolution in computer technology and numerical computations has enhanced analysis and optimization speed and precision, and the search for optimal designs has become an essential requirement in the industry. Today the design of a system is usually formulated as a problem of optimization, in which a measure of performance is to be optimized while satisfying all constraints [7]. This is defined as the "Optimum design process", opposed to the conventional design process, as illustrated in Fig.1.1.

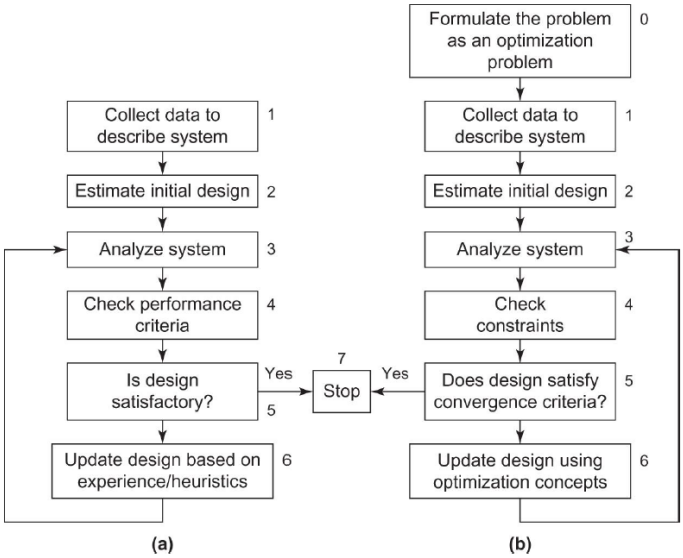

Figure 1.1 (a) Conventional design procedure VS (b) Optimum design procedure [7]

In most applications, projects are interdisciplinary environments which consider the interaction between various disciplines. However, it is still advised to use a break down strategy to face several sub-problems which can be treated independently. In the following, the structural design sub-problem is addressed, posed as an optimum design problem.

Many numerical methods have been developed and used for lightweight structure design. Fig.1.2 shows the three main FEM-based optimization methods developed to reduce the mass of structural components [8]:

- Size optimization, that determines optimal properties of the elements in the mesh;

- Shape optimization, that determines optimal coordinates of the nodes on the boundary;
- Topology Optimization (TO), introduced in 1988 by Bendsøe and Kikuchi [9], that determines the optimal material layout within a specified domain.

Topology optimization is generally used early in the design process to inspire engineers to create innovative structures. Size and shape optimization are used in the preliminary and detailed design phase using low to high-fidelity structural models

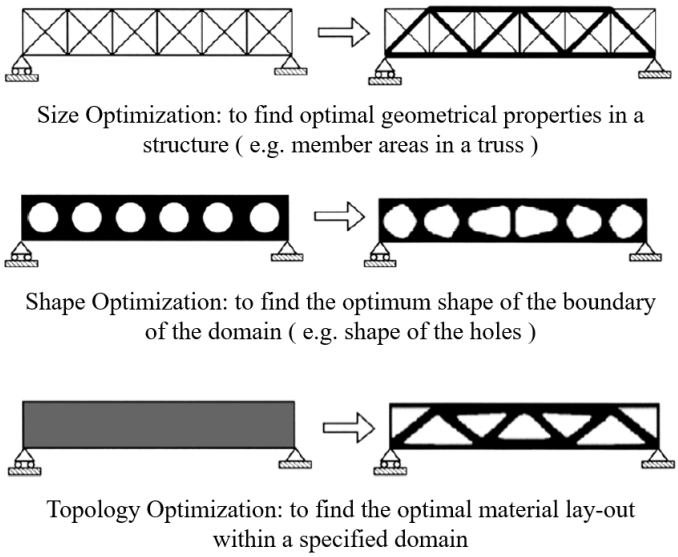

Figure 1.2 Three categories of structural optimization [8]

TO is a powerful tool for least-weight design, capable to be a creative partner in the conceptual phase of a design process. In a nutshell, TO allows to redistribute the material layout within a given design domain and to reveal the optimal load carrying path, for specified objectives, constraints, and boundary conditions [10].
Unlike other techniques, TO can support the design process at stages where the structural configuration is not yet determined and optimize the structure from a global perspective.
The interest for this technique has increased greatly for aircraft structural design, even if the process integrating it is still not mature enough to constitute a mainstream practice [11].

Aircraft structures are characterized by an extensive use of stiffened panels, which are metallic or composite thin sheets, composing the "skin", reinforced by beam-columns elements, named "stiffeners" or "stringers"(see Fig.1.3). This kind of assembly is employed in aircraft and space-vehicles, as well as ship and off-shore constructions, because of their efficient balance between structural efficiency, ease of manufacturing, installation and maintenance [12].

The design of these structures can be carried out using a two-phase process. First, the

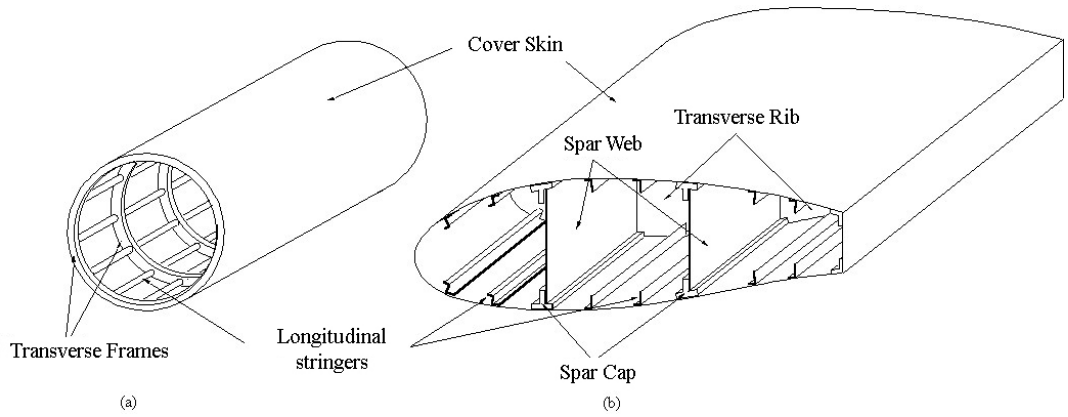

Figure 1.3 Stiffened panels in aircraft structures - (a) fuselage and (b) wing-box sections. [13]

stiffening layout, as seen from the top of the panel, must be sketched. This consists of selecting number, placement, orientation and connections of the set of stringers attached to the plate. Second, the characteristics of the panel cross-section must be defined: plate thicknesses, types and cross-sectional sizes of stiffeners.

Since size and shape optimization can only reduce mass of an a priori chosen stiffeners layout (e.g. orthogrid or equispaced longitudinal stiffeners), then there is no doubt that TO may have a role in innovative designs of stiffened panels assemblies. It can address the problem of finding the optimal stiffening layout with a higher level of conceptual freedom, considering that new competitive manufacturing processes continue to appear today.

However, many challenges exist from modelling, analysis and optimization point of views. A crucial point is related to ensuring that a proper stiffener geometry is obtained from the TO problem. Constraints on "manufacturability" must be added to constraints on the structural responses, and thus limiting the set of acceptable solutions.
Then another open challenge in the context of TO is the full integration of buckling in the optimization criteria [10, 14].

Buckling is a critical condition corresponding to a sudden increase in mechanical strain which occurs when the initial equilibrium loses its stability under an increasing load. It is a major concern in slender members and thin-walled elements, where membrane forces are converted in bending strain because of solid's imperfections [15]. Usually, the bending stiffness of these type of components is orders of magnitude smaller than their membrane stiffness. For this reason, the membrane-to-bending energy conversion results in critical conditions that occur at levels of loading lower than the elastic material limit.

Considering a finite elements based optimization, the Linearized Buckling Analysis (LBA)

is the simplest way to include the critical load estimation in the responses (objectives and constraints). In the LBA an eigen-value problem is formulated on the structure discretized by means of the finite element scheme. Among the eigen-values, the minimum positive one is the significant value for the analysis, also said the fundamental Buckling Load Factors (BLF), because it represents the scalar multiplier for the applied load to have the critical load. When the critical load is reached, new equilibrium configurations, alternative to the one provided by the static analysis, become possible. This appearance of multiple equilibrium is also referred as "bifurcation" [15].
However such a value may or may not be associated to failure of a stiffened panel assembly, which presents multiple buckling mechanisms, represented in Fig.1.4:
(1) the skin can buckle locally in the un-stiffened portion between two stiffeners (a bay);
(2) the cross section of a stiffener can buckle with a width band of possible wavelengths;
(3) the stiffeners can buckle as whole column-like modes or torsional modes;

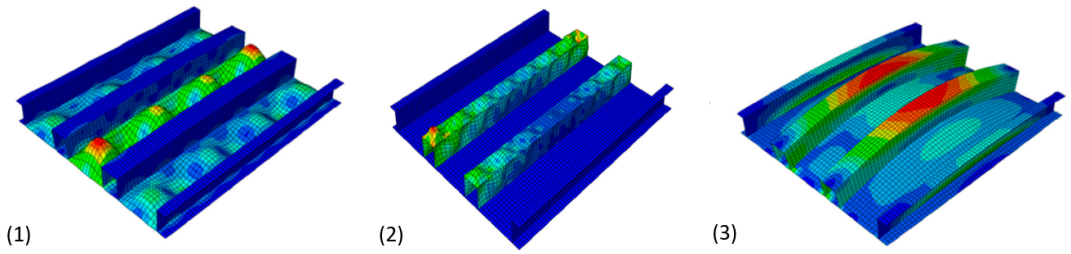

Figure 1.4 Different buckling modes for a compression stiffened panels depending on the relative bending stiffness of the U-stiffeners, showed by a parametric study in [16].

The nature of the fundamental buckling mode depends on many controlling parameters: type of loads, geometry, contact conditions, and relative size of the interacting components [16]. In aeronautical metallic stiffened panel, usually the stiffeners are relatively stiff compared to the thin skin, and the first type of buckling mechanisms is the most frequent. This kind of buckling does not lead to catastrophic failure, thanks to a redistribution of stresses from the buckled sheet to the attached columns. Indeed, experiments have shown that further weight savings are possible by allowing the panel to move into this post-buckling state [12, 17, 18].

While on one hand the LBA is easily incorporated into an optimization routine, on the other hand the estimation of final failure for a reinforced panel may not be fully addressed by these approaches. This is why, despite recent literature [14, 19] shows important developments towards the integration of the linearized buckling constraint in the topology optimization, there is still a gap between the academic research and the practical engineering application.

In addition to academic, also industrial research is very active in this field. The work conducted at Airbus UK [11] identified the full integration of buckling criteria as the main road block towards the performance improvement of TO-based designs in aerospace application. In the Airbus A380 wing leading edge rib design, a two-phase design process was developed. This can be considered as the most advanced TO procedure for aerospace applications [10].

Finite element-based topology and size optimization are performed sequentially:

— In the first phase, TO defines the structural members layout based on a stiffness criteria, i.e. minimum compliance for a given material volume.

— In the second phase, after the identification of discrete structural members, the resulting frame is sized with stress and buckling criteria for minimal mass.

Although the study case was successful, the authors underlined how post-processing TO results has been a manual operation, which required engineers judgement to adjust the geometry and add features to stabilize the design in buckling before passing to final sizing.

An overview of the two-phase Topology Optimization design process is given in Fig.1.5.
It is emphasized that the transition between the two phases is done through a heuristic interpretation of the layout suggested by TO and a manual re-construction of the model used for optimal sizing.

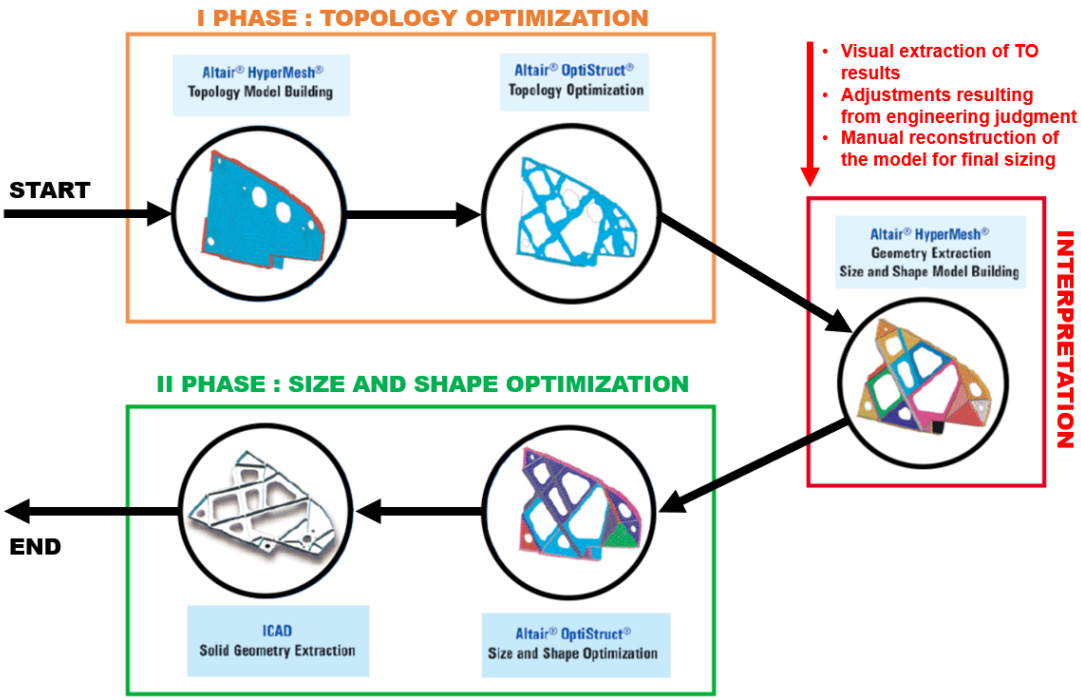

Figure 1.5 Two-phase procedure for Topology Optimization based design from [11]. The heuristic transition (interpretation) in between the phases is underlined in the flow-chart.

1.3 Problematic

Merging the concepts introduced above, some challenges to solve for a practical application of the two-phase procedure to preliminary design of stiffened panels are identified and discussed in this section.

There is still a lot of research effort required to make TO robust with regards to boundary conditions, and to lower computational needs for large scale applications. But here, special attention is given to the specific aspects of this application, which are:

(1) **Controlling the proper geometry of the stiffeners**
Innovative layouts can be further analysed and successively manufactured, only if the resultant material distribution maintains a clear description of each stiffener. That is, topological features can be extracted easily and without ambiguity. This can be done either by imposing "manufacturing" (geometric) constraints or by automating the interpretation task.
In the traditional density-based SIMP method these constraints can be very complex to formulate, because of the implicit nature of the topological variables. In the same way, systematic procedures for the extraction of explicit geometric information from a pixel-based density distribution [6, 20] is another on-going research topic in the field.

(2) **Integrating the linearized buckling criteria in the layout optimization**
Typical material distributions obtained from the compliance-based TO look alike trusses/frames, hence the idea to exploit the technique for the stiffening layout of thin plates. The optimal layout for compliance efficiently stiffens the sheet, but it does not consider the second function of stiffeners to provide stability to the skin.
Flat plates carry the loads in their plane but their buckling mechanism consists in an out of plane deflection. Then the linear strain energy for in plane loads is not linked to the buckling resistance.
Moreover, in metallic stiffened panels, the failure comes beyond the onset of the skin buckling, because the attached columns can continue to carry additional load beyond that level [12]. The fundamental BLF may not be associated with the panel final collapse, and the linearized buckling criteria cannot be an exhaustive tool to estimate the final failure.
For this reason, it is needed to limit the scope of the linearized buckling criteria to skin buckling prevention only. Last but not least, by adding buckling criteria the optimization problem becomes non-convex and navigating the design space using gradient-based solvers in the SIMP method becomes further difficult.

1.4 Research Objectives

This research work aims at developing a design procedure for stiffened panels based on topology optimization that can be used in industrial practice.
For this reason, the methodological choice is inspired by the TO-based design procedure by sequential steps shown above, since it proved to be easily deployable in industry, as well as capable of reducing the weight of many structural components.
However, in order to allow its application for the design of stiffened panels, it is necessary to solve the problematic issues related to this specific case.

The main objective (MO), consisting of the development of such a new procedure, is decomposed into sub-objectives (Soi) of narrower scope, which address these issues one at a time. Formally, the SOi are expressed as necessary steps to achieve the MO.

- **(MO)** Develop a design procedure based on Topology Optimization (TO) applicable to the design of stiffened panels.
- **(SO1)** Formulate an explicit description of the stiffener layout to automate interpretation of the TO results.
- **(SO2)** Integrate the stability criterion in the layout optimization to increase the skin buckling resistance.

To achieve the main objective, various approaches will be selected from the literature, based on their potential to meet the two sub-objectives, and will be reformulated in order to integrate them into a design procedure for stiffened panels.

The first sub-objective motivates the search for methods in which the geometry is explicitly controlled, allowing an automatic interpretation of TO results, as well as the imposition of any manufacturing constraint. S01 is therefore related to the definition of the optimization variables. Meanwhile, the second asks to consider the main function of the stiffeners, that of increasing the stability of the thin sheet, when optimizing their layout. S02 is instead related to the definition of optimization criteria.

Finally, this introduction to the objectives and their origin related to the limitations of the state of the art is summarized in the diagram of Fig.1.6.
By reading the diagram from right to left, one moves from the initial situation, in which the problem is present, to the ideal situation attainable through the achievement of the research objectives. Instead, by following the direction of the branches, one can read the cause-and-effect relationships between various key elements, contained in the nodes of the graph.
A letter and an operator are associated with each of these relationships. The letter indicates how the relationship was determined: i.e. deduced from an assumption [A], from consid-

erations in accordance with the literature [L], or from the experience gained in conducting the work [E]. Meanwhile, the operators indicate how the increase (+) or decrease (-) in the quantity/quality of each element is related to each other.

The basic assumption is that the use of TO in the design of aircraft components will reduce the structural mass, and consequently the fuel consumption, that is needed to lower aircraft costs and environmental impact. To do this, it is necessary to address the issues that prevent the application of the technique in stiffened panel design.

Therefore, the focus of the research is on the achievement of the two sub-objectives, which would ideally increase the benefits due to the use of the procedure and decrease the effort required of the designer to conduct it.

To monitor the progress towards these two ideal outcomes, some measurable indicators are defined: (1) the number of design variables, which determines the numerical computational cost; (2) the time to complete a design cycle, which depends on the ease of automation of the procedure, and determines the total time to arrive to the target design by means of multiple design cycles; (3) the performance-to-weight ratio of the structure (e.g. specific strength), which is actually what it is sought to be increased by using the TO.

These indicators are related to how complex the problem to be solved is, how much time and efforts are spent to solve it, and how beneficial the solution obtained is.

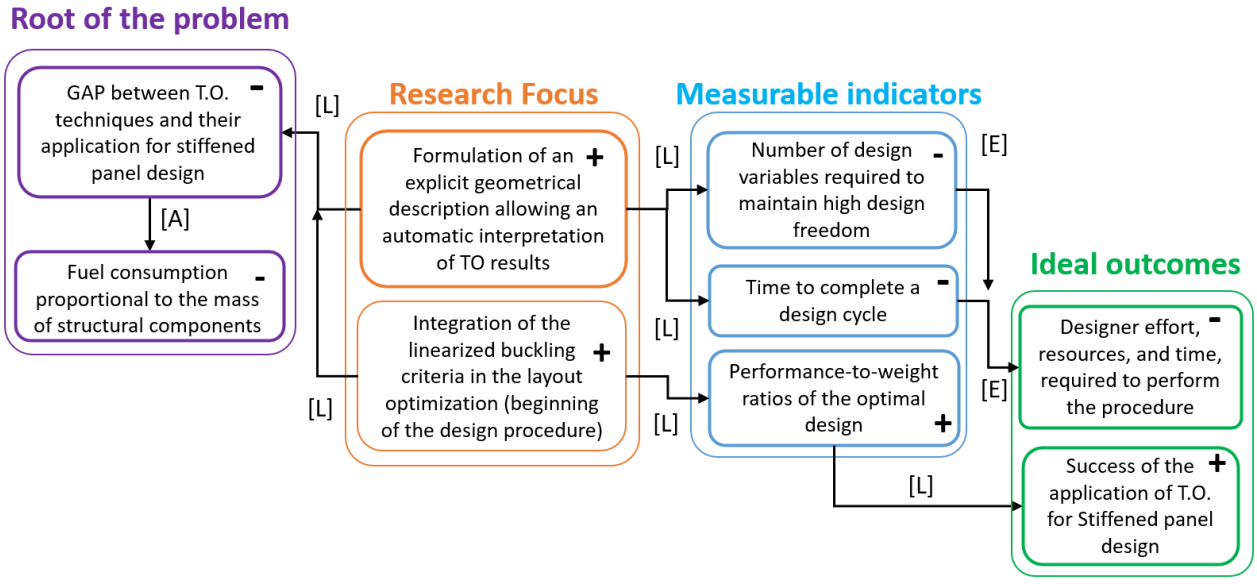

Figure 1.6 Reference diagram - A graph to visualize the effects of progress in achieving research objectives on solving the initial problem and achieving ideal outcomes

1.5 Thesis Outline

This first chapter introduced the key concepts, problematic, and research objectives that guide the work conducted in the rest of this thesis, which is structured as follows:

Chapter 2 conducts a critical literature review. A selection of some approaches to be further investigated in this work is made and previous applications of topology optimization for plate/shell stiffening are reviewed. Some issues occurring in structural optimization with eigenvalue criteria are discussed, as well as strengths and weaknesses of the optimization solvers which can be used. Finally, the results of the review are summarized and the desired contribution of the research work is stated.

Chapter 3 presents an original application of the Ground Structure Topology Optimization approach for the compliance-based stiffened panel design. A MATLAB code has been implemented to test the use of this approach for the stiffeners layout identification. The method is presented and compared to alternative approaches. The design of a pressurized stiffened panel representing an aircraft bulkhead is carried out using the two-phase design procedure. A final section shows the possibility to use the method for general geometries and loads by exemplifying a rib reinforcement layout conceptual design.

In Chapter 4, the Moving Morphable Component approach is adapted to the layout optimization problem for maximum linearized buckling load factor. Curvilinear components described by explicit topological variables are used to represents the stiffeners on a simplified panel model. Two approaches to optimize the geometrical parameters of the stiffeners paths are formulated and their MATLAB implementation is described. The first is based on selecting the best configuration after a parametric study. The second one use the Particle Swarm Optimization algorithm in order to find optimal set of stiffeners parameters for maximum BLF under volume constraints.
Some parametric studies discuss the effects of spacing and curvature of stiffeners in simple load cases, then two case studies are performed using the two-phase design procedure for upper wing skin panels.

Finally, Chapter 5 summarizes the work done. Limitations of the current implementations are pointed out, and from there some recommendations for future research are given.

CHAPTER 2 LITERATURE REVIEW

This chapter firstly presents an overview on topology optimization and its traditional approaches proposed in literature. A brief introduction to local and global optimization algorithms focuses on presenting the advantages and disadvantages of these two families of methods in the context of traditional topology optimization, but also in the problem addressed by this work: the layout optimization of the stiffeners reinforcing and stabilizing thin plates. Then it reviews past research works conducted on the optimal stiffening of plate using the SIMP method in the 2-phase procedure, and two application of the more recent MMC approach in this context.
The linearized buckling analysis is also introduced, and principal issues of structural optimization with buckling criteria are discussed.
A final subsection introduces the two main developments of this work and explains their links with the research objectives. The limitations of the consulted literature are also emphasized.

2.1 Basic concepts and Methods of Topology Optimization

Before entering different formulations, the general Topology Optimization (TO) problem is presented. To give a simple idea of the aim of this technique it is worth quoting Ole Sigmund [21], who transcribes the mathematical problem into the following fundamental design question: "How to place material within a prescribed design domain in order to obtain the best structural performance?".
This problem can be mathematically stated in this general form:

$$\begin{array}{ll} \min\limits_{\boldsymbol{x}} & f(\boldsymbol{x}) \\ \text{s.t.} & \int_\Omega \rho(\boldsymbol{x})\, d\Omega - V_{max} \leq 0 \\ & g_i(\boldsymbol{x}) \leq 0 \qquad\qquad i = 1 \dots m \\ & \boldsymbol{x}_{void} \leq \boldsymbol{x} \leq \boldsymbol{x}_{solid} \end{array} \tag{2.1}$$

Where f is the objective function, ρ represent the material density, V_{max} defines the upper bound for the material volume to be placed in the domain Ω, g_i are the m constraints on the structural responses (e.g. stress, displacement, or critical buckling load) and the vector of design variables $\boldsymbol{x}$ determines the spatial material/void distribution.
Different ways to define the topological variables x_i and their relations with structural geometry and responses represent the differences between the different approaches.

2.1.1 The Ground Structure Method (GSM)

The Ground structure method (GSM) is the first of the list. Its basic idea was anticipated in an early work of Dorn et al. [22], but it is still relevant and re-proposed constantly in new forms due to the advantages derived from the direct use of discrete structural elements, such as beams and bars.
In this method the domain is discretized in a grid of nodal points connected by the so-called ground structure: i.e. the mesh collecting all the candidate structural members.
The problem of identifying the optimized material distributions is recast in the form of a sizing optimization [8] by allowing the elements to become structural or vanishing members. This is done by considering the cross-sectional areas of the 1-D elements as the continuous design variables. At the end of the optimization, members with low cross-sectional area (below a prescribed threshold) are removed from the design domain to obtain the final layout.
This process is exampled in Fig.2.1, for the classical MBB beam 2D TO-problem [8].

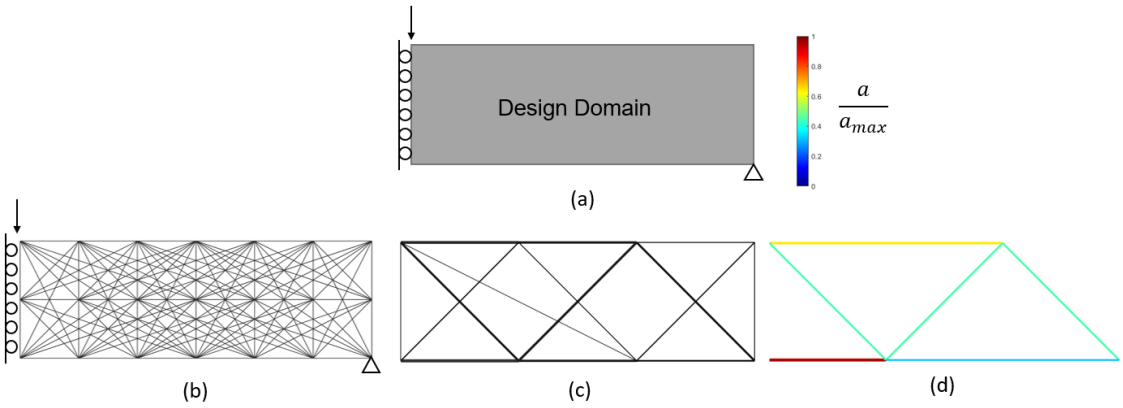

Figure 2.1 Ground Structure (GS) Method - The design domain (a) is discretized in the initial GS (b) which is iteratively optimized (c) to obtain the final design (d)

Since it does not require the use of advanced finite elements for the analysis, it is the easiest method to implement and results to be cheap for large-scale structures where a coarse mesh can be used, as demonstrated by many application in bridges and buildings design [23]. This methods is largely used to optimize trusses (bars with pinned connections) and frame structures (beams with moment-resisting connections), while its application in stiffened panel design is still unexplored [24].

2.1.2 The Solid Isotropic Method with Penalization (SIMP)

The SIMP, can be considered as the standard method in TO. It has widely spread and implemented in several FEA software, due to its compatibility to any kind of finite element.

In this method, the design space is discretized by means of continuous finite elements, such as solids (for 3D domains) or plane quadrilateral elements (for 2D domains).
Each element of the mesh is associated with a scalar optimization variable x_e, called "density", which ranges from "0 to 1", to indicate the presence of "void" or "full material" in the portion of the domain occupied by the e-th element.
The optimization algorithm seeks to optimize the element-wise density distribution in order to maximize a certain objective function, e.g. the stiffness of the structure, for a prescribed maximum volume of material. This process is exampled in Fig.2.2.

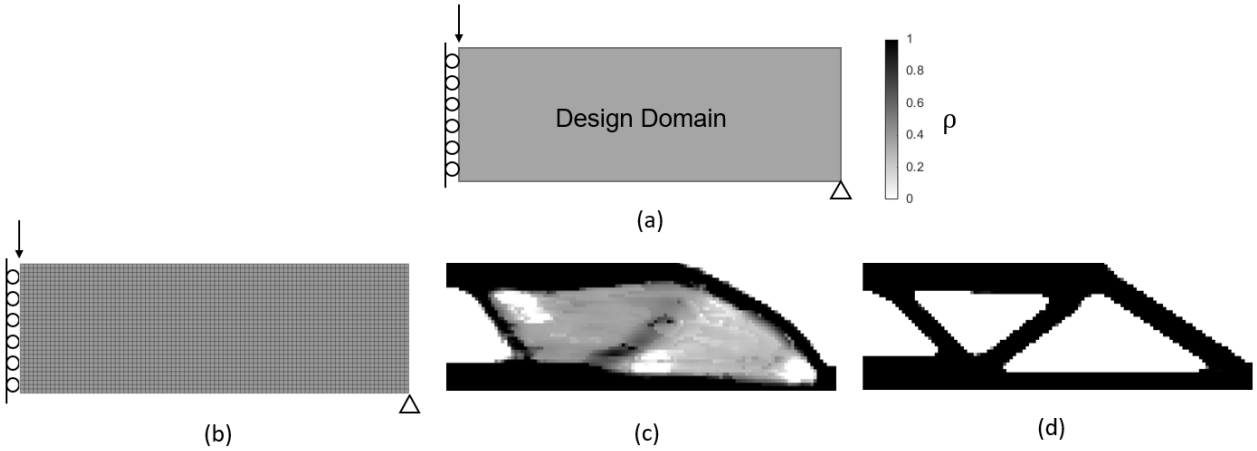

Figure 2.2 The SIMP Method - The design domain (a) is meshed (b), ρ_e distribution is iteratively optimized (c) and the final material layout is obtained (d)

The analysis model is then based on the heuristic assumption that the mechanical properties of the mesh are interpolated between the "void" and the "full material" properties according to the value assumed by the density in each finite element [8]. The use of a simple power-law interpolation for the Young Modulus, efficiently characterizes the elemental stiffness matrix $\boldsymbol{K}_e = \boldsymbol{K}_e(x_e)$ of a given linear elastic isotropic material, with Eq.2.2:

$$\boldsymbol{K}_e = \left(E_{min} + x_e^p \left(E_0 - E_{min}\right)\right) \boldsymbol{K}^0 \tag{2.2}$$

where K^0 is the stiffness matrix of any kind of finite element with unitary Young modulus, E_0 and E_{min} are the moduli of solid and void, x_e is the density variable of the eth element and p is an integer called the penalization factor.

The penalization of intermediate values relaxes the binary 0-1 problem, and it is obtained for $p > 1$, because while the volume (cost) remains proportional to the density x_e, the stiffness (the objective) becomes less than proportional (for $x_e \in [0, 1]$).
Numerical problems appearing in the SIMP method, regarding the ill-ponesedness of the problem and the non-uniqueness of the solution are categorized and discussed in [25]:

1. **Checkerboard** refers to formation of regions of alternating solid and void elements ordered in a checkerboard like fashion in the final solution, which unrealistically overestimate the model stiffness;
2. **Mesh dependence** invalidates the concept of FE convergence. Even in simple problems, mesh-refinement may not result in a more clear description of the same optimal structure, but can lead to topologically different solutions.
3. **Local minima** refers to the problem of obtaining different solutions to the same discretized problem when choosing different starting guesses.

Some prevention techniques developed over time have partially overcome these issues [25]:
• **Mesh independent filtering** mitigates (1) and (2) by averaging design variables (densities) or design sensitivities of each element over the element's direct neighbors.
• **Continuation techniques** try to avoid less efficient local minima, at least in the minimum compliance problem. For $p = 1$ the problem is convex, but the global optimum would like to present large grey regions [8]. For $p \geq 3$ grey regions disappear from the final solution, but the problem has more local minima. The continuation consists in gradually increasing p while the optimization is advancing. In this way, TO evolution to a black and white design is enforced, while the chances to descent to the best minimum are increased.

2.1.3 The Moving Morphable Components (MMC) Method

The MMC is the most recent TO method, proposed by Guo and Zhang [26] in 2014.
Its main novelty over traditional approaches is the use of design variables that explicitly describe the optimal material distribution.

In above mentioned implicit TO methods, the optimization algorithm finds the density or cross-sectional area distribution, and gives the optimal topology of the structure as a set of elements "filled with material". For example, in the SIMP, the optimal material distribution is described by a $0-1$ "pixel-based" representation.
In contrast, in the MMC method, the algorithm optimizes a set of parameters controlling the geometry of the structure, and gives the final topology description by means of an explicit analytical function constructed with the optimal parameters.

The structure is decomposed in a set of components that can change position, length, thickness, orientation, as well as merge each other, in order to reach an optimal topology [26]. This approach is depicted in Fig.2.3, for a 2D example in which each component is a rectangular member with linearly varying thickness.

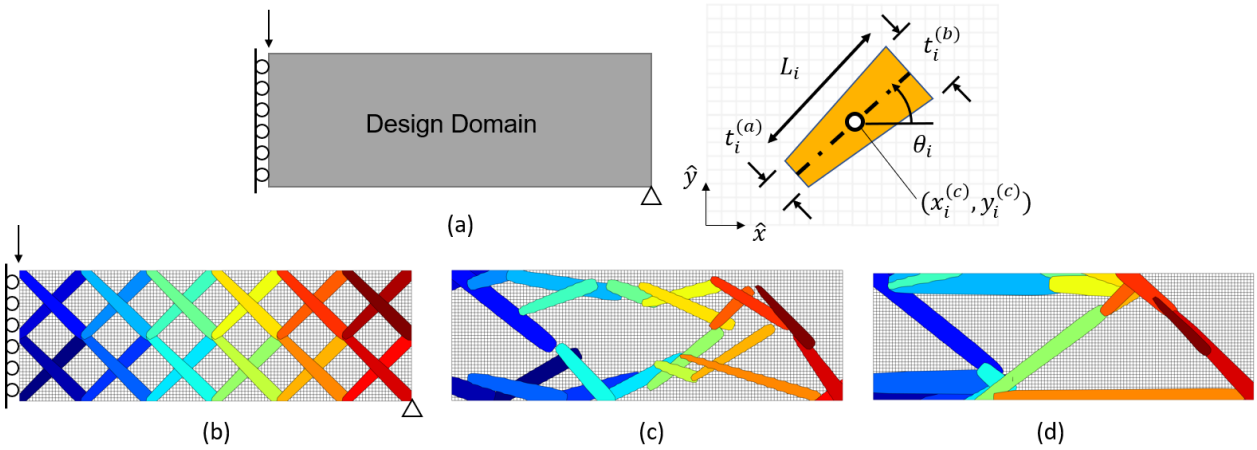

Figure 2.3 The MMC Method - The design domain (a) is meshed and a set of component is mapped over it (b), geometric variables of each components are iteratively optimized (c) and the final material layout is obtained by the superimposition of solid members (d)

The set of parameters $\boldsymbol{d}_i$ describing the ith-component, as depicted in Fig.2.3, groups the coordinates of the center point $(x_i^{(c)}, y_i^{(c)})$, the thickness at both ends $t_i^{(a)}, t_i^{(b)}$, the length L_i, and the angle between its mid-line and the global horizontal axis θ_i. Collecting the parameters of all the N components, the complete design vector $\boldsymbol{d}$ is defined:

$$\boldsymbol{d} = \{\boldsymbol{d_1}, ..., \boldsymbol{d_N}\} \tag{2.3}$$

The parameters in $\boldsymbol{d}_i$ map the portion Ω_i, over the coordinates $(X_{\Omega_i}, Y_{\Omega_i})$ occupied by the i-th solid component, in the following way:

$$\begin{Bmatrix} X_{\Omega_i} \\ Y_{\Omega_i} \end{Bmatrix} = \begin{Bmatrix} x_i^{(c)} \\ y_i^{(c)} \end{Bmatrix} + \begin{bmatrix} \cos(\theta_i) & \sin(\theta_i) \\ -\sin(\theta_i) & \cos(\theta_i) \end{bmatrix} \begin{Bmatrix} \xi \\ \eta \end{Bmatrix} \tag{2.4}$$

Where: $\xi \in [-L_i; L_I]$ and $\eta \in [-f(\xi); f(\xi)]$ with $f(\xi) = t_i^{min} + \frac{,t_i^{max} - ,t_i^{min}}{L_i}\xi$.

By looking at this description, the main differences between implicit and explicit representations can be caught. The link between the geometry of each component and its design variables is made explicit by a function having as the image the spatial coordinates of the points belonging to the solid member and as the argument a set of design variables.

Such a function cannot be defined in the SIMP method, where the solid region Ω_S is defined as the portion of the design domain where the density is over a certain threshold. Mathematically this is expressed as an implicit relation in Eq.2.5, for a 2D domain.

$$\Omega_S = \{X, Y : x_e(X, Y) - \epsilon \geq 0\} \tag{2.5}$$

where X, Y are the spatial coordinates, x_e is the elemental density and ϵ is a numerical value near to 1. It can be seen that the mathematical condition for which a point in the domain belongs to the solid is an implicit function of the density.

In contrast, within the MMC framework, defining the geometry of each component of the structure from its design variables vector $\boldsymbol{d_i}$, leads to an explicit function, as showed in Eq.2.4.

Finally, to define the finite element model, a projection-scheme is needed to map the properties of the solid region over a fixed mesh. This is done by means of a Topology Description Function (TDF), which depends on the explicit parameters contained in the design vector considering all the components $\boldsymbol{d}$ and on the spatial coordinates (X, Y).
The TDF identifies the solid region using a level-set method [26]:

$$\begin{cases} \Phi(\boldsymbol{d}, X, Y) \geq 0, & if\ (X, Y) \in Solid \\ \Phi(\boldsymbol{d}, X, Y) < 0, & if\ (X, Y) \in Void \end{cases} \tag{2.6}$$

It can be remarked that this passages comes back to describe the structure in an implicit way, but this description is used only in the analysis model, while the explicit information desired for post-processing are still available due to the nature of the design variables.

Finally the material properties for each element (Young Module E_e) are interpolated using the value of the TDF at its nodes. This is referred as the Ersatz material model [26], exampled here for a 4-nodded 2D-element, where the Heaviside function H is used:

$$E_e = \frac{E}{4} \sum_{i=1}^{4} H(\Phi(x_i, y_i)) \tag{2.7}$$

This method receives a great interest because:

1. It is easy to couple with Computer-Aided-Design (CAD) modeling systems, where geometries are described by parametric entities like NURBS curves and surfaces [27].
2. In the SIMP method it is difficult to have precise control over the geometric characteristics (i.e. min/max number/size/curvature of members). While by using explicit design variables this control is done automatically when the set of parameters and side constraints are defined.
3. Finally, the computational burden of the optimization can be reduced, since the number of design variables can be decoupled from the number of elements in the analysis model.

However, this decoupling comes at a cost. Implicit methods can efficiently use gradient-based optimizers in problems with smooth structural responses. While the use of the highly nonlinear projection scheme makes the MMC method always have nonconvex objective functions and constraints. So it suffers more from the existence of multiple local minima even in the compliance problem with the volume constraint.

2.2 Gradient-based and Global Optimization Methods in TO

The success of TO has roots in the possibility to become a finite elements based optimization. Avoiding re-meshing operations and using gradient-based solvers maintain practical running time and feasible amount of computational resources even if the number of the design variables is immense w.r.t to other kinds of optimization. However, there is no restriction on the type of algorithm to be used to solve the problem. Non Gradient based Topology Optimization (NGTO), which encompass Genetic Algorithms, Simulated annealing, Particle Swarms etc., are commonly seen in the literature as reported in the survey of [28]. Depending on the nature of the problem, the various optimization methods exhibit advantages and disadvantages.

2.2.1 Gradient-based Solvers using Sequential Convex Programming

Gradient based optimizers are extremely efficient in the classical TO problem of minimum compliance under volume constraint, or in problem with smooth objective and constraints functions. Since mass, stiffness and stress-stiffness matrices are assembled by linear operators, their derivatives are reduced at the element level, and the use of the adjoint method avoids the derivatives of the displacement to be computed [8].
Iterative algorithms are used which solve a series of convex sub-problems built using gradient information, such as the Method of Moving Asymptotes (MMA) [29]. Typically the sub-problems are solved using the primal-dual interior-point approach [30], which is numerically convenient in TO because "*If the primal problem has n variable and m constraints, the dual problem will have m variable and n constraints*" [7].
The number of constraints can be maintained low by aggregating sets of responses (e.g. element stresses) with the use of the KS-function [31] or the p-norm function [32].
Another high-performing method for large scale programming problems is the Interior Point Method [33], based on a series of barrier sub-problems in which a linear approximation of the KKT condition is solved at each step.

The major limitation for gradient based solvers is in the exploration capability in case of multi-modal objectives or constraint functions. SIMP and GSM methods are supposed to start from an uniform material distribution and are required to end in a clear material/void layout. This is hard to obtain when considering design dependent constraints. For example, when the buckling constraint is added, large “grey” regions or shapeless agglomerates of material in portion affected by local modes are likely to appear.

On the other hand, the price for solving the 0-1 binary TO problem with a combinatorial process is $N_C = 2^{N_e}$, i.e. a number of combinations N_C exponentially growing with the

number elements N_e in the mesh [34]. Also evolutionary algorithms, which are designed for dealing with discrete problems, have poor performance in terms of running time and optimal objective value when the number of value is very high [28]. As a consequence, there is no doubt that implicit methods require the use of gradient-based solvers.

2.2.2 Global Optimization Methods and the Particle Swarm Optimization (PSO) Algorithm

In the context of explicit TO methods, the potential of non gradient-based approaches can be re-evaluated. Provided that the problem is formulated with a minimal number of design variables, all the advantages of global optimization techniques could be exploited.
First of all, 0-order methods do not require gradients, hence they are easy to implement. But this is not the main concerns since a finite-difference based sensitivity analysis has computational cost growing linearly with the number of variables.
The main advantage of global optimization techniques is indeed the possibility to avoid local minima and to be able to explore the whole design space. This is important for the practical purpose of TO: that is exploring promising solutions at a conceptual level, rather than locating the optimal design point with high precision.

The MMC approach could leverage the use of global search techniques, as the number of variables can be kept as low as desired. As shown in the work of Guo et al. [35], the use of curvilinear shape members can reduce the length of the design vector to a few tens of variables.

A survey of global optimization techniques suitable for problems with continuous variables reveals that the Particle Swarm Optimization Algorithm (PSOA) of Kennedy, Eberhart and Shi [36–38] could be efficiently coupled with the MMC approach, because of the similarity of the latter to a shape optimization problem.
Fourie and Groenwold [39] showed that in the sizing of a 25-bar truss and the shaping of a torque arm with 7 parameters, the PSOA outperformed two different genetic algorithms, and showed a number of function evaluations to reach the final design comparable with the ones of a Sequential Quadratic Programming (SQP) algorithm.
Finally in the context of the optimum design of curvilinear stiffeners layout, the work of Mulani et al. [40] has already demonstrated the PSOA applicability for this problem.

The PSOA is a derivative-free population-based method which mimics social behaviors of bird flocking and fish schooling, which adjust their physical movement to avoid predators, seek food and mates [36]. As in genetic algorithms, a population of individuals exists. The progression toward better solutions is driven by both cognitive and social mechanisms [38].

In the sense that each particle in the swarm updates its position using its own flight experience and that of its companions. This biology-inspired strategy is based on the paradigm that social sharing of information among members offers an evolutionary advantage [36].
Finally, a factor of randomness and a personal inertia are added along to the swarm intelligence. These two terms are fundamental to limit the dependence on the initial positions of the swarm and to avoid stagnation in local minima.

All these principles are merged in the simple updating scheme of the PSOA:

$$\begin{gathered} \boldsymbol{x}_i(t+1) = \boldsymbol{x}_i(t) + \boldsymbol{\Delta x}_i(t) \\ \boldsymbol{\Delta x}_i(t) = w\ \boldsymbol{\Delta x}_i(t-1) + c_1\ r_1\Big(\boldsymbol{p}_i(t) - \boldsymbol{x}_i(t)\Big) + c_2\ r_2\Big(\boldsymbol{g}(t) - \boldsymbol{x}_i(t)\Big) \end{gathered} \tag{2.8}$$

Where: $\boldsymbol{x}_i$ and $\boldsymbol{\Delta x}_i$ are the ith particle's position and step (or "design change") vectors; the non dimensional time (t) represents the current iteration; r_1 and r_2 are two uniformly distributed random scalars ($r_i \in [0, 1]$); w, c_1 and c_2 are respectively the inertia, the cognitive and social coefficients [38]. The dimensional units of the Eq.2.8 depend on the units of the design variables, while all coefficients are non-dimensional weights.

The design points (particles) update is given by a weighted sum of three vectors:
• The previous step $\boldsymbol{\Delta x}_i(t-1)$;
• The difference between the personal best and the current position $\boldsymbol{p}_i(t) - \boldsymbol{x}_i(t)$, where the personal best is the position in which the ith particle found the best value of the objective function up to iteration t;
• The difference between the global best and the current position $\boldsymbol{g}(t) - \boldsymbol{x}_i(t)$, where the global best is the location of the best value of the objective function found by the entire swarm up to iteration t;

A common practice is to set c_1 and c_2 to 2, such that statistically half of the particles exceed their target and half undershoot it [41]. While, the inertia parameter w is progressively decreased (from 1.4 to 0) as the optimization proceeds, such that the search is global at first and becomes increasingly local as $\boldsymbol{x}_i$, $\boldsymbol{p}_i$ and $\boldsymbol{g}$ get closer [41].
As in all global optimisation techniques, there is no mathematical proof of convergence to the absolute global minimum. However, the probability to approach it increases with the size of the swarm and the time slot allowed for the search.

According to [38] the PSOA has been found to be robust and fast in solving highly-nonlinear and multi-modal problems, like the stiffeners layout optimization considering buckling.

2.3 Topology Optimization Applications for Stiffened Panels Design

The use of TO for plate stiffening was first suggested by Afonso et al. [42], who proposed that the placement of stiffeners could be interpreted from the optimal density distribution obtained with the SIMP method. This idea has been further developed to derive the two-phase procedure described in Chapter 1, in which optimal stiffeners positing is defined by means of a TO, and successively a sizing optimization considering stress and buckling constraints is performed on the interpreted panel model where standardized stiffeners are added [5, 11].
Many application of SIMP TO in aircraft structure, can be found in the survey [10], where also its use for stiffened panel design cases is discussed.
In little scale examples, the design space is modeled as a box of solid elements, see Fig.2.4(a) from [43], in which the lowest 2-3 layers representing the thin plate are imposed to be a passive region. One large scale example of application includes the model of an entire front fuselage of a commercial jet aircraft, see Fig..2.4(b) from [44]. In this case, the model includes only the skin made of shell elements and reinforcements are not modeled. The optimized density distribution on shell elements, obtained with the SIMP method implemented in Optistruct [1], is proposed to be considered as a suggestion for redesigning the airframe.

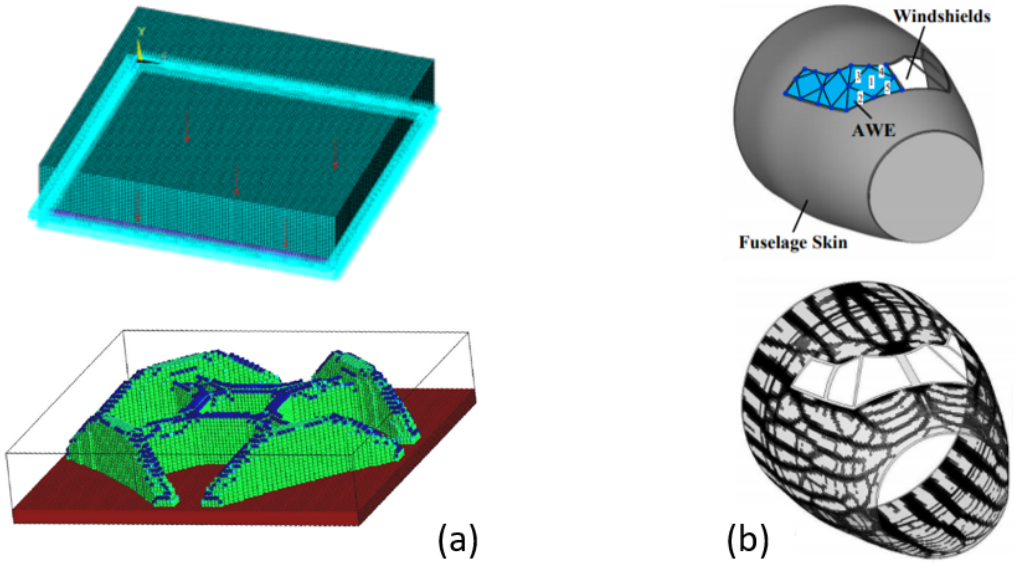

Figure 2.4 Stiffened panel application of TO: (a) A square simply supported plates modeled with solid elements, from [43]. (b) A front fuselage skin modeled with shell elements, from [44]

To model skin-stringers using two different properties this work used a two-thickness shell model, depicted in Fig.2.5 from [45], in which the properties of each element are interpolated

1. the structural analysis and optimization solver used Altair Hyperworks

between those of an element with a core thickness T_0 and those of an element with a higher total thickness T which simulates the ribbed portions.
This can be modeled in the following way:

$$\boldsymbol{K}_e(x_e) = \boldsymbol{K}_{T0} + (x_e^p)\ (\boldsymbol{K}_T - \boldsymbol{K}_{T0}) \tag{2.9}$$

Where $\boldsymbol{K}_e$ is the elemental stiffness matrices, interpolated between $\boldsymbol{K}_{T0}$ and $\boldsymbol{K}_T$, the stiffness matrices of an element with the core thickness or the total thickness respectively, according to the value of x_e, which is the density of the e-th finite element. The interpolation is a polynomial law with exponent p, a integer number greater than one that penalizes intermediate densities [21], as done in the classical SIMP method.

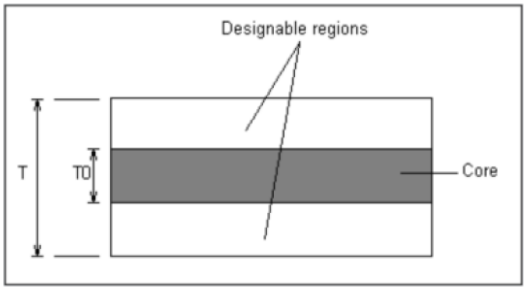

Figure 2.5 Two thickness plates TO [46] - Where the density goes to 1.0, the total thickness is assigned to the element, while where it goes to 0.0 just the core thickness is retained.

All the publications mentioned so far, do not consider buckling during the TO phase, and they miss discussion about weights saving w.r.t. to traditional designs. Still, they underline that clarity and simplicity of layouts, as well as low computational cost of the optimization, are difficult to maintain when practical structural constraints are added to the minimum compliance problem.

Alternative to the use of SIMP, few recent articles propose the MMC approach to address this challenge. In the following, two works belonging to this framework has been reviewed. Zhang [47] optimized 3D rib-stiffened plate structures discretized by solid bi-linear finite elements. The buckling constraint is considered, but only in a simple load case with one single-point concentrated force, which is not characteristic of a real plate loading. In addition, the use of solid elements for large stiffened panel assemblies makes the computational cost of the problem out of proportion to be solved on a personal computer.
Of course, the need for computational power does not daunt future prospective of TO. In a work of the TopOpt Group [1] an entire aircraft semi-wing model has been optimized, using a

huge discretization including more than one billion voxels. However in that case, the massive amount of computational resources was provided by a supercomputer, which runned for 5 days on 8,000 CPUs to solve the linear compliance problem. These resources are out of the ones available in this project.

In the perspective of using lighter finite elements models, a second work on the MMC approach applied for the design of stiffened panels [48], uses an equivalent stiffness method (ESM) to smear the stiffeners' properties into the plate mesh.
In order to replace the original stiffened panel by a clean plate model with the same stiffness, equivalent properties are derived from the original geometry using the classical lamination theory. Once the properties are obtained, "*the problem of stiffeners layout optimization can be considered as a TO problem for two kinds of materials with different mechanical properties*" [48]. That is, the optimization is asked to determine the distribution of two material phases in a design domain by setting the parameters of the TDF, the characteristic function of the MMC method, which maps the subdivision of the domain by the law defined in Eq.2.6, as shown in Fig.2.6.
However, in this case the panels are optimized for minimal compliance without considering neither buckling nor stress constraints.

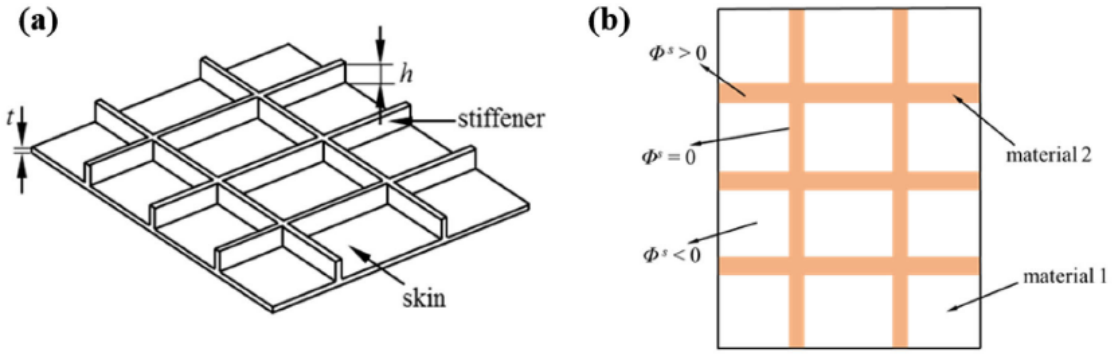

Figure 2.6 An MMC approach for TO of stiffened panels whew the a geometric model (b) is simplified in an equivalent stiffness model (b), from [48].

2.4 Structural Optimization with Buckling Criterion

Outside of the compliance minimization problem, when dealing with slender members and thin walled structures, the requirement that must be addressed first for consistent lightweight design is the stability under compressive loading. That is, it is necessary to ensure that the critical load of the structure is greater than the load to be sustained.

2.4.1 Linearized Buckling Analysis

The critical load is derived from the LBA, which is an eigenvalue problem, whose non banal solutions are the eigenpairs $(\lambda_i, \boldsymbol{\varphi_i})$ representing respectively the BLFs and the associated buckling modes. One way to derive the eigenvalues problem is to include the works done by the initial stress $\boldsymbol{\sigma}_0$ for the nonlinear part of the displacements gradient $\boldsymbol{\epsilon}_{NL}$ in the total potential energy of the structure. By introducing the finite elements scheme, the stress stiffness matrix $\mathbf{K}_\sigma$ is obtained [15]:

$$\frac{1}{2}\int_\Omega \{\boldsymbol{\epsilon}_{NL}\}^T\{\boldsymbol{\sigma}_0\}d\Omega = \frac{1}{2}\ \{\mathbf{u}\}^T[\mathbf{K}_\sigma(\mathbf{u})]\{\mathbf{u}\} \tag{2.10}$$

This matrix depends on the stress level in the pre-buckling (linear equilibrium) solution $\mathbf{u}$ and represents the stiffening/softening effect, due to tension/compression axial stress, generating the loss of stability of the equilibrium. According to the bifurcation theory the linearity is maintained up to the critical load and it can be stated that:

$$\mathbf{K}_\sigma(\mathbf{u}) = \mathbf{K}_\sigma(\lambda\mathbf{u}_0) = \lambda\ \mathbf{K}_\sigma(\mathbf{u}_0) \tag{2.11}$$

By referring to the state 0 (reference condition) as the equilibrium point found by the linear static analysis, the eigen-problem comes up when searching for new equilibrium conditions $\mathbf{u} = \mathbf{u}_0 + \boldsymbol{\varphi}$ alternative to the reference one:

$$[\mathbf{K} + \lambda\mathbf{K}_\sigma(\mathbf{u_0})]\boldsymbol{\varphi} = \mathbf{0}, \qquad \boldsymbol{\varphi} \neq \{\mathbf{0}\} \tag{2.12}$$

Considering proportionality between the applied load and the static solution, Eq. 2.13 gives the physical meaning of the first positive eigenvalue. The fundamental BLF is the scalar multiplier for the load $\boldsymbol{f}$ applied in the static analysis, to obtain the critical load $\boldsymbol{f_{cr}}$:

$$\boldsymbol{f}_{cr} = \lambda_1\boldsymbol{f} \tag{2.13}$$

2.4.2 Issues in Topology Optimizations with Linearized Buckling Criterion

TO considering buckling is an active research subject because of both the importance of the stability in the design of many structural elements and the several issues hampering the optimization process [14, 49]. Here the main issues of an eigenvalue optimization are discussed, together with some strategies proposed to overcome mathematical pitfalls.

Eigenvalue multiplicity - When dealing with eigenvalues in gradient-based optimizations, it is recommended to considered a set of firsts eigenvalues instead of a single one in the constraint/object functions. This because it is likely that at the optimum point more than one buckling modes become actives, as exampled by Seyranian et al. [50] in the optimization for the maximum BLF of a clamped-clamped column of variable cross section.

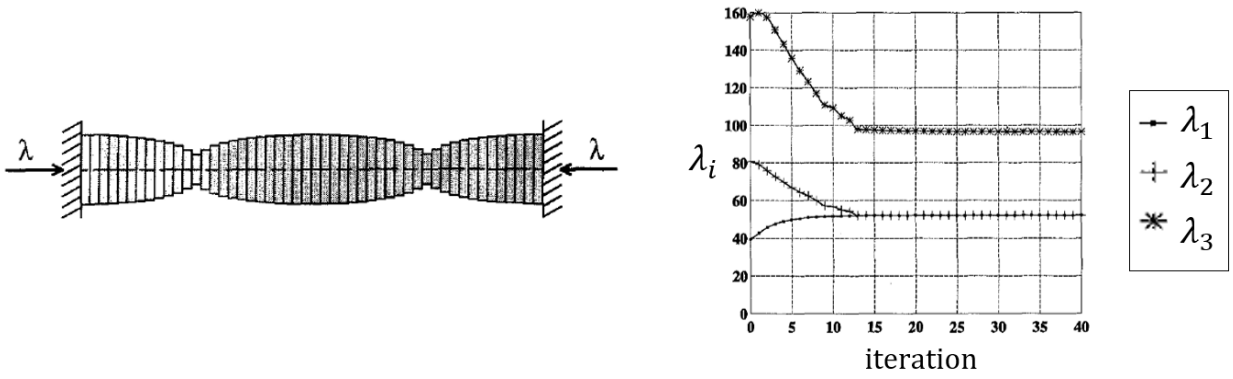

Figure 2.7 Bimodal fundamental buckling load factor of Clamped-clamped column with optimal cross-sectional area distribution [50]

In case of multiple eigenvalues, the adjoint sensitivity equation does not give univocal value for the derivatives of repeated eigenvalues (see [51] for further details), because eigenvectors of the repeated eigenvalues are not unique. To overcome the lack of differentiability of multiple eigenvalues, the strategy adopted in many works [14, 52, 53] is to use the KS aggregation function [31], which gives a smooth and differentiable approximation of the minimum eigenvalue even at design points where λ_1 is not [54].

Mode switching - Mode switching is typical of assemblies with interacting components (e.g. stiffened panel) [55], where during the optimization "the order" of the buckling mechanism may change and create a non-smooth progression of the fundamental BLF.
Referring to the Fig.2.8, a possible mode switching mechanism for a size optimization of blade stiffeners reinforcing a flat panel in compression is discussed.
For relatively weak stiffeners and a thick plate, mode (a) consisting in a global plate buckling is likely to happen. Increasing the moment of inertia of the stiffeners leads to a passage

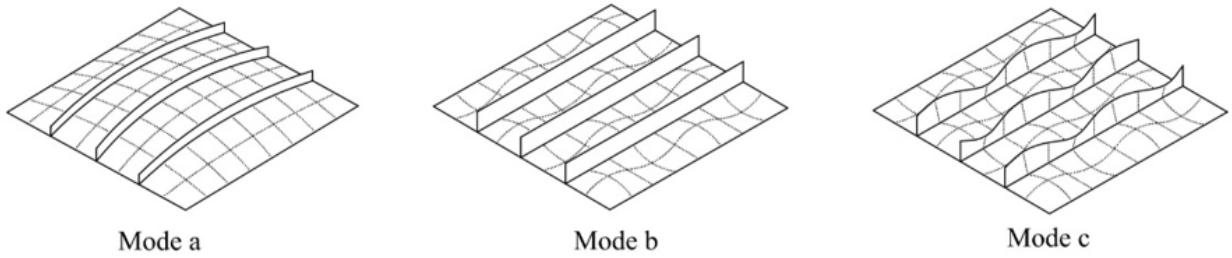

Figure 2.8 Mode switching in stiffened panel size optimization, from [55]

from mode (a) to mode (b), where there is local buckling of the plate between the stiffeners. Again, from mode (b) is possible to pass to mode (c), when the height of the web is increased too much. Such a switching between modes can cause slowness or loss of convergence [55] because it can it affects the smoothness of the buckling factor trend.

Artificial buckling modes - An issue hampering TO with eigenvalue objective/constraint is the appearance of "artificial modes" in the regions of voiding elements: e.g. low density regions in SIMP TO, or very thin bar/beam in Ground Structure TO [14, 49]. In these regions, the ratio stiffness over mass (for vibrations problem) or elastic stiffness over stress stiffness (for buckling), tends to zero. As a consequence, localized non-physical buckling modes associated to numerically small eigenvalues appear, and this prevents the search for real stability indicators.

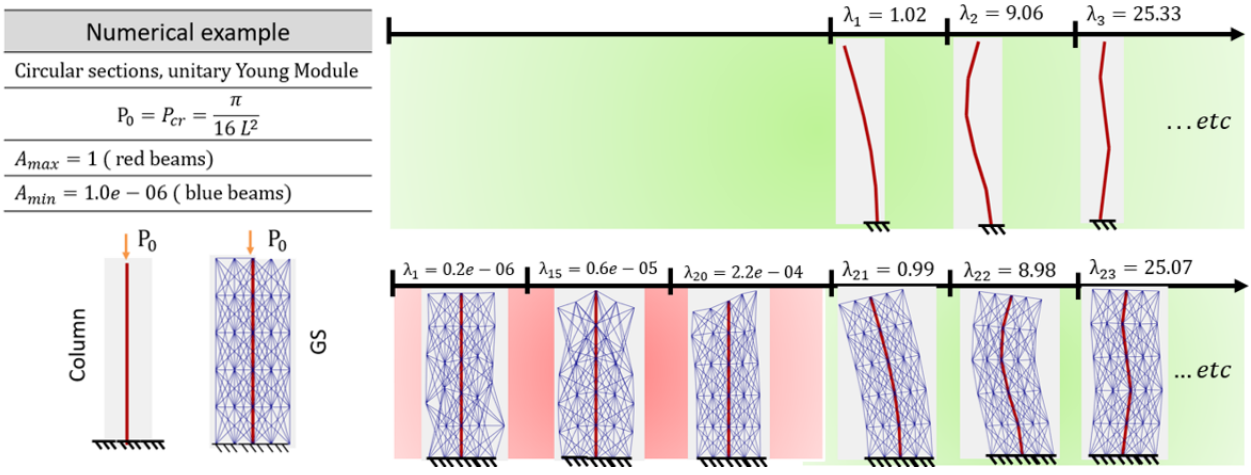

Figure 2.9 Artificial buckling modes appearing in quasi-void regions are underlined in the red band. From comparison to the "real" column, modes in the green band are considered real

An exemplification of this phenomenon is shown in Fig.2.9, in which the linearized buckling analysis is conducted for two models representing a column in compression. The cross-

sectional area distribution in the Ground Structure (GS) model recreates the same column as the clean model (Column). It is observed that the presence of infinitesimal areas in the GS model, although outside the main load path, results in localized buckling mechanisms that do not have a corresponding mode in the Column model.

Bendsoe and Sigmund [8] suggested to adopt different interpolations for elastic and stiffness matrix such that the Rayleigh coefficient remains finite in the vanishing density areas. Or, as suggested by Gao [49], the pseudo-modes can be identified, by measuring if the most of deformation energy is associated quasi-void regions, and then ignored.

2.4.3 State-of-art in Buckling-based Topology Optimization

There is a large literature on TO considering buckling for 2-3D truss design [56–60], and recent works have remarkably pushed ahead the knowledge frontier of SIMP topology optimization considering buckling for continuum solid, within 2D plane-stress finite element formulations [14, 19]. However, the class of problems studied always goes backs to truss-like structure design, but using 2D continuum models.

Instead, very few works have been found that address the problem of maximizing the fundamental buckling load of plates/shell models. A paper from Pedersen [61] introduced the prestress in topology optimization, for the first time, according to the author knowledge. The optimization is formulated for maximum fundamental eigenfrequency of flat Mindlin plates with a given membrane pre-stress. After that, Townsend et al. [62] proposed a TO-level set method for the reinforcement of plates subjected to buckling, where the strategy adopted to prevent spurious buckling modes is conceptually equivalent to the use of two different interpolation schemes for K and K_σ as proposed for the SIMP buckling methods [8].In this work optimization of both plate with holes and two-thickness flat plate without holes were addressed, since in many application placing holes in plates/shell structures in not possible.

Then this review has been able to identify one more works considering buckling in TO of plate/shell models, by Chin and Kennedy (2016) [52] which used a density method to incorporate the buckling constraints in a wing-box portion optimization. Although a practical design case is addressed, the paper does not discuss the extraction of the final layout after performing topology optimization, mainly because discrete 0-1 layouts are not obtained.

2.5 Literature Review Conclusions

In this section, two knowledge gaps highlighted by the literature review have been identified and from these, the research work carried out in the following two chapters is planned.
Furthermore, by analyzing the advantages and disadvantages of the two families of numerical optimization algorithms, local and global techniques, it is possible to identify the appropriate choice of the solver for each TO method.

(1) The comparison between the methods reviewed in Sect. 2.1. and the TO applications in Sect. 2.3 showed that the Ground Structure Method has a certain potential both in reducing the computational cost of the analysis model and in achieving a more explicit description of optimized stiffeners layout.
The computational cost of the analysis model is decreased because, using beam elements, only the degrees of freedom associated with translations and rotations of points along the beam axis are considered. Furthermore, in this type of representation, the coordinates of the end points of each element are known and the beam axis is considered as a segment joining the two points. With this information, one can explicitly represent any approximate layout by means of polygonal chains. This may simplify the interpretation task for the designer in a 2-phase design process.
The method could efficiently use a gradient-based optimizer, therefore a formulation which uses a mixed plates-beams ground structure could be investigated as a low-computational cost alternative to the SIMP method in the context of optimal plate stiffening (compliance problem).

(2) In Sect. 2.3-4, the weaknesses of the SIMP method in the stiffeners' layout optimization has been underlined. The large number of design variables becomes an issues in highly non linear problem, where gradient based solver are less efficient to navigate the design space and reveal clearly defined (hence manufacturable) layouts. To increase the chances of success in this problem, the design space should be reduced by minimizing the number of variables and the geometry of the stiffeners should be controlled explicitly.
This gave rise to the idea of implementing an MMC approach for the layout optimization problem, aiming to integrate the buckling criterion, maintain a low number of the design variable to use global optimization techniques, and provide an explicit final geometry which could be automatically extracted in order to complete the 2-phase design process.

CHAPTER 3 Generating Concepts for Optimal Stiffening Layout of Plates using Ground Structure Topology Optimization

In this chapter an original formulation of the Ground Structure Method (GSM) is proposed to address the problem of finding the optimal stiffening layout for plane pressurized stiffened panels. The GSM is well-known in the literature for trusses and frames design [23,63], but its application in the context of stiffened panels has not been investigated yet. The numerical framework to solve the topology optimization (TO) is implemented in MATLAB.
The proposed approach uses an inexpensive yet suitable finite element model to represent these types of structural assemblies. In addition, the use of beam elements to represent the layout of the stiffeners simplifies the interpretation of the topology optimization results. A comparison with SIMP and MMC methods highlights the potential of this approach.
A practical engineering problem is also addressed to demonstrate the feasibility of this formulation in a two level TO-procedure: the design of a rectangular bulkhead subject to differential pressure.
Finally, the possibility of extending the formulation to generic stiffened panel assemblies is briefly presented by using the method to explore some conceptual layout for a wing-box rib.
The content of this chapter has been submitted and accepted for ICTAM 2021 congress in Milano. The extended abstract accepted by the jury for the congress presentation can be found in the Appendix A.

3.1 The Ground Structure Method using a Hybrid Plates-Beams Model

Identifying a discrete set of stiffeners using a continuous solid mesh has the major drawback that the size of the starting mesh depends on stiffeners' cross-sectional dimensions. In the optic of applications to large structures one could easily realize that the continuous solid models can be computationally expensive for a TO.
The potential of a Ground Structure TO method, which uses a mesh made of plates and beams, comes from two basic considerations:

1. A combination of plate elements and beams is a very cheap and accurate way to model large structures made of stiffened plates. Structural idealizations of this type are commonly used in the industry for global wing finite elements model used for preliminary size purposes [12, 13, 64];
2. The GSM has been found to be an easy-to-implement formulation which can deal with the structural members of interest in aircraft constructions. Provided that a

clear stiffeners distribution can be obtained after the removal of members members with low cross-sectional areas, the model contains explicit information on the final layout of the reinforcement.

3.1.1 Design Space Modeling Hyphotesis

A ground structure constitutes a dense set of structural members which connect the nodal points discretizing the domain and constitute the candidates for the final topology.
The construction of the ground structure is the main task of the designer when using this approach. Its definition sets the domain discretization for the analysis as well as the design space for the optimization.
Zegard and Paulino (2014) [23] efficiently implemented the generation of arbitrary ground structures composed by bar elements. They also provided educational codes for building 2D and 3D ground structures with arbitrary level of connectivity, automatic removal of overlapping members, and the possibility to non-design spaces in the domain.
An adaptation of these algorithms for the automatic placement of beams elements on a plate mesh has been developed and used in this work. Building the ground structure requires the following steps, shown in Fig.3.1.

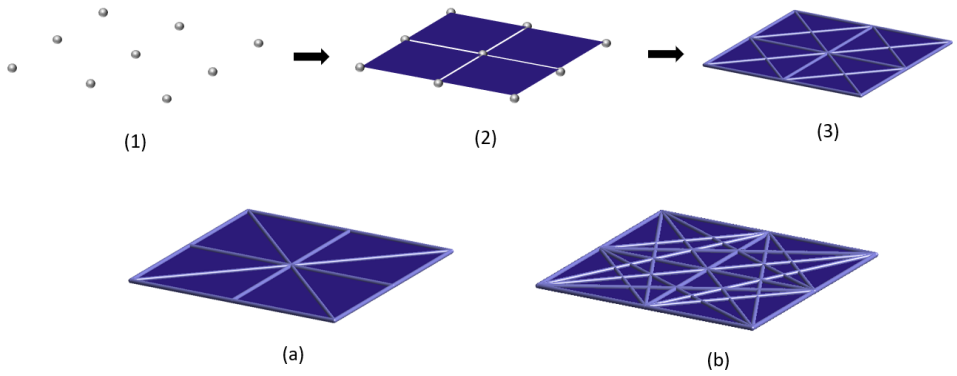

Figure 3.1 Construction of the plates-beams Ground Structure - Steps for automatic meshing of the mixed plate-beams model (1-3). Different levels of connectivity between nodes (a-b).

(1) Place nodal points in the domain, e.g. as a 2-D grid of regularly spaced points (Fig.3.1.1).
(2) Connect this grid by using plates elements. This results in a thin plate model, which is referred to as the fixed part of the ground structure or the plates ground structure (Fig.3.1.2).
(3) Superimpose a dense mesh of beams on the model. This is the variable part of the ground structure, and it connects each node to its neighbors according to the level of connectivity.

Connections between nodes contained in adjacent elements belong to the first level (Lvl1), as in Fig.3.1.3. Some connections can be skipped, as in Fig.3.1.(a)). Or conversely, connections can also be extended to the nodes of the elements immediately attached to those considered in the first level (Lvl2), as in Fig.3.1.(b).

To simplify the optimization model, the offset of the stiffeners from the plates mid-plane has been neglected. This eccentricity must be considered for accurate deflection and stress evaluation, but does not affect the main load path, which is sought in the conceptual design of the layout.

3.1.2 Stiffeners Idealization

The possible geometries that can be represented increase as the number of members in the ground structure increases. Since using more than one variables per member does not lead to additional layout possibilities, it is preferable to keep only one variable per member.
Changizi and Jalalpour [63], proposed to map cross-sectional properties of practical beam sections used in civil engineering by performing a regression analysis of the data from design manuals. In their work all the coefficients of the beam element stiffness matrix are expressed as polynomial functions of the value of the cross sectional area. For simple sections, a straightforward reduction to one independent variable can be achieved by keeping fixed proportions between various widths, heights and thicknesses. This was also adopted in the present work for rectangular sections (blade stiffeners).

When considering a pressurized plate, the bending/torsional stiffness ratio of the beam elements can have a significant effect on TO results. This effect is investigated in the current work by varying the parameter k, representing the high/width ratio of the rectangular section. For blade stiffeners, the stiffness coefficients could easily be written in an analytical form, since the second moment of inertia and the torsional constant are proportional to the square of the design variable (area), as described in Fig.3.2. The latter can be written in terms of the coefficient $\beta(k)$, whose empirical values could be found in [65].

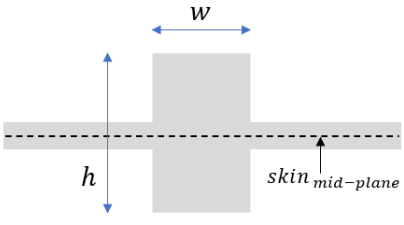

Properties as a function of cross-sectional area a, considering $h = kw$		
Cross section width	$w(a)$	$w = \sqrt{ka}$
Inertia w.r.t. to plate mid plane	$I(a)$	$I = \frac{1}{12} k\, a^2$
Torsion constant	$J(a)$	$J = \frac{\beta(k)}{k} a^2$

Figure 3.2 Stiffeners properties parametrized on the cross-sectional area

The effect of the height/width ratio parameter on these geometric properties is reported in Tab.3.1. It could be noticed that as the parameter k increases, the bending efficiency of the sections increases, while the torsion constant decreases. Consequently, high or low values of k will be used in the numerical examples to model more efficient sections in bending or torsion, respectively.

Table 3.1 Effect of the value of k on the properties of the rectangular section

$k = \frac{h}{w}$	$I = \frac{1}{12}ka^2$	$J = \frac{\beta(k)}{k}a^2$	$\frac{EI}{GJ}$
1	$\frac{1}{12}a^2$	$0.141a^2$	1.5721
3	$\frac{1}{4}a^2$	$0.088a^2$	7.5568
5	$\frac{5}{12}a^2$	$0.058a^2$	19.1092

3.1.3 Optimization Problem Formulation

In the model used here, Euler-Bernoulli beams are coupled with Discrete Quadrilateral Kirchhoff plates [15]. Metallic structures are considered, so an isotropic material model is used for both the elements type in the linear static analysis.
A compliance-based formulation for the optimization problem, can be written as follows:

$$\begin{aligned} find \quad & \{\boldsymbol{x}\} = \{x_1, x_2, ..., x_{N_b}\} \\ \min_x \quad & c(\boldsymbol{x}) = \boldsymbol{f}^T \boldsymbol{u}(\boldsymbol{x}) \\ \text{s.t.} \quad & \boldsymbol{K}(\boldsymbol{x})\boldsymbol{u}(\boldsymbol{x}) = \boldsymbol{f} \\ & \boldsymbol{l}^T \boldsymbol{x} - v_{max} \leq 0 \\ & \boldsymbol{a}_{min} \leq \boldsymbol{x} \leq \boldsymbol{a}_{max} \end{aligned} \tag{3.1}$$

where lowercase letters symbolize scalar quantities, bold lowercase are vectors and uppercase letters are matrices. The vector $\boldsymbol{x}$ contains the design variables (the cross-sectional areas of each beam element), N_b is the number of beams composing the variable ground structure; c is the structural compliance [1]; $\boldsymbol{f}$ and $\boldsymbol{u}$ are the load and nodal displacement vectors expressed in the global reference system. $\boldsymbol{l}$ is the vector of beams lengths and v_{max} is the estimated maximum volume of material allowed for the reinforcement. Finally, $\boldsymbol{a}_{min}$ and $\boldsymbol{a}_{max}$ are vectors that contain the lower and upper bounds for the design variables.

1. Compliance represents the integral of the strain energy in the structure. This measure is inversely proportional to stiffness, since the higher the value, the more the structure deforms under the prescribed load. The TO formulation for minimum compliance, which seeks the stiffest structure, is widely used in the conceptual phase as a structural layout identification criterion, since it can improve structural integrity through a convex programming problem.

Finite Elements Model for the Bending Problem In this paragraph, the finite element model for the linear elastic bending problem of flat panels subjected to lateral loads is developed in detail.

Let consider the skin panel laying in the xy plan, and the straight axis of each beam element placed on this surface. If the panel is subjected only to lateral loads the significant Degrees Of Freedoms (DOFs) are vertical displacements w and out-of-plan rotations θ_x and θ_y, as remarked in Fig. 3.3, since they are decoupled from in the in plane displacements for these elements kinematics assumptions.

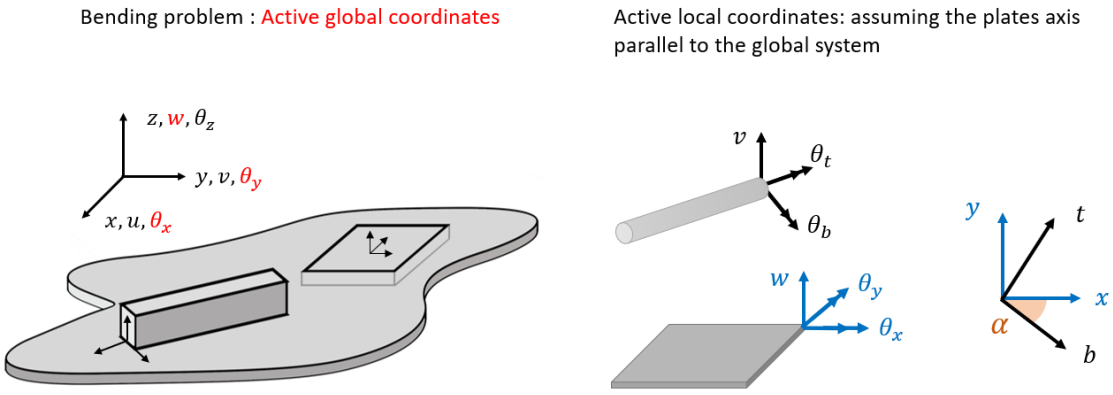

Figure 3.3 DOFs for the bending problem

The part of the ground structure representing the skin, modelled by plate elements, can be considered a "passive region" of the optimization model, because elemental stiffness matrices for the plates do not depend on the design variables.

Since in Kirchhoff hypotheses bending and axial behaviors are uncoupled for isotropic (and orthotropic) plates, the deformation energy for the problem considered on a single plate reads:

$$U = \frac{1}{2}\int_{\Omega}(\mathbf{D}_b\, w)^T[\boldsymbol{D}](\mathbf{D}_b\, w)\, d\Omega \tag{3.2}$$

where:

$$\begin{aligned}\mathbf{D}_b &= \{-\tfrac{\partial^2}{\partial x^2},\ -\tfrac{\partial^2}{\partial y^2},\ -\tfrac{\partial^2}{\partial x \partial y}\}^T \\ [\boldsymbol{D}] &= \tfrac{Et_p^3}{12(1-\nu^2)}\begin{bmatrix}1 & \nu & 0\\ \nu & 1 & 0\\ 0 & 0 & \frac{1}{2}(1-\nu)\end{bmatrix}\end{aligned} \tag{3.3}$$

with E being the Young Modulus, t_p the plate thickness and ν the Poisson's ratio.

In Eq.3.2, w represents the continuous transverse displacement fields, and the kinematic assumption of the Kirchhoff theory [66] have been used to link the rotations θ_x and θ_y to the partial derivatives of w.

Introducing a finite element approximation with the use of a non-conforming Hermite interpolation functions [66], 4-nodded plate elements consider as degrees of freedom the vertical translation w and its partial derivatives with respect to x and y, $w_{/x}$ and $w_{/y}$, for each node (subscript $i = 1...4$):

$$\mathbf{u}_{eP} = \{w_1,\ w_2,\ w_3,\ w_4,\ w_{/x1},\ w_{/x2},\ w_{/x3},\ w_{/x4},\ w_{/y1},\ w_{y2},\ w_{/y3},\ w_{/y4}\}^T \tag{3.4}$$

The coefficients of the interpolation functions N_i are defined according to Hermite shape functions [66], so the local stiffness matrix for a plate element can be expressed as:

$$[\boldsymbol{K}_{eP}]_{12\times12} = \int_{-1}^{.1}\int_{-1}^{.1} [\boldsymbol{B}]^T[\boldsymbol{D}][\boldsymbol{B}]\det(\boldsymbol{J})\,d\xi\,d\eta \tag{3.5}$$

with: $[\boldsymbol{B}] = \mathbf{D}_b[\boldsymbol{N}]$ and $\boldsymbol{J}$ being the Jacobian matrix of the transformation from natural to physical coordinates. The integration can be done by selecting a Gauss integration scheme, and the inverse of the Jacobian matrix $\boldsymbol{J}^{-1}$ needs to be numerically evaluated at Gauss points for the computation of the shape functions derivatives w.r.t. the physical coordinates .

The "active" part of GS, which depends from the design variables, is composed by Euler-Bernoulli beams, whose shape functions are Hermitian for the vertical displacement and linear for the torsional rotation. Then each beam elements has the following DOFs:

$$\mathbf{u}_{eB} = \{w_1,\ w_2,\ \theta_{b1},\ \theta_{b2},\ \theta_{t1},\ \theta_{t2}\}^T \tag{3.6}$$

Using subscripts “b” and “t” for bending and torsion submatrix, the elemental stiffness matrix, analytically available [66], for a beam element is:

$$[\boldsymbol{K}]_{eB} = \begin{bmatrix} [\boldsymbol{K}_b]_{4\times4} & \mathbf{0}_{4\times2} \\ \mathbf{0}_{2\times4} & [\boldsymbol{K}_t]_{2\times2} \end{bmatrix} \tag{3.7}$$

To assemble the ground structure explained earlier, compatibility can be applied to the nodes by equating the displacements of the nodal points for the elements connected to the same nodes. It should be mentioned that this is a weak compatibility condition, since the equality of nodal displacements does not imply that the displacements in the beams and plates are equivalent along the segments shared between the nodes. Strong compatibility is verified if triangular plate elements are used, or if this method is reformulated with isoparametric rectangular Mindlin plates (4 nodes) coupled to Timoshenko beams (2 nodes), since both use linear shape functions.

The global displacements vector is organised as follows:

$$\mathbf{u} = \{\mathbf{u}_1, ...\mathbf{u}_i, ...\mathbf{u}_n\}^T \quad , where: \quad \mathbf{u}_i = \{w_i, \theta_{xi}, \theta_{yi}\}^T \tag{3.8}$$

Thus, beams (B) and plates (P) contributions to the panel stiffness matrix are respectively:

$$\begin{aligned} \boldsymbol{K}_B &= \textstyle\sum_{i=1}^{N_B} [\boldsymbol{\Omega}_i]^T [\boldsymbol{T}(\alpha_i)]^T \boldsymbol{K}_{eB_i} [\boldsymbol{T}(\alpha_i)][\boldsymbol{\Omega}_i] \\ \boldsymbol{K}_P &= \textstyle\sum_{i=1}^{N_P} [\boldsymbol{\Omega}_i]^T [\boldsymbol{P}]^T \boldsymbol{K}_{eP_i} [\boldsymbol{P}][\boldsymbol{\Omega}_i] \end{aligned} \tag{3.9}$$

where the transformation matrices $\boldsymbol{T}(\alpha_i)$ and $\boldsymbol{P}$, defined as in Fig.3.4, and the location matrix $\boldsymbol{\Omega}_i$ are needed to complete the assembly of the global stiffness matrix. The matrices $\boldsymbol{T}(\alpha_i)$, with α_i being the angle by which the ith-beam is inclined to global x-axis, and $\boldsymbol{P}$, transform the stiffness matrices of individual beams and plates respectively from local to global coordinates. While, the location matrices $\boldsymbol{\Omega}_i$ perform the operation of positioning the contributions of individual elements into the global matrices.

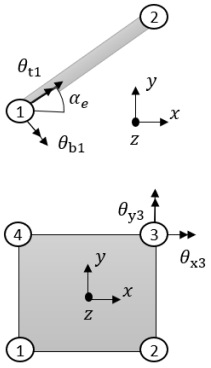

For Beam elements	For Plate elements
$\{ue_i\} = [T(\alpha_e)]^T \{u_{eB}\}$	$\{ue_i\} = [\mathrm{P}]^T \{u_{eP}\}$
$T(\alpha_e) = \begin{bmatrix} 1 & 0 & 0 & 0 & 0 & 0 \\ 0 & 0 & 0 & 1 & 0 & 0 \\ 0 & -n & m & 0 & 0 & 0 \\ 0 & 0 & 0 & 0 & -n & m \\ 0 & m & n & 0 & 0 & 0 \\ 0 & 0 & 0 & 0 & m & n \end{bmatrix}$	$P_{ij} = \begin{cases} 1 & if \quad (i,j) \in ind+ \\ -1 & if \quad (i,j) \in ind- \\ 0 & otherwise \end{cases}$
$m = cos(\alpha_e)\,, n = sin(\alpha_e)$	$ind+ = [(1,1),(2,4),(3,7),(4,10),$ $(9,2),(10,5),(11,8),(12,11)]$
	$ind- = [(5,3),(6,6),(7,9),(8,12)]$

Figure 3.4 Globalization of local stiffness matrices - [66]

After completing the global assembly of beams and plates, the total stiffness matrix results in the linear superposition of the two contributions:

$$\boldsymbol{K}(\boldsymbol{x}) = \boldsymbol{K}_B(\boldsymbol{x}) + \boldsymbol{K}_P \tag{3.10}$$

where it should be noted that the dependence on design variables is contained only in the contribution from the beam elements.

Load Vector In the following examples, two types of loads are applied to the plate: pressure loads and concentrated lateral loads. In case of concentrated loads, the generalized force variable is energetically conjugated with the correspondent displacements. In case of pressure loads, the generalized force vector is considered acting on the plates elements, hence it is introduced through the plates interpolation functions:

$$\boldsymbol{f}_e = \int_{-1}^{1}\int_{-1}^{1} p\boldsymbol{N}^T \det(\boldsymbol{J})\, d\xi, d\eta \tag{3.11}$$

Sensitivity Analysis Since the equilibrium is written in the reference condition, loads can be considered design independent, thus the sensitivity of structural compliance can be written using the adjoint method, where the derivatives of the displacement are not calculated explicitly [8] :

$$\frac{\partial c}{\partial x_e} = -\boldsymbol{u}^T \frac{\partial \boldsymbol{K}}{\partial x_e}\boldsymbol{u} = -\boldsymbol{u}^T \frac{\partial \boldsymbol{K}_B}{\partial x_e}\boldsymbol{u} = -\sum_{e=1}^{Nb} \boldsymbol{u_e}^T \ \frac{\partial [\boldsymbol{K}]_{eB}}{\partial x_e}\ \boldsymbol{u_e} \tag{3.12}$$

$\boldsymbol{u}_e$ referred to the elemental (e-th beam) nodes displacements vector, and to obtain the derivative of the elemental stiffness $[\boldsymbol{K}]_{eB}$, it is only needed to replace each properties with the relative property sensitivity w.r.t. to the cross sectional area inside the stiffness matrix expression:

$$\frac{\partial [\boldsymbol{K}]_{eB}}{\partial x_e} = \begin{bmatrix} \frac{\partial [\boldsymbol{K}_b]_{4\times 4}}{\partial x_e} & \boldsymbol{0}_{4\times 2} \\ \boldsymbol{0}_{2\times 4} & \frac{\partial [\boldsymbol{K}_T]_{2\times 2}}{\partial x_e} \end{bmatrix} \tag{3.13}$$

where:

$$\frac{\partial [\boldsymbol{K}_b]_{4\times 4}}{\partial x_e} = \frac{E\frac{\partial I_e}{\partial x_e}}{L_e^3} \begin{bmatrix} 12 & 6L_e & -12 & 6L_e \\ & 4L_e^2 & -6L_e & 2L_e^2 \\ & & 12 & -6L_e^2 \\ sym & & & 4L_e^2 \end{bmatrix} \tag{3.14}$$

$$\frac{\partial [\boldsymbol{K}_t]_{2x2}}{\partial x_e} = \frac{G\frac{\partial J_e}{\partial x_e}}{L_e} \begin{bmatrix} 1 & -1 \\ -1 & 1 \end{bmatrix}$$

So only the $\frac{\partial I_e}{\partial x_e} = \frac{k}{6}x_e$ and $\frac{\partial J_e}{\partial x_e} = 2\frac{\beta(k)}{k}x_e$ sensitivities needs to be evaluated.
Finally, the sensitivity of the total volume is given by:

$$\begin{gathered} V = \textstyle\sum_{e=1}^{Nb} {x_e}^T l_e = \boldsymbol{x}^T \boldsymbol{l} \\ \\ \frac{\partial V}{\partial x_e} = l_e \end{gathered} \tag{3.15}$$

3.2 Implementation flowchart

Based on the FE analysis and sensitivity analysis introduced earlier, the TO problem of Eq. 3.1 can be solved by using any generic gradient-based optimization algorithm.
For example, the Interior Point Method [67], implemented in the MATLAB Optimization Toolbox, is called in the code provided in Appendix B. Meanwhile, the Method of Moving Asymptotes (MMA) [30], considered in literature as the standard TO solver, has been used for the comparison against SIMP and MMC methods reported in Sect.3.3.
The pseudo code of the current implementation is represented in Fig. 3.5, supported with a visualization of the main steps of the process.

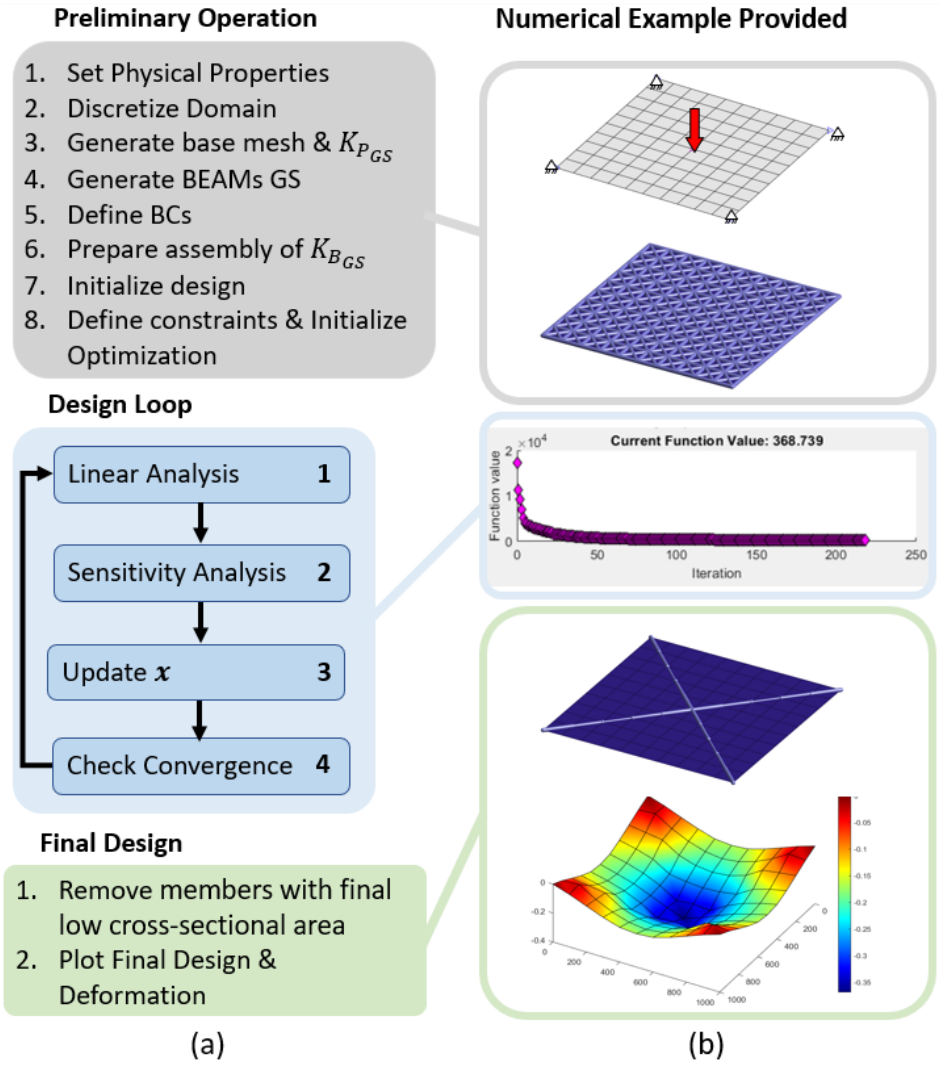

Figure 3.5 (a) Flowchart of the code provided in Appendix B. (b) Illustration of the main steps based on the numerical example provided in the code.

Pre-processing operations are carried out in the block referred as "Preliminary operations". This part includes the definition of the total panel dimensions, material properties and boundary conditions, and it sets the operators needed to assemble the global stiffness matrix. Since the optimization is performed on a fixed mesh, rotation matrices and collocation indices are constants during the whole process.

The second block is called "Design Loop" and it is the iterative part of the code. As long as the stopping condition is not satisfied, the static analysis solution is recalculated, the sensitivity analysis is repeated the design is updated.
Sensitivity analysis is the calculation of the gradients of the objective function and the constraints with respect to the design variables [7]. This information is used to find the direction of maximum descent of the objective function and thus improve the design at each iteration. This phase, which is fundamental in case the problem is solved with a gradient-based algorithm, can also be carried out through the approximate calculation of sensitivities using the method of central finite differences.
In contrast, if a non-gradient based algorithm is used, this step is not present.

In all the examples discussed in this work the stopping criterion considers an upper bound for the iteration as well as a "StepTolerance". When the solver attempts to make a design change shorter than a certain threshold, the iterations end.
In the code reported here, this block is coded in the nested function "Compliance" called by the fmincon MATLAB command.
The use of sparse matrices and vectorized operations, as suggested in [68], increases code execution speed and reduces the memory required by the software.
Further improvement of the code can be made by vectorizing the sensitivity analysis. However, the computational time required for the examples discussed in this work remained on the order of a few minutes. Thus a further increase in code efficiency was not deemed necessary.
The function "GenerateGSBEAMS" is the adaptation of the educational algorithm of Zegard and Paulino [23] for a ground structure composed of beams elements. The function "getKeP", providing the elemental stiffness matrices for the plates elements, is adapted from [66].

An example is provided to automatically run the code: the optimization of the stiffeners layout for a square panel supported on the corners and loaded with a central concentrated force. The X-shape reinforcement, which bears the load to the supports, is found in 181 iterations.

3.3 Testing and Comparison on a Benchmark Problem

In this section, the proposed GSM for the design of the reinforcement layout of plates is compared with SIMP and MMC methods in an exemplary test commonly used in the literature as a benchmark problem for minimum compliance TO of plates in bending [8, 69].

The SIMP and MMC implementations are based on the open source codes of the articles [68] and [70] respectively. For these, the lines of code concerning the finite elements analysis, given in the articles for 2D plane stress problems, have been adapted to the problem introduced in Sect.3.1.3 .

To ease the comparison, a problem is selected where symmetry of the geometry and boundary conditions ensure that the different methods yields the same optimal topology, which consists of a central cross armature connected to the centers of the four sides by tapered elements.

The methods are compared quantitatively based on the computational cost of the analysis model and the rate of convergence of the optimization.
While a qualitative comparison discusses the level of designer involvement for pre-processing and post-processing operations. These operations consist of:
(1) Design initialization;
(2) Design cycles, to verify the robustness of the solution with respect to perturbations in optimization parameters, such as the starting guess;
(3) Extraction of the resulting geometry.

The numerical example, described in Fig.3.6, is constructed with a square plate subjected to multiple out-of-plane forces and clamped on all four sides. The same boundary conditions are applied on the models of the three different methods.

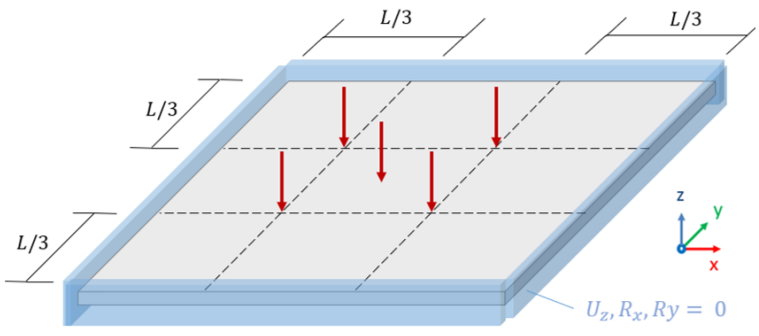

Example's parameters		
Young modulus	$\boldsymbol{E}$ $[\boldsymbol{MPa}]$	70000
Poisson coeff.	$\boldsymbol{\nu}$	0.3
Plate thickness	$\boldsymbol{t}$ $[\boldsymbol{mm}]$	2
Plate length	$\boldsymbol{L}$ $[\boldsymbol{mm}]$	1000
Applied forces	$\boldsymbol{F}$ $[\boldsymbol{N}]$	200
For SIMP and MMC		
Core thickness	T_{core}	t
Full thickness	T_{full}	$10t$

Figure 3.6 Benchmark problem - A square clamped plate subjected to concentrated out-of-plane loads. Numerical data used in the comparison.

The GSM uses a model made of beams and plates, while SIMP and MMC models use the two-thickness plate model as presented in Sect.2.3 of the literature review.
For a completely neutral comparison, the three algorithms:
- use the same block of code for the FEA of the problem bending of discrete quadrilateral Kirchoff plates with 3 dofs per node;
- use the same solver for optimization, i.e. the MATLAB cod of the MMA provided by [30].
For GSM and SIMP methods the standard parameters for the MMA suggested in the article that introduces the solver [30] have been used, while for the MMC method the parameters suggested by Guo in [70] are selected.

(1) Design initialization The initialization of GSM and SIMP is straightforward, since it consists in choosing the constant value of the material distribution such as to meet the constraint. For the MMC method, choosing the number of components, their shape, and initial parameters is up to the user. As is usually done for simplicity, a uniform grid of orthogonal components with a constant thickness is assumed.
Thus, it can be seen in Tab.3.2 that the definition of the initial starting guess involves a gradually increasing number of user choices, moving from SIMP to GSM to MMC.
The last item is the proper mesh size selection. For SIMP and MMC it is necessary to refine the mesh until it can describe the reinforcement in its short side with at least three/four elements. While in GSM, the mesh size is decided according to the size of the plate and the set of reinforcements that the designer wants to include in the design space.

Table 3.2 Designer choices (input)

GSM	**SIMP**	**MMC**
- Mesh size	- Mesh size	- Mesh size
- Level of connectivity	- Density ρ_i	- No. of morphanle components
- Cross-sectional area a_{max}		- Components shape parameters $\{d_i\}$

There are no theoretical restrictions on the initial configuration that can be selected. However, simple initial designs for each method can be defined in the following ways:

starting cross sectional area in GSM [23]: $a_i = \frac{V_{max} N_b}{\sum_{i=1}^{N_b} l_i} \quad \forall i = 1 \dots Nb$

starting element densities in SIMP [71]: $\rho_i = v_f \quad \forall i = 1 \dots Ne$

starting components width in MMC [26]: $t_i = \frac{v_f \ L^2}{\sum_{i=1}^{Nmc} l_i} \quad \forall i = 1 \dots Nmc$

where: V_{max} and v_f are respectively the maximum volume and volume fraction allowed; L and l_i are the total panel length and the ith candidate component length; $Nb, Ne \ and \ Nmc$

are the number of beams in the GS, the total number of plate elements with variable density in the SIMP, and the number of morphable component composing the design space of the MMC method.

Optimization routine For the minimum compliance problem with constrained volume, Table 3.3 summarizes the results of the comparison. To determine the optimization convergence, the step tolerance on the minimum current design update was selected as: $tol = 1e-04$.

Table 3.3 Summary of the comparison GSM vs SIMP vs MMC

	GSM	**SIMP**	**MMC**
Design variables	$d_i = \{a_i\}$	$d_i = \{\rho_i\}$	$d_{MCi} = \{x_0, y_0, L, t_1, t_2, sin\theta\}$
g_1	$V \leq 2.5L^2\ mm^3$	$v_f \leq 0.15$	$v_f \leq 0.15$
Side constraints	$a_i \in [10^{-3}; 1000] mm^2$	$\rho_i \in [0; 1]$	$(x_{0i}, y_{0i}, L) \in [0; L]$ $(t_1, t_2) \in [0; L/10]$ $sin\theta \in [-1; 1]$
No. of design variables	1332	10000	192
No. of Plate (P) and Beam (B) elements	324 P + 1332 B	10000 P	10000 P
No. of DOFs	1083	30603	30603
Iterations to converge	389	83	248
Time per iteration [s]	0.97	0.56	2.16

From Table 3.3 it can be seen that SIMP has the least iterations. MMC maintains the lowest number of design variables. The least computationally intensive finite element model is within the GSM.

Additionally, it is noted that SIMP is also the fastest in terms of time per iteration considering the average time taken in the first 10 iterations. GSM loses a portion of time to recalculate the beams local stiffness matrices at each iteration, whereas the MMC formulation uses finite difference calculations for the sensitivity of the topology description function.

A graphical summary of the comparison is presented in Fig.3.7 and Fig.3.8, where graphs of the optimization history and progression to the optimal design for the three methods are shown respectively.

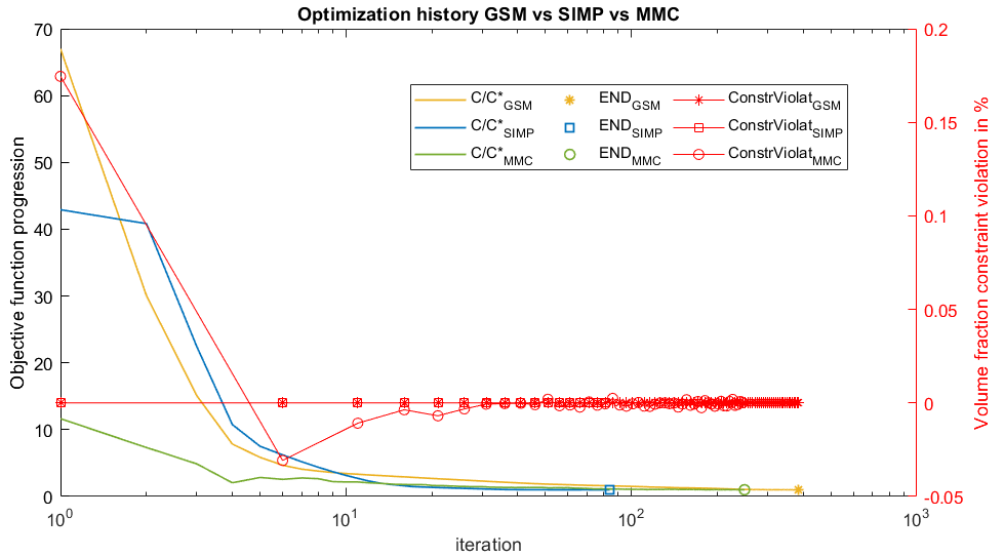

Figure 3.7 Comparison GSM vs SIMP vs MMC: The values of the compliance normalized on the optimum value (left axis), and the volume constraint violation (right axis) are plotted against the current iteration for each method.

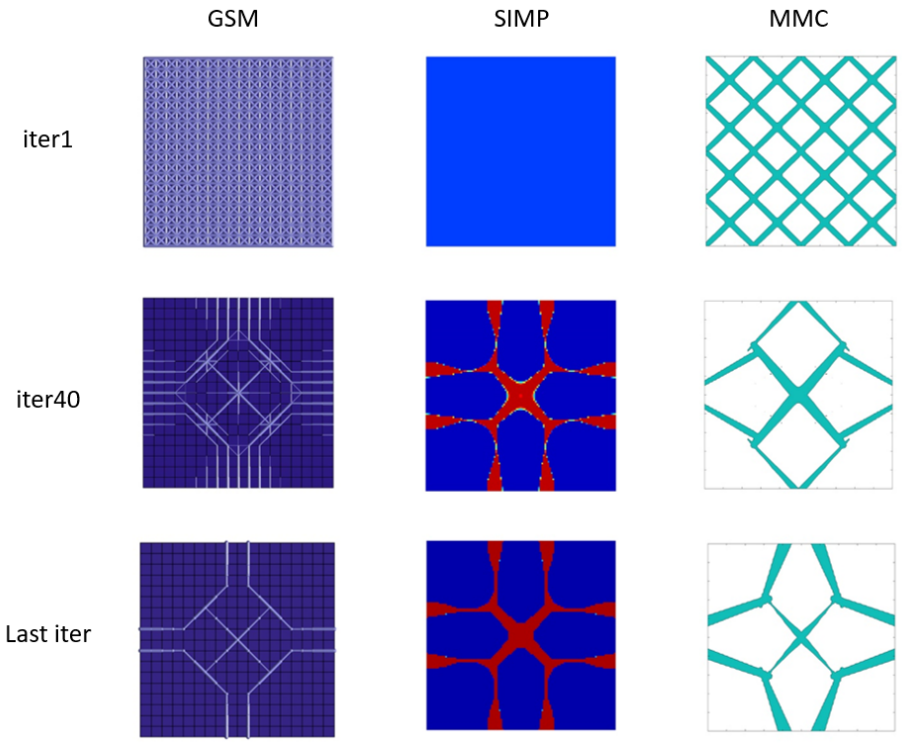

Figure 3.8 Comparison GSM vs SIMP vs MMC: Plot of initial, intermediate (iter=40) and final layout for each method.

(2) Design cycles and use of different parameters In a practical design, the above optimization problem cannot be expected to be run only once. Depending on the complexity of the problem, the user usually has to try multiple initial starting designs or optimization parameters to arrive to a satisfying layout.
The level of dependence of the results on this type of inputs, causes a certain level of involvement of the final user in carrying out the procedure, which ideally should be kept as minimal as possible.
In this regard it was noted that GSM and SIMP are much more user friendly than MMC. It was also noted the strong oscillatory behavior of the MMC method. The result shown in the Fig.3.6 is the most efficient among the tests performed. Changing the number of morphable components or their initial arrangement radically changes the convergence history. For example, starting from a grid of orthogonal components 0-90° needs about 600 iterations to find the layout in the figure. In some cases the optimization for the MMC method has caught up the imposed limit of 1000 iterations, and presented incoherent disconnections of the components in the final design. On the other hand, SIMP when used with typical filter radius values (between 2 and 6 times the mesh size) does not result in topology changes, for a fixed mesh and $p = 3$.

In this particular case, different initial values of the starting guess reinforcement volume do not result in topology changes for GSM. The only parameter that plays a role in the final design using GSM is the discretization choice: mesh size and level of connection. Mesh dependency, a typical feature of topology optimisation [8], is shown in Fig.3.9.

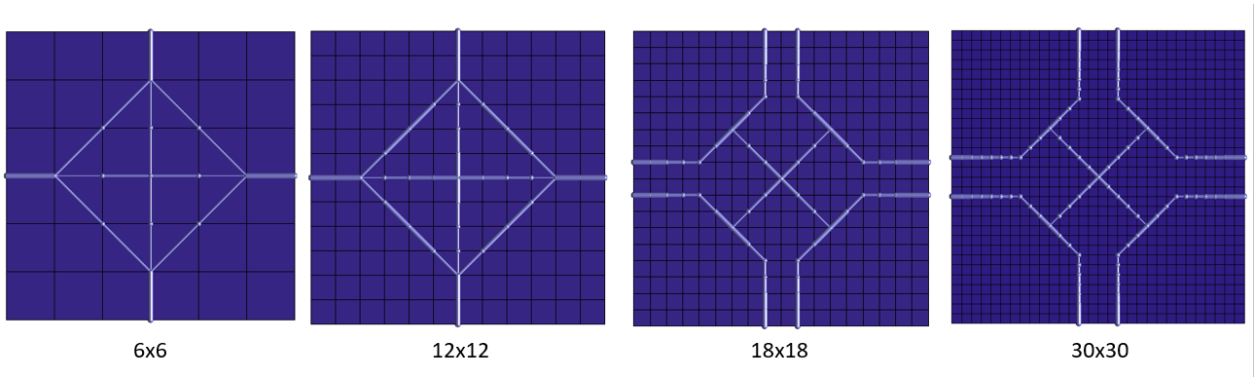

Figure 3.9 Mesh Dependency test

It is observed that going from a mesh of 12×12 plates to a 18×18 one radically changes the resultant topology. However, in this particular case the solution has moved towards a better value of the objective function.
Refining the starting ground structure has expanded the design space and increased the

Table 3.4 Result for the mesh dependency test

Test	**1**	**2**	**3**	**4**
No. of plate elements in the mesh	6×6	12×12	18×18	30×30
No. of beam elements in the final design	20	40	60	100
No. of stiffeners in the final design	12	12	16	16
Max area in the optimum design $a^*_{max}[mm^2]$	1000	1000	1000	1000
Min area in the optimum design $a^*_{min}[mm^2]$	468.8	230.5	209.5	201.5
Optimal compliance value $c^*[Nmm]$	17.9	17.2	15.1	14.8
No. of iteration to converge	202	274	389	502

possibility of finding better layouts. In this case the 30×30 mesh includes all the possible designs of the 6×6 mesh: i.e. the new refined mesh is "embedded" in the old one. Thus, the possible solutions of the refined mesh include all those of the old mesh.
Finally, the examples showed that with mesh refinement the number of steps required for convergence also increases, due to larger design space.

(3) Final layout extraction Interpreting the layout of the stiffeners is another important operation in the practical use of these tools, so that one can move on to models with higher fidelity of representation for more advanced stages of the design.
Assuming a clear topology is obtained for each method, the SIMP approach is the only one that needs an additional tool to extract the final geometry.
GSM clearly defines any kind of piece-wise linear layout by defining skeletons and connections (ends of each reinforcement) uniquely.
MMC is the one that provides the geometric information most explicitly. The starting components merge and intersect, but starting from the solution x^*, the geometry is automatically rebuildable in a CAD software.

Lessons learned By summing up the experience gained in these tests, a typical characteristic of the structural optimization subject has been encountered: there is no method which performs better than the competitors on every single aspect.
Table 3.5 synthesizes main strengths and weaknesses for each method. Some observations on the expected ideal application, based on remarked advantages, as well as possible ways to mitigate drawbacks for each method are also reported.

Table 3.5 Strengths-Weaknesses underlined

	GSM	**SIMP**	**MMC**
STRENGTH	Low-cost finite element model. Good physical representation.	Rapid convergence. Simple pre-processing.	Possibility to limit the number of variables.
Suitable applications	Large structures using beam-like structural elements.	Structures that do not have special concerns regarding manufacturability.	Structures that do have special concerns regarding manufacturability.
WEAKNESS	Design freedom depending on the initial GS. Iterative recalculation of local stiffness matrices.	Poor control on geometrical features	Optimization problem always non-convex High dependence on the starting guess
Possible improvements	Making GS construction smarter by leveraging information from BCs. Use of an interpolation scheme to avoid local stiffness matrices recalculation	Addition of manufacturing constraints Computer-vision support for the interpretation of the results	Use of a continuation strategy (following the example of the one explained for the SIMP method in Sect.2.1.2)

3.4 Conceptual Design of a Simplified Pressure Bulkhead

In this section, the use of the GSM is tested in a two-level procedure for a TO-based design of a flat pressure bulkhead.
Even if this kind of structures also sustain in-plane loading coming from connections with fuselage airframe, the out of plane loading (pressure) is dominant and can be isolated for preliminary sizing purpose [12].

The problem of reinforcing a rectangular panel has been chosen, because this simple domain allows to carry out an easy and fast comparison with the semi-analytical formulas contained in handbooks.
Focus can be kept on the procedure, rather than a particular geometry. For a conventional configuration, the design usually consists of N equals stiffeners with a constant pitch, which is a simple and low cost solution. For this layout, the design variables are the number of stiffeners (related to the pitch), the type and dimensions of stiffeners cross sections.
Topology optimization is asked to propose different configurations, which after optimal sizing reveals if there is a considerable impact in terms of weight reduction. It is recalled that conceptual stiffeners layouts are found by minimizing the compliance for a given material volume.

The baseline of Fig.3.10, extracted by a rapid parametric study (discussed in Sect.3.5) is considered for an initial estimation of the geometrical dimensions of the reinforcement. These information are used to set the volume upper bound and the variable side constraints in the optimization problem. I-beam are considered because of their bending efficiency, but in the topology optimization problem they are modeled as blade stiffeners.

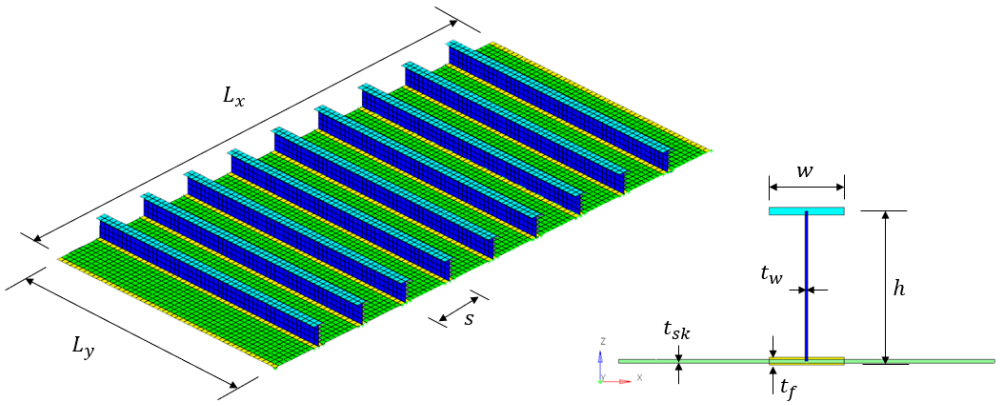

Figure 3.10 Simplified Rectangular Bulkhead - Baseline

The properties of a typical aeronautical aluminum alloy (Al7075) and the sizes of the domain

Table 3.6 Baseline Design

Baseline Design	
Skin thickness [mm]	2.25
No. of stiffeners (pitch [mm])	9 (125)
Pressure [MPa]	0.083
Young Modulus [GPa]	71.7
Material density $[\frac{Kg}{mm^3}]$	$2.8 * 10^{-6}$
Long side [mm]	2500
Short side [mm]	1250
Stiffeners Cross-sectional Area $[mm^2]$	≈ 450
Total Stiffeners Volume [mm^3]	$5 * 10^6$

are reported in the table 3.6. The numerical value of 0.083 Mpa is estimated considering a 1.5 Safety Factor above the limit pressure of 0.055 Mpa, which is the flight pressurization profile of a typical civil aircraft as per FAR 25 specifications [72].
For front bulkheads which separate nose radome and cockpit, flat stiffness panels are usually adopted because the lack of space prevents the use of more efficient hemispherical shells [12].

The design domain, the GS used as starting guess and the boundary conditions are showed in Fig.3.11.

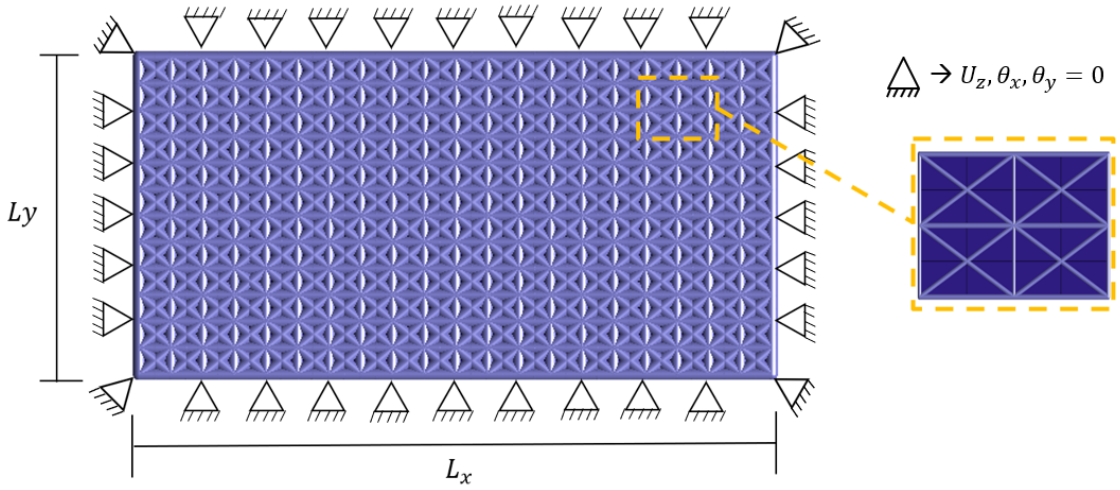

Figure 3.11 Design Space: The ground structure

The skin is discretized with a mesh of 40x24 rectangular elements. The connection between the bulkhead and the fuselage airframe is modeled by constraining all displacements at some equidistant points. The ground structure presents the modular repetition of the portion highlighted in Fig.3.11. The starting guess has an initial uniform area distribution which

satisfy the constraints without slack, and the design space consists in 1984 stiffener's segments candidates.

The optimization problem of 3.1 is solved, and the results are summarized in Fig.3.12 and the corresponding Tab.3.13. The TO suggested layouts (k3 and k5) are compared with the a parallel stiffeners layout (EP) and an orthogonal grid stiffeners layout (OG) in terms of compliance. All the layout are iso-volume, and the high/widht ratio for stiffeners' section, $k = 3$ is used for all the cases, except for concept k5.

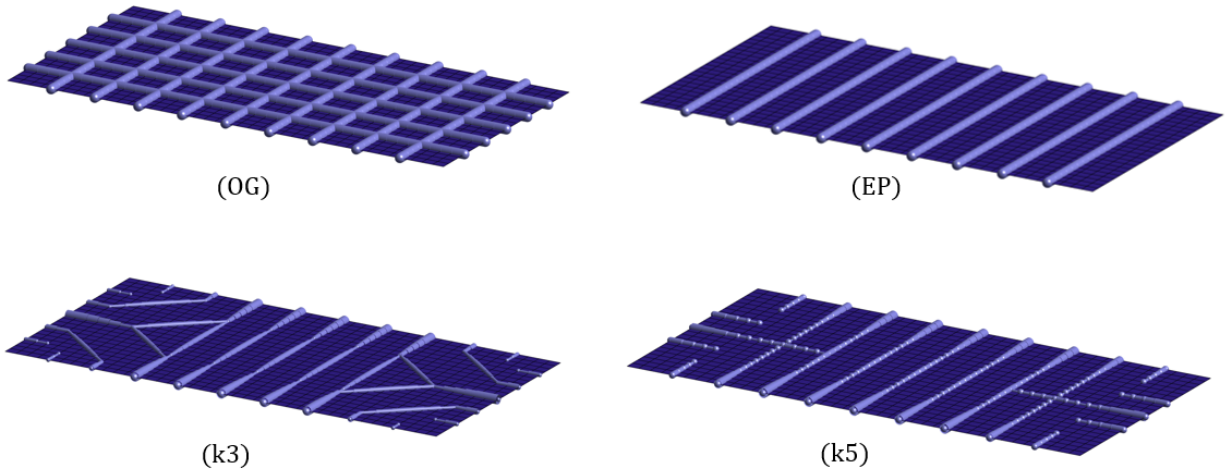

Figure 3.12 Two conventional layouts: Ortho-grid (OG) and equispace parallel (EP). Two TO suggested layout (k3) for $k = 3$ and (k5) for $k = 5$

Table 3.7 Compliance values for Conventional and TO-suggested layouts

	OG	**EP**	**k3**	**k5**
Max plate deflection [mm]	13.54	8.66	13.37	7.02
Optimal compliance value c^* [Nmm]	$1.40e+06$	$1.08e+06$	$9.10e+05$	$6.83e+05$

It is found that novel configurations, depicted in Fig. 3.13, do have better compliance value: i.e. the integral of their deformation over the entire domain has been decreased, indicating that new solutions are stiffer.

For novel configurations, it is observed that straight stiffeners are placed in the middle. However their axis-wise stiffness distribution is non-constant at the optimum design. A qualitatively same axis-wise area distribution is found in the 2 novel layouts. A physical justification for this distribution can be given by examining the "bending" diagram of an un-stiffened panel subjected to uniform pressure (Fig. 3.14).

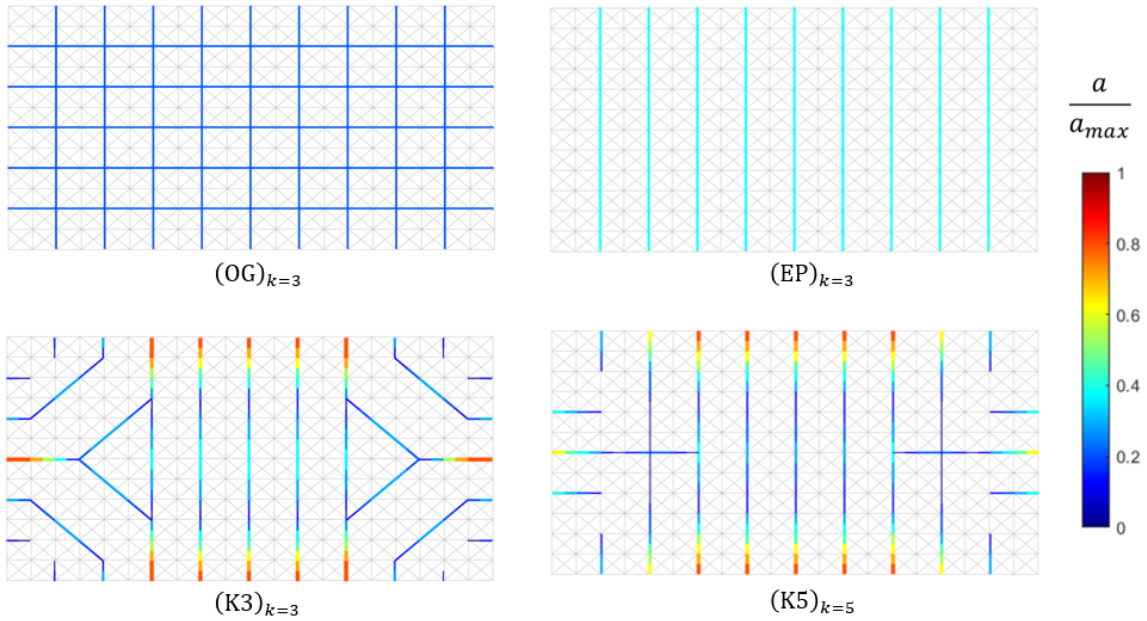

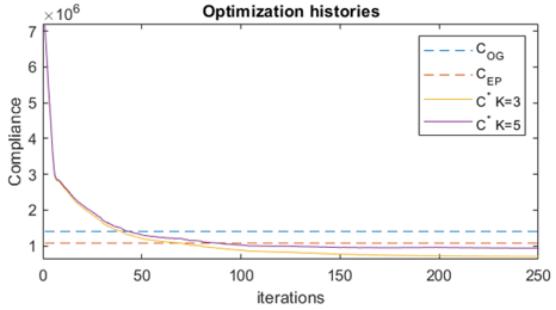

Optimization formulation	
Min	*Compliance*
Sbj to	$V \leq 5 + e06$
	$1e-03 \leq x \leq 1e+03$
Optimization parameters	
$iter_{max}$	250
toll	$1e-04$

Figure 3.13 Summary of the optimization: Results, history and formulation.

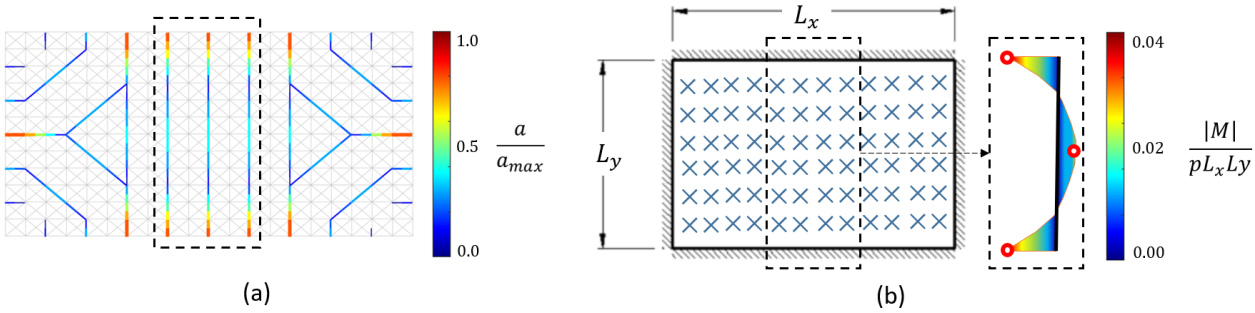

Figure 3.14 Interpretation of mechanical features suggested by TO in the optimal layouts. A direct correlation is present between the cross-sectional area distribution in the optimal layout (a) and the bending moment diagram of the un-stiffened panel subjected to uniform pressure (b), sketched using empirical coefficients [12].

Along the short sides the biggest reinforcements grow in the middle (for the same reasons), while very near the corners there is no need of additional material.
In between these regions, the optimal distribution seems to depends on the ratio bending/torsion efficiency of the beam elements, which grows for a bigger k. Dependency from the initial ground structure is pronounced in this zone, especially from the level of connectivity which enlarge possible beams' orientations.

The choice of boundary conditions has an important impact on the solution, since the positioning of the concentrated supports fixes the starting point from which the stiffeners branch off towards the centre of the panel.It is worth mentioning two main effects of the boundary conditions on the TO results, depending on whether the constraint is: (1) Simply supported or clamped and (2) concentrated or distributed loading.

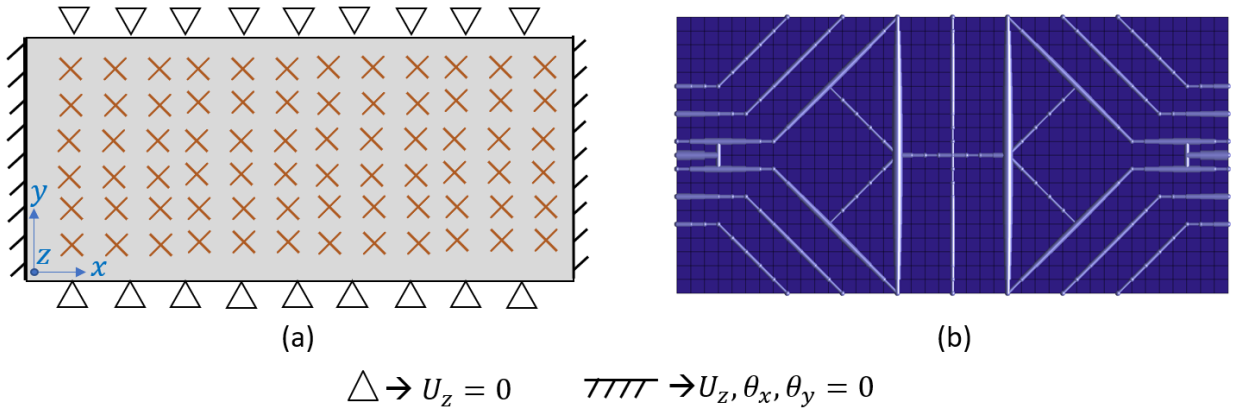

Figure 3.15 Supports are applied to the long sides of the panel at equally spaced locations, and a clamping condition is applied along the entire length of the long sides (a). The impact of these two different conditions on the stiffeners attached to the long/short sides of the panel can be seen in the resulting layout (b) , in terms of spacing and tapering.

The example in Fig.3.15, showed both the effects on the optimal reinforcement layout:
(1) As opposed to clamping, the simply support causes the bending moment to be maximum at the center of the panel and zero along the constrained sides. This results in placing larger sections in the middle of the panel and smaller section near the support.
(2) By imposing a "distributed constraint" all along the sides, the number of stiffeners increases, since the "main load path" that the TO must reveal is less concentrated.
In conclusion, the example have demonstrated that GSM results showed to be mechanically efficients in term of compliance. The physical interpretation of the features suggested by TO can be easily found by looking at the initial stress distribution in the un-stiffened panel.

However, stress concentrations at stiffeners connections (and interruptions) cannot be considered within this formulation. This turns out to drastically reduce the efficiency of the layout when moving to final sizing, as is discussed later.

Finally, by comparing the discussed results with the ones obtained with SIMP Method [5] and MMC [48] in similar test cases, the competitiveness of the GS-Method for the minimum compliance design of this kind of structure is further validated: similar features are suggested regardless of the method, but the finite element model adopted by the GSM formulation is is much lighter and therefore very promising for large size models.

3.5 Baseline Estimation

Before moving on to the sizing of the various concepts obtained, the reference model used so far for total volume estimation is introduced. This baseline consists of a flat rectangular "thin plate" and N equispaced stiffeners. As shown in Fig.3.10, this configuration considers the following design variables: the constant skin thickness of the panel t_{sk}, the I-section total height h and width h, and two independent thicknesses for the web t_w and the flanges t_f. Assuming that the bending stiffness of the beams is orders of magnitude greater than adjacent portions of the panel, an initial guess for skins and stiffeners size can be found by using the criteria given in Table 3.8.

Table 3.8 Initial estimation of the Baseline Design

Parametric study. For N=[5:15] find $\{t_{sk}, t_f, t_w, h, w\}$ s.t. :		
Objective	$min\ M$	$M = \rho * (Ly + (Lx + N(Ht_w + 2Wt_f)))$
g1: Plate deformation (center) [mm]	$w_{sk} \leq 5t_{sk}$ *	$w_{sk} = 0.00126 * (p(\frac{Lx}{N+1})^4) * \frac{Et_{sk}^3}{12(1-\nu^2)}$
g2: Stiffeners deformation (midspan) [mm]	$w_{st} \leq t_{sk}$	$w_{st} = \frac{qL_x^4}{384EI}$, $q = p\frac{L_x}{N+1}$
g3: Stiffeners maximum axial stress (at root) [Mpa]	$\sigma_{max} \leq 300$ **	$\sigma_{max} = \frac{qL_y^2 h}{24I}$
g4: Stiffeners max shear stress (at root) [Mpa]	$\tau_{max} \leq \sqrt{3}\ 300$	$\tau_{max} = \frac{qL_y Q}{16t_w I}$, $Q = wh^2 - w(h-2t_f)^2 + t_w(h-2t_f)^2$
g5: Stiffeners' web critical stress [Mpa]	$\sigma_{max} \leq \sigma_{cr,web}$	$\sigma_{cr,web} = 21.6 * E(\frac{t_w}{h})^2$

*According to [12], "thin plates", deflection in thin plates encountered in metallic airframe structure are limited to not overcome $\delta/t < 5$. ** Since fatigue is not considered, a reduction of the of the aluminium ultimate strength (575MPa) is applied.

To make a coarse initial estimation, a decoupling between the components is assumed, so that

the classic beam theory (for stiffeners) and classic plate theory with empirical coefficients (for panel bays), taken from chapter 7 of the practical handbook for airframe design of Niu [12], are used to set design criteria. With these analytical formulas, a parametric study is performed, and reported in Fig.3.16, to see the optimal design for different numbers of stiffeners.

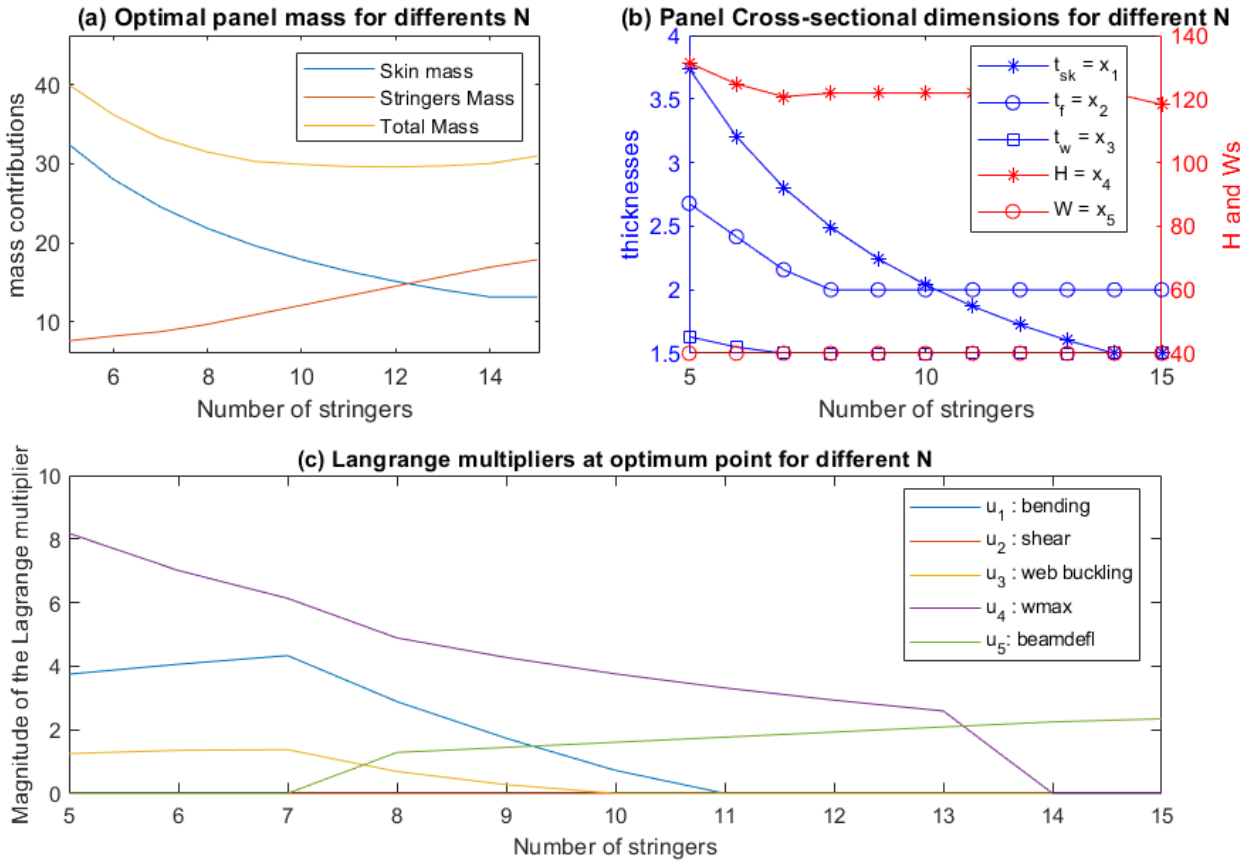

Figure 3.16 Results of the analytical parametric study

The study shows that from 9 stiffeners onwards the optimal mass is on a plateau Fig.3.16(a). The configuration with 9 stiffeners is then taken as the baseline, and its dimensions can be extracted from graph fig.3.16(b). The graph in Fig.3.16(c), on the other hand, shows the trend of the Lagrange multipliers at the optimal point for increasing values of N.

The magnitude of the Lagrange multipliers (at the solution) reveals useful information about the effect of each constraint on the optimal objective function value:

- The constraint on the max skin deflection results to be associated with the largest Lagrange multiplier. This means that it has the greatest importance on the value of the optimal panel mass. By augmenting the number of stiffeners, the bays dimensions are reduced and the constraint gradually loses importance because the skin portion became thinner. However it results to be active until 14 stringers are placed.

- Constraints on maximal bending and web buckling became inactive as the skin panel is split in more portions. However beams dimension reach a plateau because the stiffness constraint (middle beam point deflection) takes place. Finally from the variables trends, we can observe that some design variables are blocked by their side constraints. In particular, the thickness and the width of the stiffeners flanges tends to the lower allowable value, because their impact the bending stiffness is little w.r.t to the impact of the stiffeners height. This constrained are relaxed for the finite element optimization, but not so much because of manufacturing limitations.

With this information, a finite element model of the baseline is modeled in Hypermesh FEA. The model is clamped along the four side and a normal pressure is applied using PLOAD4 card on the un-stiffened side of the skin. The I-stiffeners are modeled using CQUAD4 for the web and CBAR for the flanges. The results of the analysis are reported in Fig. 3.17. As expected, the final element analysis reveals to have higher stresses and displacements w.r.t. to simplified analytical formulas, where empirical coefficients assumed the connection with stiffeners to be a perfect clamping for the plates. The sizes of finite element model of Fig. 3.17 are assumed used from now on as a initial values for new concepts size optimization.

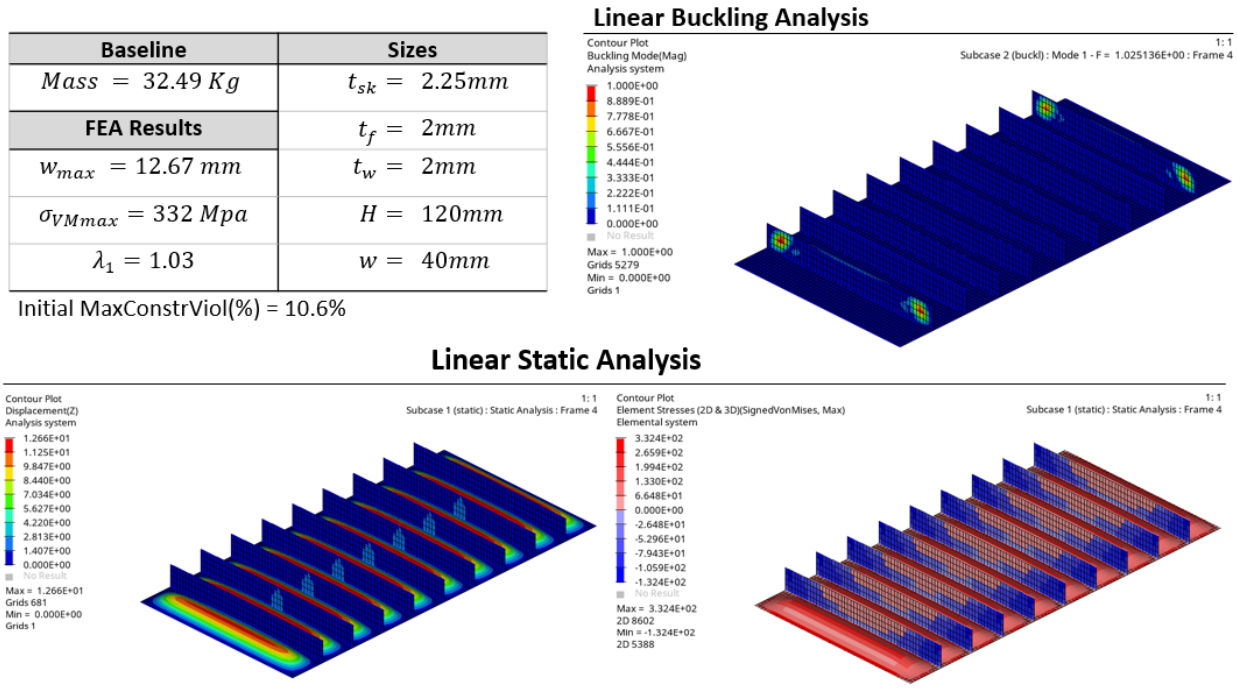

Figure 3.17 Analysis of the Baseline Design

3.6 Optimal sizing of suggested concept

New concepts suggested by TO are modeled and resized via a size optimization. At this stage, the optimization variables are the cross-sectional dimensions of the stiffeners, whose topology is now determined. It is assumed that all stiffeners have an I-section, and the three-dimensional panel is modeled using the following types of finite elements:
- PSHELLs, contained in the XY plane, to represent the skin;
- PSHELLs, positioned orthogonally to the XY plane, to represent the web of stiffeners;
- CBARs with rectangular section to represent the stiffeners flanges.

The panel is loaded with a uniform pressure of 0.083 Mpa, considered as per Tab.3.6, and it is clamped all along the four sides.
Then, for each stiffeners, the sizing variables are the width W and thickness t of each flange (independent for upper and lower flanges) and the web thickness t_{web}.
Finally, according to the optimal cross-sectional area distributions of Fig.3.13(a), stiffeners with variable cross-sectional area are considered, since the TO suggests that they can give more stiffness to the panel for a given amount of mass, compared to stiffeners with constant cross-sections. The web height is allowed to vary linearly between the endpoint values, H and h, these latter added to the vector of variables of the ith-stiffener $\boldsymbol{d}_i$.

The definition of the variables for the single stiffener is presented in Fig.3.18(a), and the different colors used for different stiffeners, in Fig.3.18(b), indicate the subdivision of layouts K3 and K5 (from Fig.3.13) into different groups of components for which the cross-sectional sizes are considered equal.

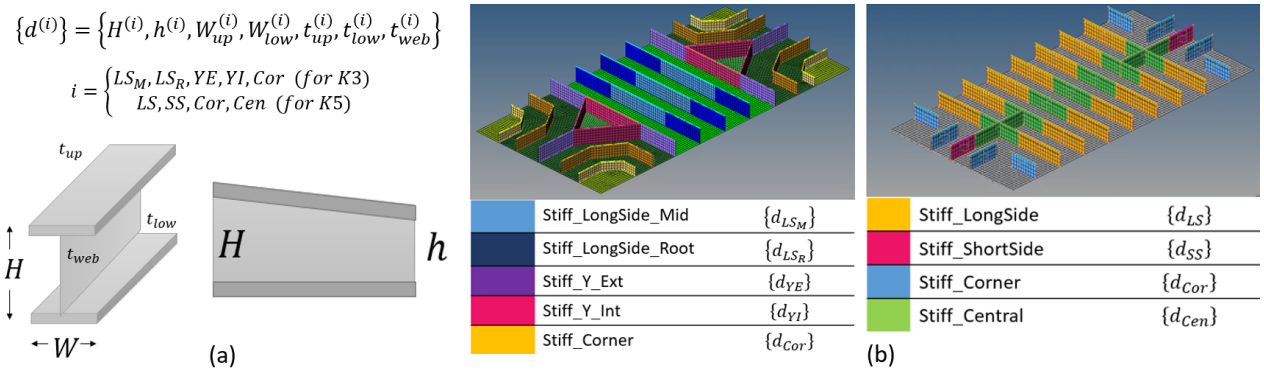

Figure 3.18 Size Optimization - (a) Definition of the ith-stiffener's variables. (b) Subdivision of stiffeners into groups with the same design variables.

Consequently, each concept is associated with a vector of design variables $\boldsymbol{d}$ that contains as many $\boldsymbol{d}_i$ as the different groups of stiffeners identified by the designer. In this exercise,

this division follows the symmetries of the structure and an arbitrary classification based on the different stiffeners placement. Final designs are then found by solving the problem in Eq.3.16, aiming at minimizing the total mass of the panel while meeting the mechanical requirements discussed in Tab.3.8. Constraints are imposed on the maximum skin deflection g_1, the maximum Von Mises stress g_2 (strength requirement for ductile materials), and the minimum BLF g_3 (linearized stability requirement). Thus, the problem is defined as follows:

$$\begin{aligned} \min \quad & Mass \\ \text{s.t.} \quad & g_1 : w_{max} \leq 12.5mm \\ & g_2 : \sigma_{VMmax} \leq 300Mpa \\ & g_3 : \lambda_1 \geq 1 \\ & \underline{\boldsymbol{d}} \leq \boldsymbol{d} \leq \overline{\boldsymbol{d}} \end{aligned} \tag{3.16}$$

The initial starting guess takes the dimensions considered in the baseline of Fig.3.17, and the range in Tab.3.9 is considered for the different design variables.

Table 3.9 Size optimization variables, side constraints and baseline values

Variable	lower bound	baseline value	upper bound
$H[mm]$	50	125	150
$h[mm]$	50	125	150
$W_{up}[mm]$	25	40	60
$W_{low}[mm]$	25	40	60
$t_{up}[mm]$	1.25	2	4
$t_{low}[mm]$	1.25	2	4
$t_{web}[mm]$	1.25	2	4
$t_{ski}[mm]$	1.25	2.25	4

In the sections 3.6.1 and 3.6.2, the results of the optimization and the analysis of the final design are reported for concept K3 and K5 respectively.
For each optimization, the progression of the objective function is presented, along with the maximum constraint violation and the values of the design variables for each iteration (Fig.3.19-3.20 for concept K3 and Fig.3.22-3.23 for K5). The analyses of the final designs (Fig.3.21 for concept K3 and Fig.3.24 for K5), show the values of the structural responses considered among the optimization criteria: deflection, stress in shell and bar elements, and fundamental buckling mode with its BLF. Observing the numerical values, it is confirmed that all the constraints are satisfied in the final design (feasible solution), and it is also noted that all the constraints are active at the optimum point. Consequently, they are well formulated and all play an active role in determining the optimal sizes.

3.6.1 Results for concept k3

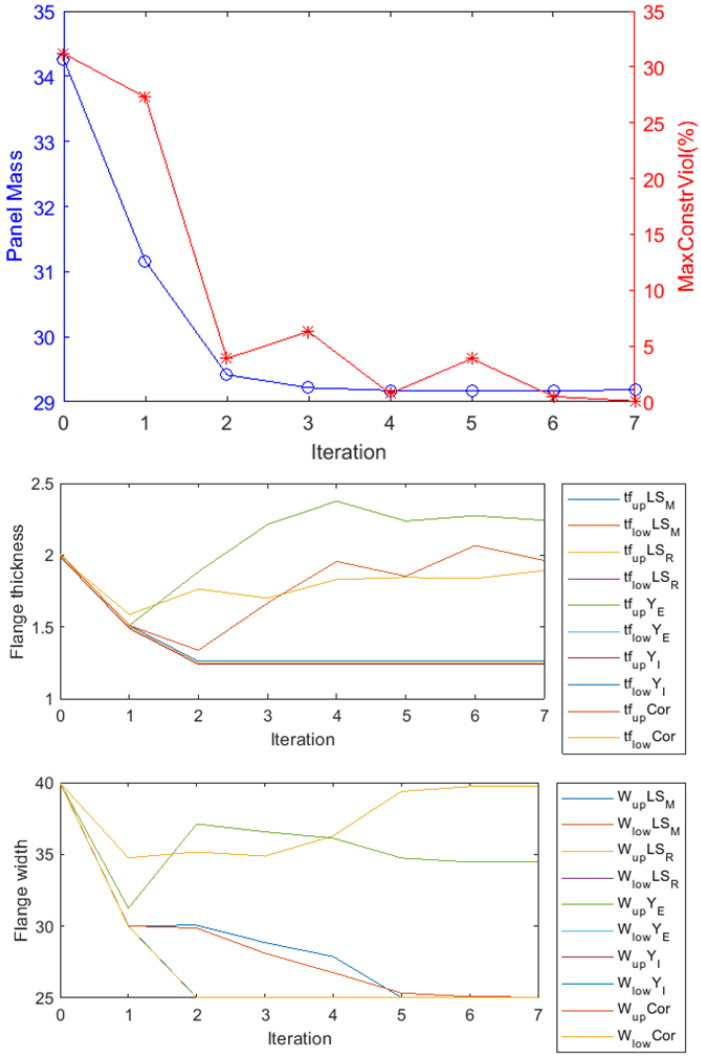

Figure 3.19 Optimization history and evolution of flanges design variables

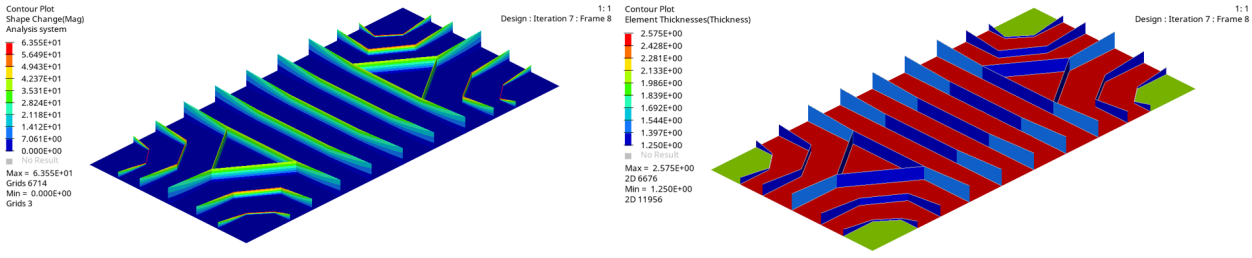

Figure 3.20 Optimal thickness and height distribution (variation w.r.t to baseline 125mm)

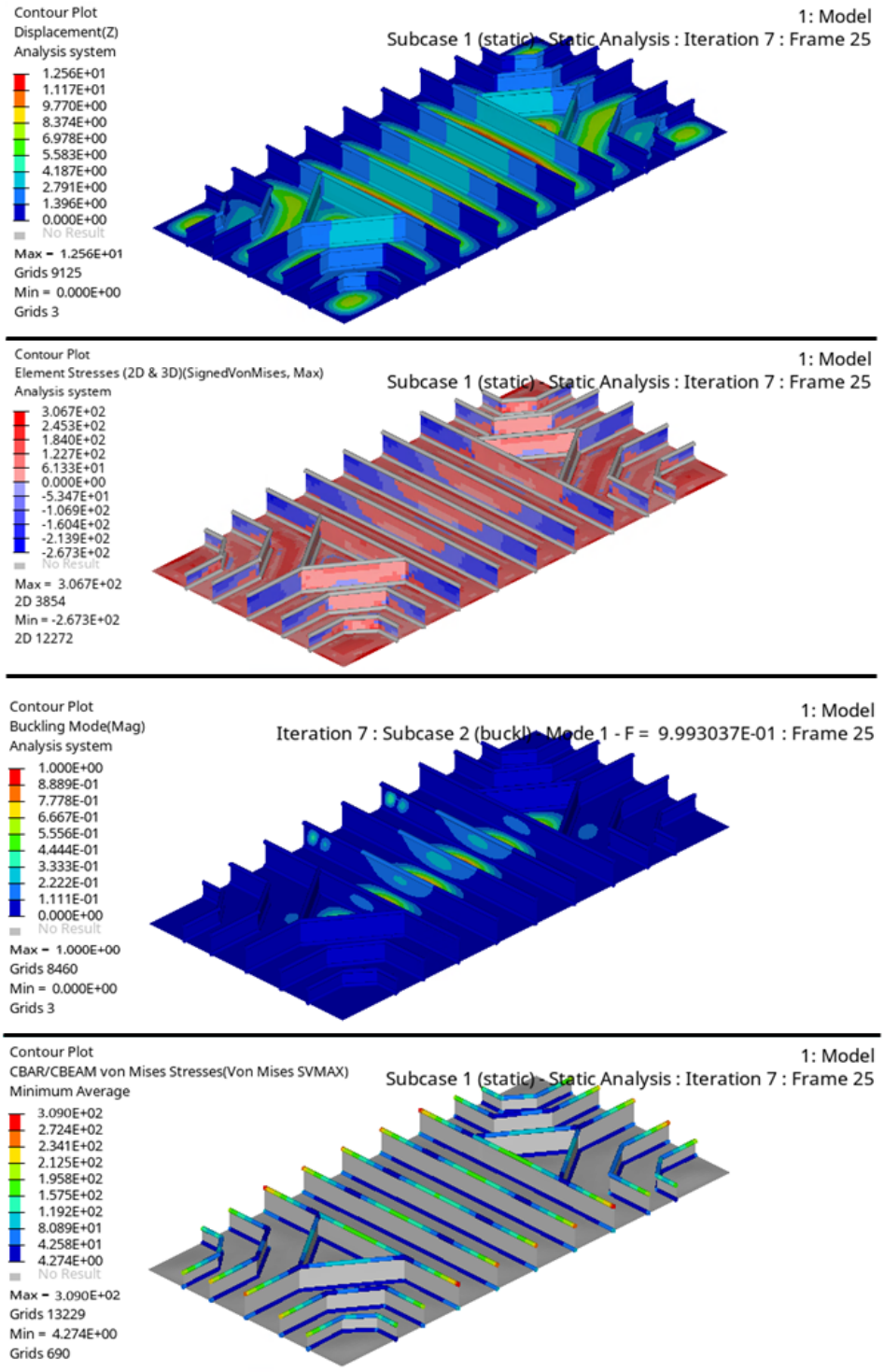

Figure 3.21 Linear static and Linear Buckling Analysis of the optimal design - The results show that all constraints (buckling, stress, and deflection) are active at the optimal design

3.6.2 Results for concept k5

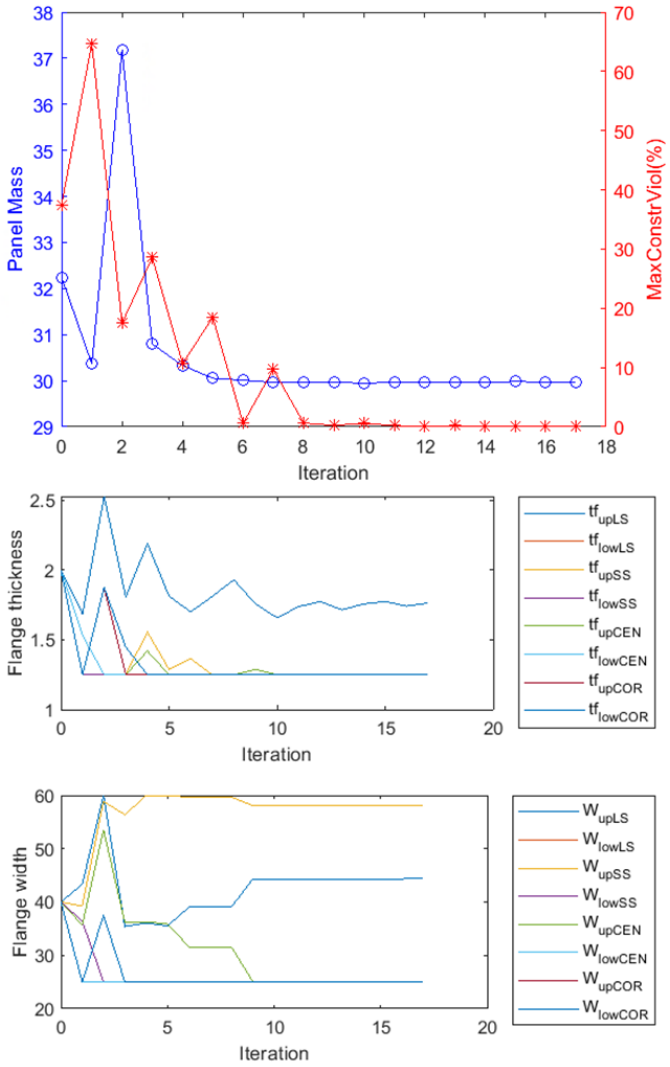

Figure 3.22 Optimization history and evolution of flanges design variables

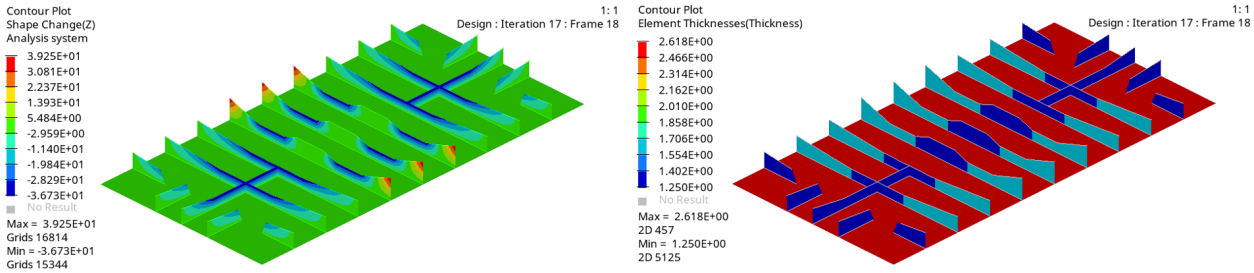

Figure 3.23 Final thickness and height distribution (variation w.r.t to baseline 125mm)

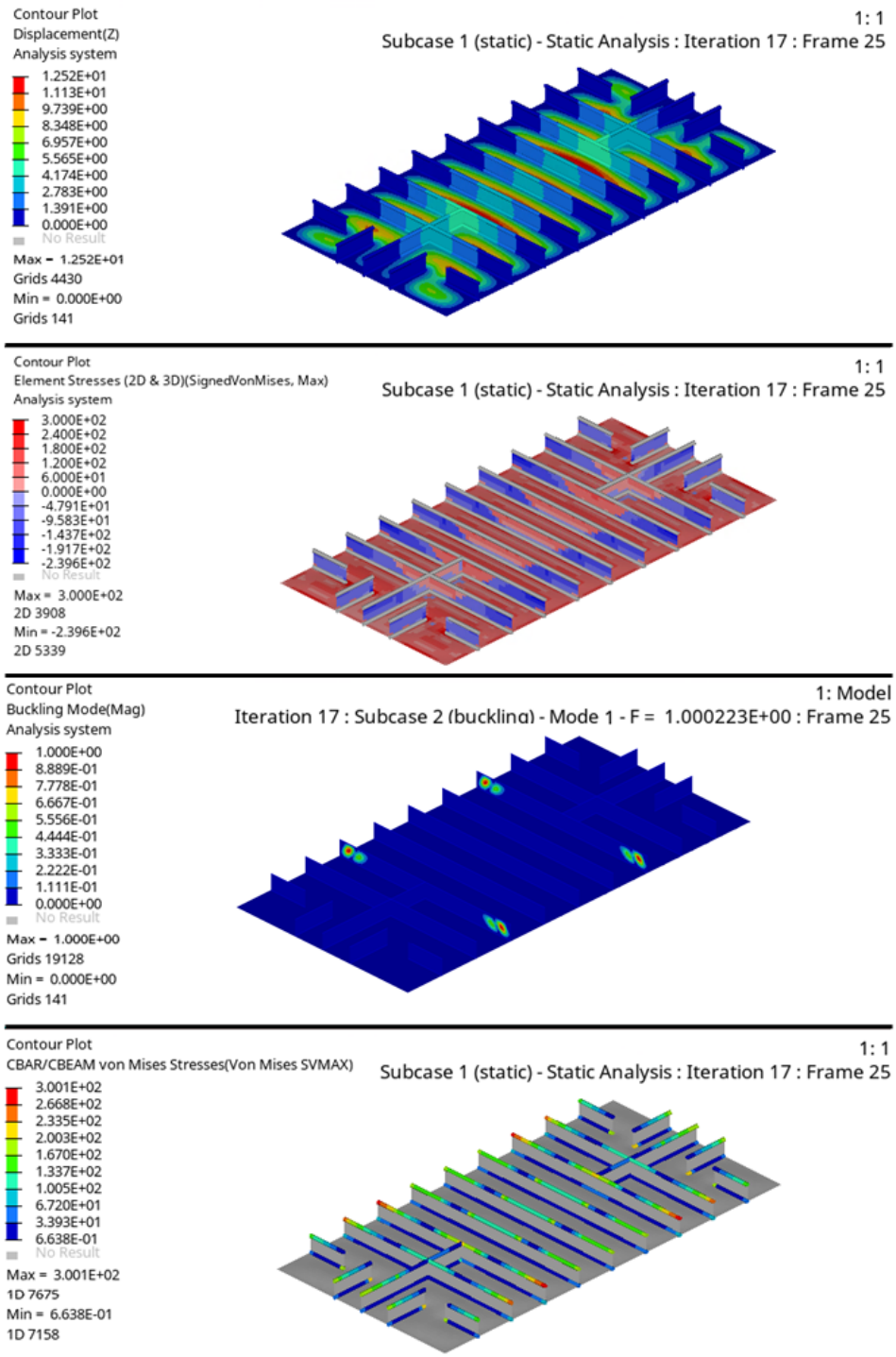

Figure 3.24 Linear static and Linear Buckling Analysis of the optimal design - The results show that all constraints (buckling, stress, and deflection) are active at the optimal design

3.6.3 Discussion on the Optimal Sizing of TO-based Concepts

For a fair comparison, the mass of the TO-based designs is compared with that of the traditional configuration in Tab.3.10, after the latter is also optimized according to the problem 3.16.

Table 3.10 TO-Based concepts VS optimized Baseline stiffened panel

Concept	Optimized-Baseline	Optimized-k3	optimized-k5
Mass [Kg]	29.7	29.2	30.1

A marginal gain of the $1,7\%$ is reached by the k3 configuration. However, it is worth noting the increase in complexity brought by this design:
- Stiffeners with variable height axis-wise;
- 5 different groups of stiffeners: the k3 design has 32 independent design variables for the stiffeners and 3 (thicknesses) for the skin. In contrast, the traditional design considered a skin with constant thickness and only 5 design variables for all equals stiffeners.

The result is on the one hand disappointing due to the poor weight gain in the face of a much more complex design, but on the other hand, the procedure has proven applicable to generic piece-linear reinforcement layouts.
The interpretation effort to go from the GS-model to the final sizing model is minimal, thanks to the explicit information available on the ends coordinates of each stiffener axis. This possibility of generalization is a potential strength point for the TO-based design process, which could have more important weight gains for more complicated geometries, where the simplicity of traditional design could be less efficient.

Finally, it is important to discuss why the k5 concept showed a poor final result, when it was the stiffest concept in the GSM model. In this concept, only one independent thickness was used for the whole skin. The design suffered from the stiffeners run-outs placed in the corners. Stiffeners interruptions bring high stress concentrations because of the discontinuity in the stiffness of the model. The skin remain thick and prevents the mass to lower below the baseline threshold.

3.7 Conclusions on the GSM for Pressurized Stiffened Panel Design

In this chapter, a new methodology based on the Ground Structure TO has been developed for the design of pressurized stiffened panels.
The basic idea of the approach is to create the design space for reinforcing the plate mesh by overlaying a dense network of beam elements over the entire panel surface. The TO reveals which elements are most important in the initial set of candidates by optimizing the cross-sectional area of each beam and removing from the final design the elements that have been thinned below a certain threshold. In the cases studied, the layout optimization criterion was that of maximum structural stiffness (minimum compliance) with a constraint on the maximum stiffeners volume.
The minimum compliance problem can be effectively applied in the layout design of pressurized panels, since in this case the main function of the stiffeners is to provide the transverse support that minimizes skin deformation. Through a comparison with other TO methods, it was shown that the GSM is advantageous in terms of computational cost of the analysis model, since it can represent stiffeners layout with a great geometrical freedom even with coarse meshes. Furthermore, the ease of extracting the optimal layout was increased compared to the SIMP method, since the geometry is explicitly described by the coordinates of the end points of each beam element.
From this information, panel models in which the stiffener geometry is represented with higher fidelity are automatically reconstructed. With the extracted models, the design procedure can then be concluded by minimizing the panel mass while meeting the design requirements (maximum stress, minimum critical buckling load and maximum deformation).

The procedure has been shown to achieve mass gains, even if small, compared to conventional layouts for a rectangular bulkhead design example. However, for more complex geometries and non-uniform loads, straight and evenly spaced stiffener configurations would be less competitive and TO-based layouts may show greater advantages.
The lack of consideration of stress concentrations appears to be the main weakness of the formulation for minimum compliance. This is because thin joints and interruptions in the stiffeners layout are advantageous in term of global compliance, but are ineffective in the final sizing when considering stress requirements.

The method can be extended to any panel geometry and general loads. This flexibility is demonstrated by an example in Appendix C, in which the conceptual design of an airfoil rib is carried out. However, to complete this extension, it is necessary to incorporate stress and buckling criteria into the layout optimization. The latter is not negligible, especially in the optimal placement of stiffeners for in-plane loaded panels.

3.8 Limits of the GSM for In-Plane Loaded Panels and the Transition to the MMC Method

In the case of transverse loads, the reinforcement's main function is to minimize skin deflection by increasing the bending stiffness of the assembly. In this case, the minimum compliance problem addresses the main design requirement, and is easily solved by using gradient-based algorithms [8]. However, stiffened panels are also used to carry compressive and shear loads. For in-plane loads, the problem for minimum compliance is not particularly significant, since, in this case, the main function of the stiffeners is to increase the critical buckling load of the thin panels by acting as supports limiting the free length of skin deflection [12].

The use of linearized buckling analysis, discussed in Sect.2.4.1, is the simplest method to estimate the critical buckling load by extracting the first positive eigenvalue (BLF) and including it among the optimization criteria, as an objective function or constraint.
This inclusion makes the optimization problem nonconvex, i.e., it has multiple local minima. Gradient-based algorithms converge to the local minimum closest to the initial starting guess [7], and this makes the problem highly dependent on the boundary conditions and the starting point of the optimization.

Moreover, another problem is related to the definition of the design space. In GSM (and SIMP), each design variable can take a continuous set of values between the extremes of the specified range, i.e., between a_{min} and a_{max} (0 and 1 in the case of SIMP). These values are considered as acceptable, but one then tries to penalize their presence in the final design. This because easy-to-interpret designs are those where one can clearly identify the elements to be removed and those to be kept.
Penalty strategies for buckling-based optimization are still being researched [73], and an efficient one has not been identified for the present work. Designs with numerous beam elements having intermediate values of cross sectional area tend to appear as results of TO with buckling criteria and can be highly complex to interpret and produce (see Fig.3.25).

In conclusion, in the GSM method, it is difficult to guarantee a priory that the TO results meet the following acceptability requirements:
1. The optimal area distribution is entirely clustered around the values of a_{min} and a_{max};
2. The paths of the stiffeners are clearly defined;
3. After the removal step, there are no stiffeners disconnected from the rest of the layout.

For the minimum compliance problem, these requirements are often met, though not imposed, due to the convex nature of the design space. However, for highly nonlinear design spaces, imposing them becomes necessary. Since these requirements, not directly related to the

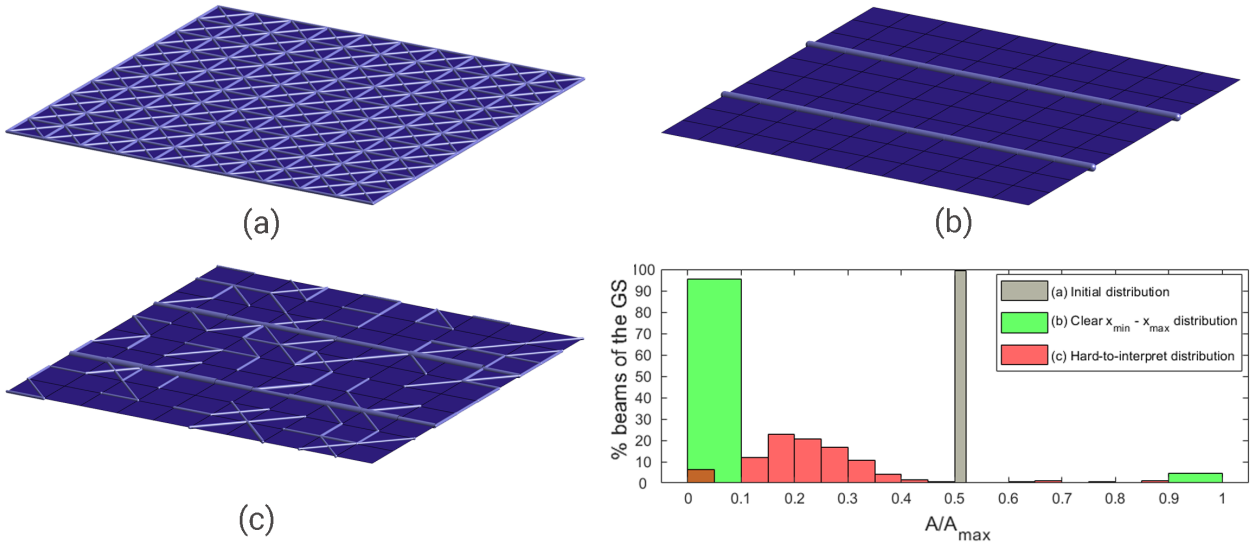

Figure 3.25 Distributions of the design variable within the design space in the GSM - Initial distribution (a), a clearly interpretable a_{min} - a_{max} distribution (b), and a hard-to-interpret distribution (c) with several beams of intermediate area

optimization variables, are difficult to enforce in the GSM method, it was decided to change the strategy and test a formulation that can guarantee them a priory.

From this point on, the focus shifts to the MMC method, identified as a promising alternative for 3 reasons:
(1) it uses geometric parameters as design variables, ensuring the absence of ambiguity in the interpretation;
(2) the shape of the stiffeners can be parameterized with some a priori assumptions, allowing, for example, a definition of the axes and connections between components;
(3) the complexity of the problem can be limited as needed by limiting the number of structural components and/or free parameters.

Reducing the complexity of the design space is considered to be of great value both from the point of view of the designer, who defines the problem, and the computer, which solves it. The designer can define what information to selectively search for and impose requirements from the beginning. While, the use of a small number of variables simplifies the problem from a computational point of view and opens up the possibility of using global optimization algorithms, which are more likely to succeed in non-convex programming problems.

CHAPTER 4 A Moving Morphable Component based Curvilinear Stiffeners Layout Optimization considering Buckling

In this chapter, a new methodology based on the Moving Morphable Component (MMC) approach is proposed for the optimization of the geometrical parameters of curvilinear stiffeners reinforcing a thin sheet.
Each morphable component gives the explicit geometric description of one stiffener through a finite set of parameters. The explicit curves used in the work consider linear, quadratic or Hermite shape functions. The skin and stiffeners are modeled as plates with different stiffness properties, derived locally through an equivalent stiffness method based on the First-order Shear Deformation laminated plate Theory (FSDT).
The stiffeners layout optimization is then formulated as a problem of assigning the equivalent properties to the elements of a fixed plates mesh, using a projection scheme based on a level-set Topology Description Function (TDF).
The stiffeners has a fixed cross section during the layout optimisation and are assumed stiff enough to force the buckling to onset locally on the skin, as done in common aeronautical application. After estimating that the low-fidelity model can approximate the displacement field with error less than 4% and the buckling load factor with error less than 11%, some parametric studies are performed to see if conventional layouts for simple test cases can be identified as optimal layouts.
Finally the model is cast in the Particle Swarm Optimization framework to solve the fundamental Buckling Load Factor (BLF) global maximization problem. Some practical examples are shown to demonstrate the potential of the procedure in the design of wing skin panels.

4.1 New Design Tools for the New Philosophy of Unitized Structures

Classical configurations employ straight stiffening members riveted to thin panels, as this solution facilitates the fabrication and design process [12].
The individual components are manufactured separately and then assembled by riveting. As for sizing, a wide range of experimental data collected in hand-books provide semi-analytical formulas that are easily implemented in digital spreadsheets [12, 64].
In this context, the "layout" of the reinforcement is assumed a priory and described by one parameter: the number of parallel stiffeners. A requirement on stringers minimum bending stiffness is obtained to promote local instability appearing first on the portion of the skin between them [74]. Then the cross sectional dimensions of the stiffeners are sized to

sustain additional loading after the skin buckling onset, according to Euler-Johnson failure prediction [12,64]. Since skin and sections size variables are coupled in ensuring stability and strength requirements, the sizing is usually done in an iterative procedure where the current estimation is improved until all the requirements are satisfied.

However, new manufacturing techniques suitable for aluminum and titanium alloys, including Friction Stir Welding (FSW) [75] and Electron Beam Free Form Fabrication (EBF3) [76], challenge classical configurations reducing material waste and weight associated to the riveted joints. A new philosophy of "unitized structures" is sought, i.e. monolithic reinforced panels where reinforcements and skin are physically integrated [77]. As manufacturing limitations are loosening, new optimization methodologies for the design of unitized stiffened panels with curvilinear stiffeners become possible [40, 78].

In order to fill this gap with the tools of topology optimization, it is necessary to:
(1) balance computational cost and representation fidelity of the finite element analysis;
(2) use global optimization techniques to navigate the design space being highly non-linear due to the presence of a buckling criteria.

The simplification of the finite element model can be achieved by approximating the stiffened panel with a clear plate that uses equivalent stiffness properties to incorporate the reinforcement [79–82]. The reduction in the number of design variables, necessary for global optimization techniques, can be done without losing freedom of representation through the use of morphable components with curvilinear paths [35].

The major foreseen strength of the unitized panels is that there is no restriction on the reinforcement layout geometry. Accordingly, this work focuses on the layout optimization phase where this freedom of configuration is leveraged to highlight new design solutions. This phase is then integrated in a sequential design procedure sketched in Fig. 4.1.

The process starts with an initial sizing of a baseline, which can be a panel with straight evenly spaced stiffeners satisfying the design requirements. When estimating baseline dimensions, analytical tools can be used, following conventional design criteria and ensuring that buckling occurs on the skin first [74]. Subsequently, a sequential process to optimize the design focuses firstly on the stiffeners' layout and finally on the cross-sectional sizing. The layout optimization aims at maximizing the skin buckling critical load for a given volume of the reinforcement. At this level, model complexity is kept low to prioritize freedom of exploration over accuracy of the analysis. For this task, an MMC approach using an equivalent plate model was selected in this work. Finally, when the stiffener arrangement has been determined, a size optimization that aims to minimize the total panel mass while satisfying the stress and stability constraints concludes the design. For this last step, the complete panel geometry is

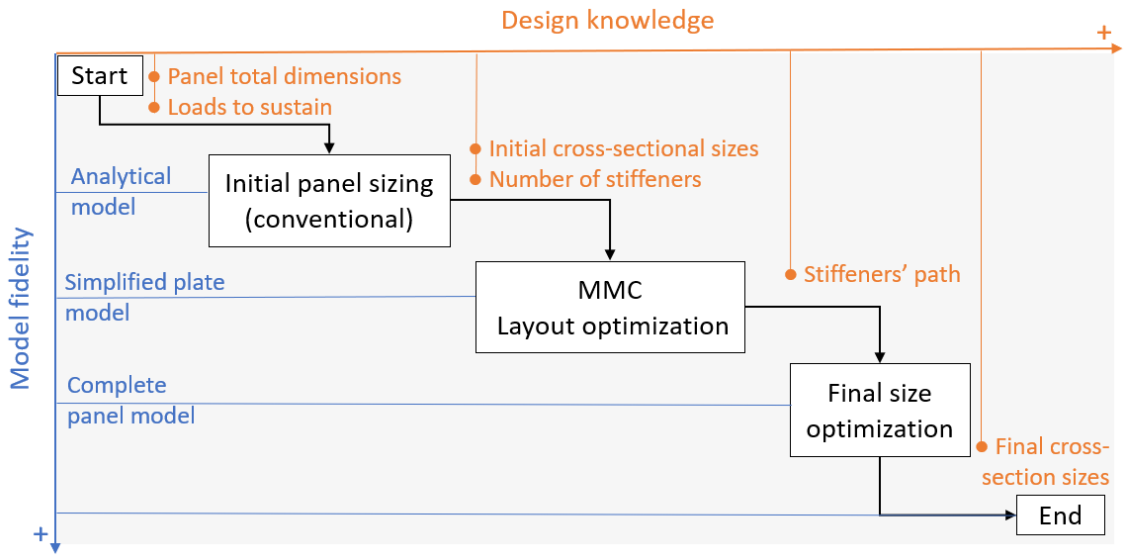

Figure 4.1 A sequential design procedure for unitized panels with curvilinear stiffeners - the complexity of the model increases as more design features are determined. Starting from a traditional layout, a first step aims to improve the skin buckling resistance by optimizing the path of stiffeners. Finally, on a fixed layout, a size optimization determines the final design.

modeled to obtain more accurate structural responses.

It should be noted that for metallic panels, the onset of skin buckling may not coincide with panel collapse, as the stiffeners continue to support additional loads [12, 18]. Consequently aircraft regulations allows the onset of panel buckling in metallic panels before limit loads. However, there are some exceptions, such as upper wing panels in commercial aircraft, panels in supersonic vehicles or composite panels [12].

4.2 An MMC approach for Optimizing the Layout of Integral Panels with Curvilinear Stiffeners

In this section an original approach based on the MMC framework is presented as a tool to optimize the stiffeners' paths of compression-shear stiffened panel for the maximum BLF, calculated using the Linear Buckling Analysis.
Two strategies are possible to search for improvement in a baseline design with a fixed number of stiffeners by allowing generic location and curvilinear path for each reinforcement.
By means of parametric studies or global optimization techniques, potential beneficial effects of shape variations and topological changes can be explored.
The rest of the chapter is organised as follows:
(4.2.1) The explicit definition of the TDF which maps the geometry of the reinforcement on

the base plate mesh is explained;
(4.2.2) An equivalent stiffness model in which the sheet-stiffeners panel is replaced by a clear plate with approximate equivalent properties is proposed;
(4.2.3) The finite element formulation for linear static and buckling analysis are reported;
(4.2.4) The use of the model to perform parametric studies is discussed, as a practical way to evaluate the effects on few meaningful parameters of interest on the structural responses;
(4.2.5) A Particle Swarm Optimization (PSO) for BLF maximization with an upper volume constraint is formulated within the current framework.
(4.3) The Matlab implementation is discussed and the flowchart of the code reported in the Appendix E is briefly explained.
(4.4) Some numerical examples of parametric studies and layout optimization for representative panel portions of an upper skin wing-box are carried out, demonstrating that this design procedure for unitized panels can reduce the mass of structural components in practical applications.
(4.5) A conclusion summarizing the novel aspects of this work and the lesson learned ends this chapter.

4.2.1 Explicit Parametrization and Projection of Curvilinear Stiffeners on a Fixed Plate Mesh

The Moving Morphable components approach proposed by Guo et al. [26], is adopted here to control explicitly the shape of the stiffeners reinforcing the thin sheet.
The explicit topology description function for curvilinear components [35] is adapted to one component-stiffeners placed on flat panels. The components have a constant width w_i and a polynomial mid-curve $y_i = f(x')$, with $x' \in [0, L_i]$ being the first axis of the local ith-stiffener system of coordinates (see Fig.4.2).
Each stiffener composing the layout is then represented by the component's TDF $\Phi_i(x, y)$, described by the component design vector D_i and expressed in the stiffener's coordinates (x', y') as:

$$\begin{aligned} &\Phi_i = min(\Phi_i^{(1)}(x', y', D_i), \Phi_i^{(2)}(x', y', D_i)) \\ &where: \\ &\Phi_i^{(1)} = (w_i/2)^2 - (y_i' - f(x'))^2 \\ &\Phi_i^{(2)} = x'(L_i - x')^2 \end{aligned} \tag{4.1}$$

$\Phi_i^{(1)}$ and $\Phi_i^{(2)}$ can be evaluated on the global coordinate system by means of the following coordinate transformation:

$$\begin{Bmatrix} x' \\ y' \end{Bmatrix} = \begin{bmatrix} \cos(\theta_i) & \sin(\theta_i) \\ -\sin(\theta_i) & \cos(\theta_i) \end{bmatrix} \begin{Bmatrix} x - x_{0i} \\ y - y_{0i} \end{Bmatrix} \tag{4.2}$$

where (x_{0i},y_{0i}) is the origin of the component local system and θ_i is the angle between the global x and local x' axes. In this way, the component design vector reads:

$$D_i = \{x_{0i}, y_{0i}, \theta_i, L_i, \{c_{ik}\}^T\}^T \tag{4.3}$$

Where the coefficients c_{ik} $(k = 1 \ldots n+1)$ characterize the polynomial shape $f(x')$.

Table 4.1 describes the shapes used in this in work, which are also depicted in Fig.4.2. The local stiffener's system is centered in its starting point. The terms and x_{0i}, y_{0i} and θ_i provide global translation and inclination with respect to the panel's system. Then depending on the shape function f considered, the end points coordinates and slopes can be controlled. Each component's TDF $\Phi_i(x, y)$ defines the region occupied by the ith-stiffener according to the following rule:

$$\Phi_i(x,y) \begin{cases} \geq 0, & if\ (x,y) \in ith - stiffener\ interior \\ = 0, & if\ (x,y) \in ith - stiffener\ boundary \\ < 0, & otherwise \end{cases} \tag{4.4}$$

If N stiffeners are placed on the panel, then the union of the reinforcement regions is straightforward to obtain by means of the following operation:

$$\Phi(x,y) = \max(\Phi_1, ..., \Phi_i, ..., \Phi_N) \tag{4.5}$$

where $\Phi(x, y)$ is the total TDF whose 0-level contour identifies all the stiffeners boundaries.

Finally, to complete the projection on a fixed mesh of finite elements discretizing the domain, the numerical relaxed Heaviside function is introduced to map the whole region where integral stiffeners are added to the base skin:

$$H(x,y) = \frac{1}{2}(1 + tanh(\beta\ \Phi(x,y))) \tag{4.6}$$

with $\beta \in [1, \infty)$. This function equals the unit value where the total TDF is positive and the zero value where the total TDF is negative.

Table 4.1 Polynomial curves for skeleton description

Order	Polynomial function	Coefficients
1st	$f^I(x') = \frac{h^I}{L}x'$	$\{c_{ik}\} = \{h^I\}$
2nd	$f^{II}(x') = 4\frac{h^{II}}{L}(x' - \frac{x'^2}{L})$	$\{c_{ik}\} = \{h^{II}\}$
3rd	$f^{III}(x') = \frac{h^{III}}{L^2}(-2x'^3 + 3Lx'^2)$	$\{c_{ik}\} = \{h^{III}\}$
Hermite (3*rd*)	$H(x') = \{1 \quad x' \quad x'^2 \quad x'^3\} \begin{bmatrix} 1 & 0 & 0 & 0 \\ 0 & 0 & 1 & 0 \\ -\frac{3}{L^2} & \frac{3}{L^2} & -\frac{2}{L} & -\frac{1}{L} \\ \frac{2}{L^3} & -\frac{2}{L^3} & \frac{1}{L^2} & -\frac{1}{L} \end{bmatrix} \begin{Bmatrix} y'_0 \\ \theta'_0 \\ y'_1 \\ \theta'_1 \end{Bmatrix}$	$\{c_{ik}\} = \begin{Bmatrix} y'_0 \\ \theta'_0 \\ y'_1 \\ \theta'_1 \end{Bmatrix}$

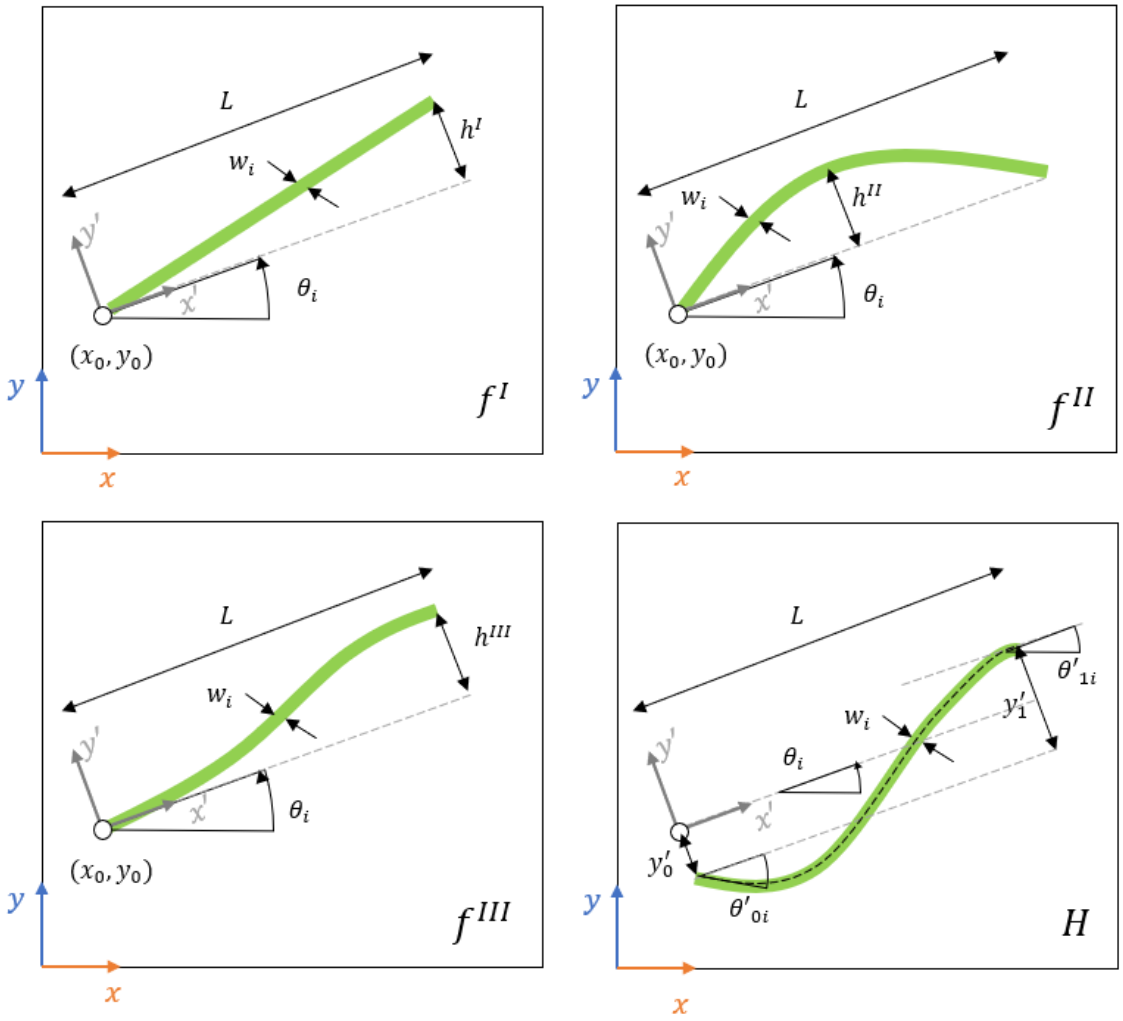

Figure 4.2 Polynomial curves for path description - definition of coefficients in Tab.4.1

As an example, the projection of 2 stiffeners on a rectangular panel, with a mesh 100x100 is depicted in Fig.4.3, where the related shape parameters of each component are reported:

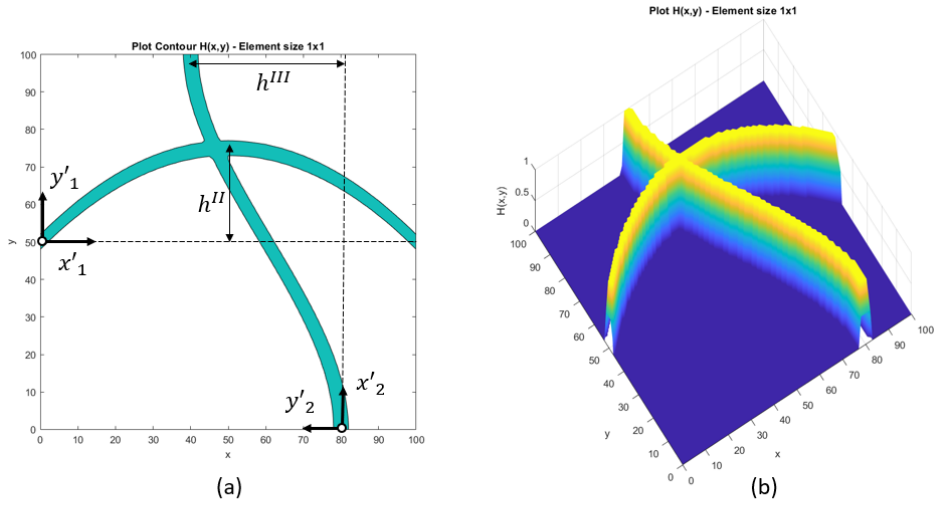

(c) Design vectors for the 2 stiffeners					
$\boldsymbol{D_1}$	$x_{01} = 0$	$y_{01} = 50$	$\theta_1 = 0°$	$L_1 = 100$	$h_1^{II} = 25$
$\boldsymbol{D_2}$	$x_{02} = 80$	$y_{02} = 0$	$\theta_2 = 90°$	$L_2 = 100$	$h_2^{III} = 40$

Figure 4.3 Example of the projection scheme on a square panel with two stiffeners
(a) The interior of the reinforcement region. (b) Plot of H(x,y) over the domain. (c) The coefficients composing the component design vectors D_i

4.2.2 Basic Idea of the 2-layer Laminate Plate model with Equivalent stiffness properties for metallic panel with integral reinforcement

Here an equivalent stiffness model in which the stiffened panel is reduced to a clear panel with two approximate equivalent properties is proposed.
Introducing such a model aims at reducing the complexity of finite element model and allow to perform parametric studies or optimization of the stiffeners layout on a fixed mesh.

Equivalent stiffness methods for composite and metallic stiffened panels have been studied to develop low-fidelity model for reasonable accuracy and high computing speed in the context of flutter-analysis for wing-box structure [82], dynamic response of plate [80] and buckling resistance estimation of grid stiffened plates [81]. The general idea of these method is to determine the extensional, coupling and bending matrices associated with the stiffeners with respect to plate's mid-plane strains and curvatures of the skin.
In this way, stiffener's force and moment contributions can be superimposed directly with

those of of the base plate, obtaining the the equivalent stiffness matrices of the whole panel.

The idea of using equivalent stiffness methods to formulate a 2-material TO is proposed in the work of Sun [48], for the minimum compliance design of composite stiffened panel modeled with the Classical Laminate Plate theory (CLPT). In this work the effect of transverse shear is also considered, by assuming the First order Shear Deformation Theory (FSDT) for Laminated Plates [83]. The load-deformation relation in the matrix form reads:

$$\begin{Bmatrix} \boldsymbol{N} \\ \boldsymbol{M} \\ \boldsymbol{Q} \end{Bmatrix} = \begin{bmatrix} \boldsymbol{A}_{eq} & \boldsymbol{B}_{eq} & \boldsymbol{0}_{3\times 2} \\ \boldsymbol{B}_{eq} & \boldsymbol{D}_{eq} & \boldsymbol{0}_{3\times 2} \\ \boldsymbol{0}_{2\times 3} & \boldsymbol{0}_{2\times 3} & \boldsymbol{A}_{eq}^{(s)} \end{bmatrix} \begin{Bmatrix} \boldsymbol{\epsilon} \\ \boldsymbol{k} \\ \boldsymbol{\gamma} \end{Bmatrix} \tag{4.7}$$

Where the in-plane strain $\boldsymbol{\epsilon}$, curvature $\boldsymbol{k}$ and transversal shear strain $\boldsymbol{\gamma}$ vectors are linked to the internal membrane forces $\boldsymbol{N}$, moments $\boldsymbol{M}$ and transverse shear forces $\boldsymbol{Q}$ vectors by means of the equivalent tensile $\boldsymbol{A}_{eq}$, coupling $\boldsymbol{B}_{eq}$, bending $\boldsymbol{D}_{eq}$ and shear $\boldsymbol{A}_{eq}^{(s)}$ stiffness matrices. These matrices depend on the spatial coordinates through the total TDF, and they are defined by the following interpolation scheme:

$$\begin{cases} [\boldsymbol{A}_{eq}] = [\boldsymbol{A}]^{(1)} + H(\Phi(x,y))[\boldsymbol{A}]^{(2)} \\ [\boldsymbol{B}_{eq}] = [\boldsymbol{B}]^{(1)} + H(\Phi(x,y))[\boldsymbol{B}]^{(2)} \\ [\boldsymbol{D}_{eq}] = [\boldsymbol{D}]^{(1)} + H(\Phi(x,y))[\boldsymbol{D}]^{(2)} \\ [\boldsymbol{A}_{eq}^{(s)}] = [\boldsymbol{A}^{(s)}]^{(1)} + H(\Phi(x,y))[\boldsymbol{A}^{(s)}]^{(2)} \end{cases} . \tag{4.8}$$

Superscript (1) and (2) refer to the matrices characterizing the "skin" lamina and the super-imposed integral "stiffeners lamina" respectively, as depicted in Fig.4.4.

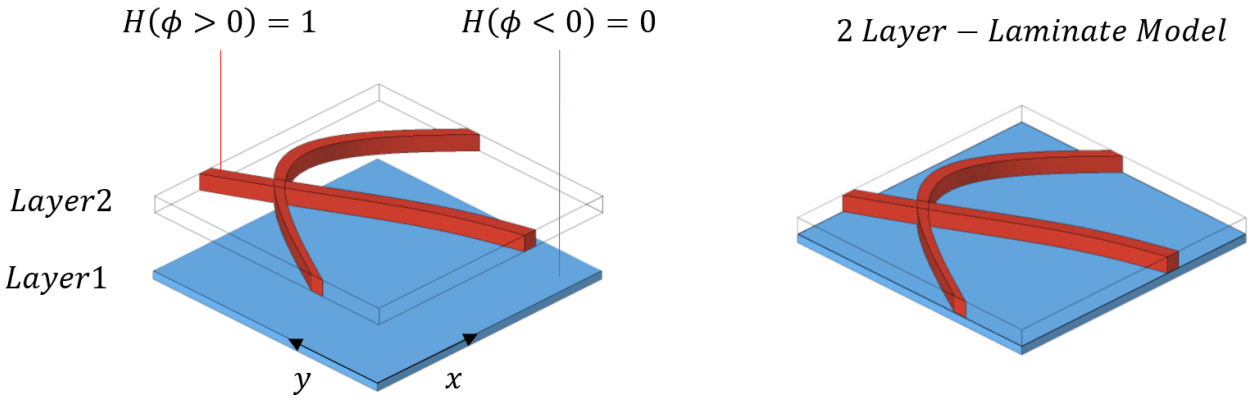

Figure 4.4 The 2-Layer Model with Equivalent Stiffness Properties

Models with arbitrary integral stiffeners layout are approximated as a laminate whose mechanical properties depends on the total TDF $\Phi(x, y)$.
According to the FSDPT the state of tension inside each lamina can be described as a plane-stress state with the addition of the transverse shear stresses (only $\sigma_{zz} = 0$) [83]. In case of metallic material, the linear constitutive relations are expressed for an isotropic homogeneous lamina as:

$$\{\boldsymbol{\sigma}\} = [\boldsymbol{Q}]\{\boldsymbol{\epsilon}\} = \begin{Bmatrix} \sigma_{xx} \\ \sigma_{yy} \\ \tau_{xy} \end{Bmatrix} = \frac{E}{1-\nu^2} \begin{bmatrix} 1 & \nu & 0 \\ \nu & 1 & 0 \\ 0 & 0 & \frac{1-\nu}{2} \end{bmatrix} \begin{Bmatrix} \epsilon_{xx} \\ \epsilon_{yy} \\ \gamma_{xy} \end{Bmatrix} \tag{4.9}$$

$$\{\boldsymbol{\tau}_z\} = [\boldsymbol{Q}_s]\{\boldsymbol{\gamma}_z\} = \begin{Bmatrix} \tau_{zx} \\ \tau_{zy} \end{Bmatrix} = G \begin{bmatrix} 1 & 0 \\ 0 & 1 \end{bmatrix} \begin{Bmatrix} \gamma_{zx} \\ \gamma_{zy} \end{Bmatrix} \tag{4.10}$$

Because of the use of the Heaviside projections, here the hypothesis of homogeneity assumed is not maintained in the stringers layer. Therefore, stress recovery is performed only in the skin layer. In particular, membrane stresses evaluated at the skin middle plane are needed to evaluate skin buckling. The calculation of the stiffness matrices is characterized for each layer starting from the relations for a generic isotropic lamina:

$$\begin{cases} [\boldsymbol{A}]^{(k)} = [\boldsymbol{Q}]^{(k)}(z_k - z_{k-1}) \\ [\boldsymbol{B}]^{(k)} = \frac{1}{2}[\boldsymbol{Q}]^{(k)}(z_k^2 - z_{k-1}^2) \\ [\boldsymbol{D}]^{(k)} = \frac{1}{3}[\boldsymbol{Q}]^{(k)}(z_k^3 - z_{k-1}^3) \\ [\boldsymbol{A}^{(s)}]^{(k)} = K_s[\boldsymbol{Q}_s]^k(z_k - z_{k-1}) \end{cases} . \tag{4.11}$$

Where K_s is the shear factor, introduced to correct the energetic contribution from the shear strains assumed constant along the thickness. The z-coordinates are normal to the panel plane, as in Fig. 4.5.

By these assumptions, contribution (1) and (2) to the equivalent stiffness properties are explicitly calculated:

$$\begin{cases} [\boldsymbol{A}]^{(1)} = t_s[\boldsymbol{Q}] \\ [\boldsymbol{B}]^{(1)} = [\boldsymbol{0}]_{3x3} \\ [\boldsymbol{D}]^{(1)} = \frac{t_s^3}{12}[\boldsymbol{Q}] \\ [\boldsymbol{A}^{(s)}]^{(1)} = K_s t_s[\boldsymbol{Q}_s] \end{cases} . \begin{cases} [\boldsymbol{A}]^{(2)} = h_r[\boldsymbol{Q}] \\ [\boldsymbol{B}]^{(2)} = e h_r[\boldsymbol{Q}] \\ [\boldsymbol{D}]^{(2)} = \frac{1}{3}\Big((e + h/2)^3 - (e - h/2)^3\Big)[\boldsymbol{Q}] \\ [\boldsymbol{A}^{(s)}]^{(2)} = K_s h_r[\boldsymbol{Q}_s] \end{cases} . \tag{4.12}$$

Where e is the stiffener eccentricity, t_s the skin thickness and h_r the height of the blade integral stiffener.

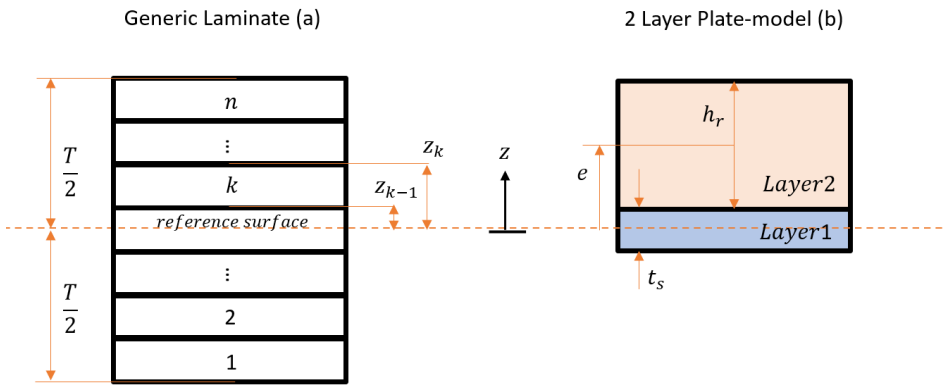

Figure 4.5 2-Layer Laminate model

In common applications $e = t_s/2 + h_r/2$, and for metallic rectangular section the shear factor is $K_s = 5/6$. Calculation of the shear factor for general laminate can be found in [83].

It is worth noting the effect of eccentricity on the membrane-bending coupling, expressed in the resultant matrix $[\boldsymbol{B}eq]$. Here the eccentricity is defined as the distance of the centroid of the rectangular blade stiffeners from the plate midplane. This effect plays a beneficial role for rectilinear and parallel stiffeners, because it augments the section's second moment of area, meanwhile it may or may not augment stability in case of curvilinear stiffeners, depending on the level of the coupling.

4.2.3 Finite Elements Formulation of Static and Linear Buckling Analysis

Since the model is reduced to an equivalent plate, the kinematics of the FSDT follows the Mindlin-Reissner assumptions [83]. The physical meaning of the displacement parameters $\{\mathbf{d}\} = \{u^0, v^0, w^0, \theta_x, \theta_y\}^T$, which are the unknowns to be determined in the FE problem, is explained in Fig.4.6.

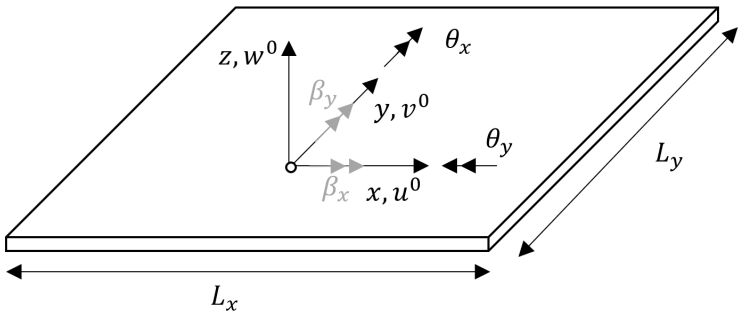

Figure 4.6 Definition of global coordinate system and plate displacement field in the FSDT

The form of the displacement field in each point of the plate is:

$$\{\boldsymbol{d}_p\} = \begin{Bmatrix} u(x,y,z) \\ v(x,y,z) \\ w(x,y,z) \end{Bmatrix} = \begin{Bmatrix} u^0(x,y) \\ v^0(x,y) \\ w^0(x,y) \end{Bmatrix} + z \begin{bmatrix} 1 & 0 \\ 0 & 1 \\ 0 & 0 \end{bmatrix} \begin{Bmatrix} \theta_x(x,y) \\ \theta_y(x,y) \end{Bmatrix} \tag{4.13}$$

where u^0, v^0, w^0 denote displacements of a point on the plane $z = 0$, and it should be remarked that if (β_x, β_y) denote the physical rotation about x and y axis, following the hand rule, then:

$$\theta_x = -\beta_y \ , \ \theta_y = \beta_x. \tag{4.14}$$

This notation, taken from [83], may be confusing to some but it is extensively used in literature, because:
(1) it binds the displacements along x and y axes (i.e. u and v) to the parameters with subscripts x and y respectively (as $\frac{\partial u}{\partial z} = \theta_x$ and $\frac{\partial v}{\partial z} = \theta_y$);
(2) leads to include all parameters as a contribution with a positive sign ("+") in the displacement relations of Eq.4.13.

The strain components, used in Eq.4.7, which depend linearly on the thickness coordinate, are described as follows:

$$\{\boldsymbol{\epsilon}\} = \{\boldsymbol{\epsilon}^0\} + z\{\boldsymbol{k}\} = \begin{Bmatrix} \epsilon_{xx} \\ \epsilon_{yy} \\ \gamma_{xy} \end{Bmatrix} = \begin{Bmatrix} \epsilon^0_{xx} \\ \epsilon^0_{yy} \\ \gamma^0_{xy} \end{Bmatrix} + z \begin{Bmatrix} k_{xx} \\ k_{yy} \\ k_{xy} \end{Bmatrix} = \begin{Bmatrix} \frac{\partial u^0}{\partial x} + \frac{1}{2}\frac{\partial w^0}{\partial x})^2 \\ \frac{\partial v^0}{\partial y} + \frac{1}{2}(\frac{\partial w^0}{\partial y})^2 \\ \frac{\partial u^0}{\partial y} + \frac{\partial v^0}{\partial x} + \frac{\partial w^0}{\partial x}\frac{\partial w^0}{\partial y} \end{Bmatrix} + z \begin{Bmatrix} \frac{\partial \theta_x}{\partial x} \\ \frac{\partial \theta_y}{\partial y} \\ \frac{\partial \theta_x}{\partial y} + \frac{\partial \theta_y}{\partial x} \end{Bmatrix}$$

$$\{\boldsymbol{\gamma}\} = \begin{Bmatrix} \gamma_{xz} \\ \gamma_{yz} \end{Bmatrix} = \begin{Bmatrix} \frac{\partial w^0}{\partial x} + \theta_x \\ \frac{\partial w^0}{\partial y} + \theta_y \end{Bmatrix} \tag{4.15}$$

At this point the displacement field can be interpolated using iso-parametric finite element formulation. Here the bi-linear Q4 plates elements are considered: see [67] for the definition of the shape functions N_i. The displacement parameters in the interior of each element are independently interpolated from degrees of freedom assigned to elements nodal points:

$$\{\mathbf{d}\} = \left[\mathbf{N}\right] \{\mathbf{u}^{(e)}\} \tag{4.16}$$

where $[N]_{[5x20]}$ collects the shape functions and $\mathbf{u}^{(e)}$ collects the elemental nodal DOFs $u^{(e)}_{ni}$ in the following way:

$$\begin{aligned} \mathbf{u}^{(e)} &= \{\mathbf{u}^{(e)}_{n1}, \mathbf{u}^{(e)}_{n2}, \mathbf{u}^{(e)}_{n3}, \mathbf{u}^{(e)}_{n4}\}^T \\ \mathbf{u}^{(e)}_{ni} &= \{u_i, v_i, w_i, \theta_{xi}, \theta_{yi}\}^T \end{aligned} \tag{4.17}$$

The elemental strain-displacement matrices $\boldsymbol{B}_m, \boldsymbol{B}_b$ and $\boldsymbol{B}_s$ are derived by including the finite element approximation in (4.15), which reads in matrix form:

$$\begin{aligned} \{\boldsymbol{\epsilon}\} &= \begin{bmatrix} \frac{\partial}{\partial x} & 0 & 0 & 0 & 0 \\ 0 & \frac{\partial}{\partial y} & 0 & 0 & 0 \\ \frac{\partial}{\partial y} & \frac{\partial}{\partial x} & 0 & 0 & 0 \end{bmatrix} \mathbf{d} = [\mathbf{D}_m]\mathbf{d} = [\mathbf{D}_m\mathbf{N}]\mathbf{u}^{(e)} = [\mathbf{B}^{(e)}_m]\mathbf{u}^{(e)} \\ \{\boldsymbol{k}\} &= \begin{bmatrix} 0 & 0 & 0 & \frac{\partial}{\partial x} & 0 \\ 0 & 0 & 0 & 0 & \frac{\partial}{\partial y} \\ 0 & 0 & 0 & \frac{\partial}{\partial y} & \frac{\partial}{\partial x} \end{bmatrix} \mathbf{d} = [\mathbf{D}_b]\mathbf{d} = [\mathbf{D}_b\mathbf{N}]\mathbf{u}^{(e)} = [\mathbf{B}^{(e)}_b]\mathbf{u}^{(e)} \\ \{\boldsymbol{\gamma}\} &= \begin{bmatrix} 0 & 0 & \frac{\partial}{\partial x} & 1 & 0 \\ 0 & 0 & \frac{\partial}{\partial y} & 0 & 1 \end{bmatrix} \mathbf{d} = [\mathbf{D}_s]\mathbf{d} = [\mathbf{D}_s\mathbf{N}]\mathbf{u}^{(e)} = [\mathbf{B}^{(e)}_s]\mathbf{u}^{(e)} \end{aligned} \tag{4.18}$$

The element stiffness matrix is then defined by using the equivalent properties of Eq.(4.8):

$$\begin{aligned}\mathbf{K}_{eq}^{(e)} = \int_{\Omega_e} \Big\{ [\mathbf{B}_m^{(e)}]^T[A_{eq}][\mathbf{B}_m^{(e)}] \ + \ [\mathbf{B}_b^{(e)}]^T[B_{eq}][\mathbf{B}_m^{(e)}] \ + \\ [\mathbf{B}_m^{(e)}]^T[B_{eq}][\mathbf{B}_b^{(e)}] \ + \ [\mathbf{B}_b^{(e)}]^T[D_{eq}][\mathbf{B}_b^{(e)}] \ + \ [\mathbf{B}_s^{(e)}]^T[A_{eq}^{(s)}][\mathbf{B}_s^{(e)}] \Big\} \, d\Omega_e\end{aligned} \tag{4.19}$$

Integrals are computed by Gauss quadrature. The stiffness integral is solved by considering 2×2 Gauss points for the bending contribution, and 1 point for the shear contribution [67].

To carry the element wise integration, it is proposed to obtain constant values for the equivalent stiffness coefficients inside each element by adapting the Ersatz material model [26] to this formulation.
Matrices $[A_{eq}], [B_{eq}], [D_{eq}]$ and $[A_{eq}^{(s)}]$ are expressed for the generic coordinates (x, y) according to the Heaviside projection in Eq.(4.8). The coefficients of the equivalent properties can be evaluated at each nodal point, and then be averaged over each element. For instance, the equivalent tensile stiffness matrix for element (e) is given by:

$$[A_{eq}]^{(e)} = \frac{1}{4}\sum_{i=1}^{4}[A_{eq}(x_i^{(e)}, y_i^{(e)})] \tag{4.20}$$

where $(x_i^{(e)}, y_i^{(e)})$ are the coordinates of ith-node associated to element e.
By considering a regular grid of rectangular elements, the assembled stiffness matrix reads:

$$\mathbf{K} = \sum_{e=1}^{Ne}[\Omega^{(e)}]^T\mathbf{K}_{eq}^{(e)}[\Omega^{(e)}] \tag{4.21}$$

Where $\Omega^{(e)}$ is a symbolic matrix operator which carries out the sorting operation of the generalized displacement vector $\mathbf{u} = \{\mathbf{u}^{(1)}, ..., \mathbf{u}^{(e)}, ..., \mathbf{u}^{(Ne)}\}$, needed to complete the assembly process.

Defining $\mathbf{F}$ as the load vector, the linear static equilibrium equation finally reads:

$$\mathbf{K}\mathbf{u} = \mathbf{f} \tag{4.22}$$

The loss of uniqueness of the reference equilibrium determined by the linear elastic equilibrium, can be predicted by means of the linearized buckling analysis.
Non linear strains are linearized in the vicinity of the elastic equilibrium configuration and their contribution to the total potential energy is considered. Then, by searching for new equilibrium conditions $\mathbf{u} = \mathbf{u}_0 + \boldsymbol{\varphi}$ alternative to the reference one, the following eigen-problem is derived:

$$[\mathbf{K} + \lambda \mathbf{K}_\sigma(\mathbf{u_0})]\boldsymbol{\varphi} = \mathbf{0}, \qquad \boldsymbol{\varphi} \neq \mathbf{0} \tag{4.23}$$

where it is remarked that the stress stiffness matrix $\mathbf{K}_\sigma(\mathbf{u_0})$ depends on the pre-buckling (linear equilibrium) solution through the stresses. This matrix is assembled in the same way as the elastic stiffness matrix, from the elemental $\mathbf{K}_\sigma^{(\mathbf{e})}$, which is defined as follows [15]:

$$K_\sigma^{(e)} = \int_{\Omega_e} [\mathbf{G}]^T [\mathbf{S}^0][\mathbf{G}] d\Omega_e \tag{4.24}$$

where $G_{[10x20]}$ is the deformation gradient having the following structure:

$$\mathbf{G} = \begin{bmatrix} \nabla\mathbf{N} \otimes \begin{bmatrix} 1 & 0 & 0 & 0 & 0 \end{bmatrix} \\ \nabla\mathbf{N} \otimes \begin{bmatrix} 0 & 1 & 0 & 0 & 0 \end{bmatrix} \\ \nabla\mathbf{N} \otimes \begin{bmatrix} 0 & 0 & 1 & 0 & 0 \end{bmatrix} \\ \nabla\mathbf{N} \otimes \begin{bmatrix} 0 & 0 & 0 & 1 & 0 \end{bmatrix} \\ \nabla\mathbf{N} \otimes \begin{bmatrix} 0 & 0 & 0 & 0 & 1 \end{bmatrix} \end{bmatrix} \quad \nabla\mathbf{N} = \begin{bmatrix} N_{1/x} & N_{2/x} & N_{3/x} & N_{4/x} \\ N_{1/y} & N_{2/y} & N_{3/y} & N_{4/y} \end{bmatrix} \tag{4.25}$$

and $\mathbf{S}^0$ is a banded matrix which rearrange the membrane stresses $\sigma_{xx}^0, \sigma_{yy}^0, \tau_{xy}^0$ as follows:

$$\mathbf{S}^0 = \begin{bmatrix} t_s\sigma^0 & 0_{2\times2} & 0_{2\times2} & 0_{2\times2} & 0_{2\times2} \\ 0_{2\times2} & t_s\sigma^0 & 0_{2\times2} & 0_{2\times2} & 0_{2\times2} \\ 0_{2\times2} & 0_{2\times2} & t_s\sigma^0 & 0_{2\times2} & 0_{2\times2} \\ 0_{2\times2} & 0_{2\times2} & 0_{2\times2} & \frac{t_s^3}{12}\sigma^0 & 0_{2\times2} \\ 0_{2\times2} & 0_{2\times2} & 0_{2\times2} & 0_{2\times2} & \frac{t_s^3}{12}\sigma^0 \end{bmatrix} \quad \sigma^{\mathbf{0}} = \begin{bmatrix} \sigma_{xx}^0 & \tau_{xy}^0 \\ \tau_{xy}^0 & \sigma_{yy}^0 \end{bmatrix} \tag{4.26}$$

One notes that membrane stresses are recovered using the isotropic lamina constitutive relations of Eq.(4.9) and considering the strains from Eq.(4.15) evaluated at the reference plane ($z = 0$). With the adopted discretization, the stress is computed in the centroid of each element, which is the stress super-convergent point for Q4 bilinear elements [15].

For a further discussion of the MATLAB implementation of the linear buckling analysis, please refer to the work Ferrari and Sigmund's [84] on the use of vector operations to assemble the matrices $\boldsymbol{K}$ and $\boldsymbol{K}_\sigma$. The exclusive use of vector operations reduces the computational burden of the analysis set-up, due to the elimination of large "for" cycles which are inefficient in terms of execution time and memory allocation. The procedure is used here to accelerate the optimization, and one can refer to appendix F for details on the rules to organize the elemental stress stiffness matrix of a Mindlin Plate in a vector form.

4.2.4 Parametric studies for BLF maximization

Arbitrary changes in the geometry, as well as topology, of the stiffeners layout can be managed by the adopted TDF and the reduced complexity of the model can be exploited in many way.

A first application can be for parametric studies, in which the designer aims at observing the variation of the response of the model for prescribed changes in the stiffeners geometry. In particular, here the focus is on determining how the critical buckling load is affected by the position, the orientation and/or the curvature of the stringers paths.

For the considered panels with integrally curvilinear blade-stiffeners, let the geometry of a panel be described by a set of parameter which can be listed in the following panel design vector $\boldsymbol{D}$.

$$\{\mathbf{D}\} = \{\mathbf{D}_0, \{\mathbf{D}_x\}\} \tag{4.27}$$

where the parameters in $\boldsymbol{D}_0$ are considered frozen, because there is no possibility or no interest in varying its component, while parameters in $\boldsymbol{D}_x$ are considered as variables.

Let a certain range for the values of $\boldsymbol{D}_x$ components be identified for the investigation, and a matrix of sample points with different parameters be defined. Then, by running the predefined set of runs and collecting the corresponding model responses, the trend of the observed value can be identified over the explored interval by fitting the data.

A study of this type can be represented in the block scheme of Fig.4.7:

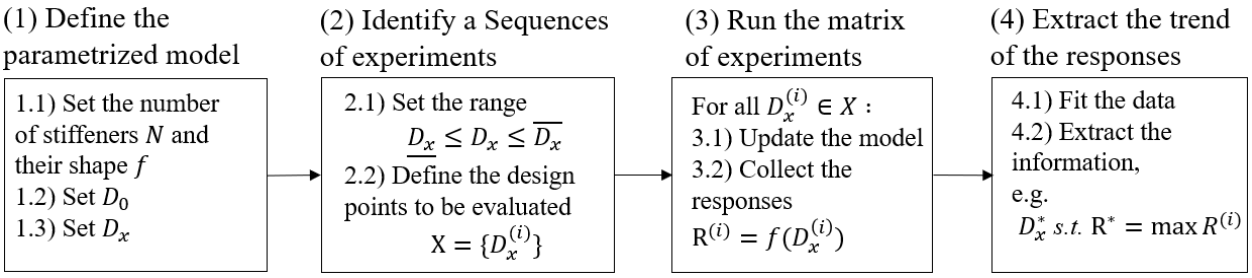

Figure 4.7 Parametric study procedure

4.2.5 Particle Swarm Optimization formulation for BLF maximization

The critical load of the stiffened panel is a function of skin thickness, stiffeners sizes, and stiffeners locations. The latter is the main factor in splitting the skin in more bays hence determining the free length of the skin buckling waves.
To simplify the problem, here it is assumed that stiffeners sizes are frozen while optimizing their locations, because for stiffeners with very high bending stiffness the critical load is mainly driven by skin thickness and bays dimensions [74].
Since the problem has multiple local maximum points, the optimization of the curvilinear stiffeners paths needs for the use of global optimization techniques [40].

Global derivative-free optimization techniques, are computationally expensive if compared to gradient based techniques. However, the adopted model allows maintaining a minimum number of design variables for the optimization problem, which can be run in parallel computing mode to further reduce the computational time. In the following the equivalent panel model is cast in a Particle Swarm Optimization (PSO) [36–38] problem.

Optimization Formulation The optimization goal is to maximize the fundamental BLF of a panel with a given number of stiffeners over a set of parameters which controls the stiffeners positioning and their skeleton. A maximum total volume for the set of stiffeners is imposed. The optimization uses a simplified model and has to be considered a tool for new concepts generation for the stiffening layout, which are subsequently sized for minimum mass and the complete set of design constraints.
The design variables of the problem are the parameters defining the TDF of the model, as described in Sect.4.3.1, when the Hermite shape function is selected to describe each curvilinear stiffener's path.

The mathematical problem can be stated as in Eq.4.28:

$$\begin{aligned} find \quad & \{\boldsymbol{D}_x\} = \{\boldsymbol{D}_{x1}, \boldsymbol{D}_{x2}, ..., \boldsymbol{D}_{xN}\} \\ \min_{D_x} \quad & \mu_1 = \tfrac{1}{\lambda_1} \\ \text{s.t.} \quad & g_1 : V/V_{max} - 1 \leq 0 \\ & g_{01} : \boldsymbol{K}(\boldsymbol{D_x})\boldsymbol{u}(\boldsymbol{D_x}) = \boldsymbol{f} \\ & g_{02} : [\mathbf{K}_\sigma(\boldsymbol{D_x}, \boldsymbol{u}) + \mu\mathbf{K}]\boldsymbol{\varphi} = \mathbf{0} \\ & \underline{\boldsymbol{D_x}} \leq \boldsymbol{D_x} \leq \overline{\boldsymbol{D_x}} \end{aligned} \tag{4.28}$$

Where:

- $\boldsymbol{D}_{xi}$ is a subset of $\boldsymbol{D}_i$ (see Eq.4.3), excluding non-variable parameters $\boldsymbol{D}_{0i}$ (see Eq.4.27);
- λ_1 is the fundamental (minimum positive) eigenvalue identifying the BLF;
- the total volume is calculated as $V = h_r \iint_\Omega H(\Phi(x, y,)) \, dx \, dy$, where Ω is the panel domain.
- g_{0i} are constraints implicitly forced when calculating the objective function;
- $\underline{\boldsymbol{D_x}}$ and $\overline{\boldsymbol{D_x}}$ are respectively the lower and upper bound values for the design variables.

An example of definition of the vector of design variables is reported in Fig.4.8.

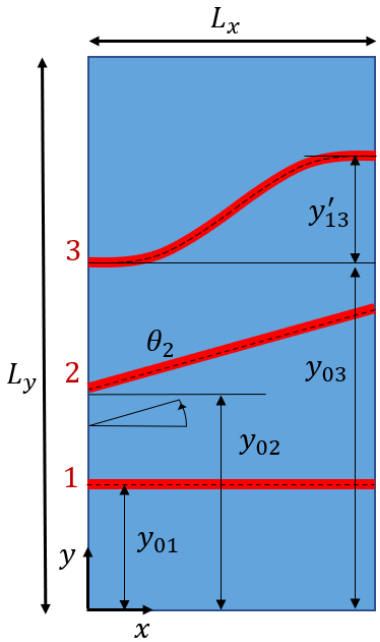

Generic component design vector
$\{D_i\} = \{x_{0i}, y_{0i}, \theta_i, L_i, \{y'_{0i}, \theta'_{0i}, y'_{1i}, \theta'_{1i}\}\}$
Example's component design vector
$\{D_1\} = \{0, y_{01}, 0, L_x, \{0,0,0,0\}\}$
$\{D_2\} = \{0, y_{02}, \theta_2, \frac{L_x}{\cos(\theta_i,)}, \{0,0,0,0\}\}$
$\{D_3\} = \{0, y_{03}, 0, L_x, \{0,0, y'_{13}, 0\}\}$
Definition of $\{\boldsymbol{D}_x\}$ and $\{\boldsymbol{D}_0\}$ in the example
$\{\boldsymbol{D}_x\} = \{y_{01}, y_{02}, \theta_2, y_{03}, y'_{13}\}$
$\{\boldsymbol{D}_0\} = \begin{Bmatrix} \{x_{01}, \theta_1, L_1, \{y'_{01}, \theta'_{01}, y'_{11}, \theta'_{11}\}\}^T \\ \{x_{02}, L_2, \{y'_{02}, \theta'_{02}, y'_{12}, \theta'_{12}\}\}^T \\ \{x_{03}, \theta_3, L_3, \{y'_{03}, \theta'_{0i}, \theta'_{1i3}\}\}^T \end{Bmatrix}$

Figure 4.8 Example of extraction of the design variables vector $\boldsymbol{D}_x$ from the total design vector $\boldsymbol{D}$ defining the TDF of a 3-stiffeners panel. Note that the generic Hermite shape is reduced to linear segment for stiffeners 1 and 2.

4.3 Matlab Implementation Flowcharts

Based on the FE modelling and analysis described earlier, the implementation to set-up the PSO problem of Eq.4.28 or to perform a parametric study is here described.
In the Appendix E, the MATLAB code which follows the PSO flowchart reported in Fig.4.9 is provided. The flowchart for parametric studies is easily obtained by extracting the objective function evaluation cycle from the optimization solver and redefining it according to the matrix of experiments.

In Fig.4.9, the yellow path characterizes the PSO pseudo code, while the green path is related to the parametric study pseudo code. The grey modules are operations contained in both processes and the blue module represents the nested function which is called iteratively to perform the model update and the FEA.

The "Pre-processing operations" block carries out all the operations performed only once when running the code. The "Set Physical Properties" part defines the domain dimensions and properties that determine the equivalent stiffnesses (i.e., skin thickness, height, and eccentricity of the integral reinforcement). The calculation of equivalent matrices is done in "the Generate K_{sk} and K_r" part. In "Define Baseline design and variables" definition of $\boldsymbol{D}$ and $\boldsymbol{D}_x$ is explicited.

The "PSO Initialization" consists of:
(1) setting the size of the swarm and the initial positions of the particles, which can also be done randomly ;
(2) define the inputs for the built-in MATLAB optimization toolbox: the objective nested function, the limit number of iterations, and the bounds for $\boldsymbol{D}_x$.

In this implementation the volume constraint is included using a barrier method [7], which penalizes the objective function in the unfeasible region of the design space. In the flowchart of Fig.4.9 the operations implemented to evaluate the objective function for each particle (namely the operation "Opt1") are listed following the order of execution.

The alternative pseudo code following the block scheme of Fig.4.7, iteratively evaluates the objective function according to a set of design point selected for the investigation. After storing the structural responses, the best design is extracted from the trend obtained by data fitting.

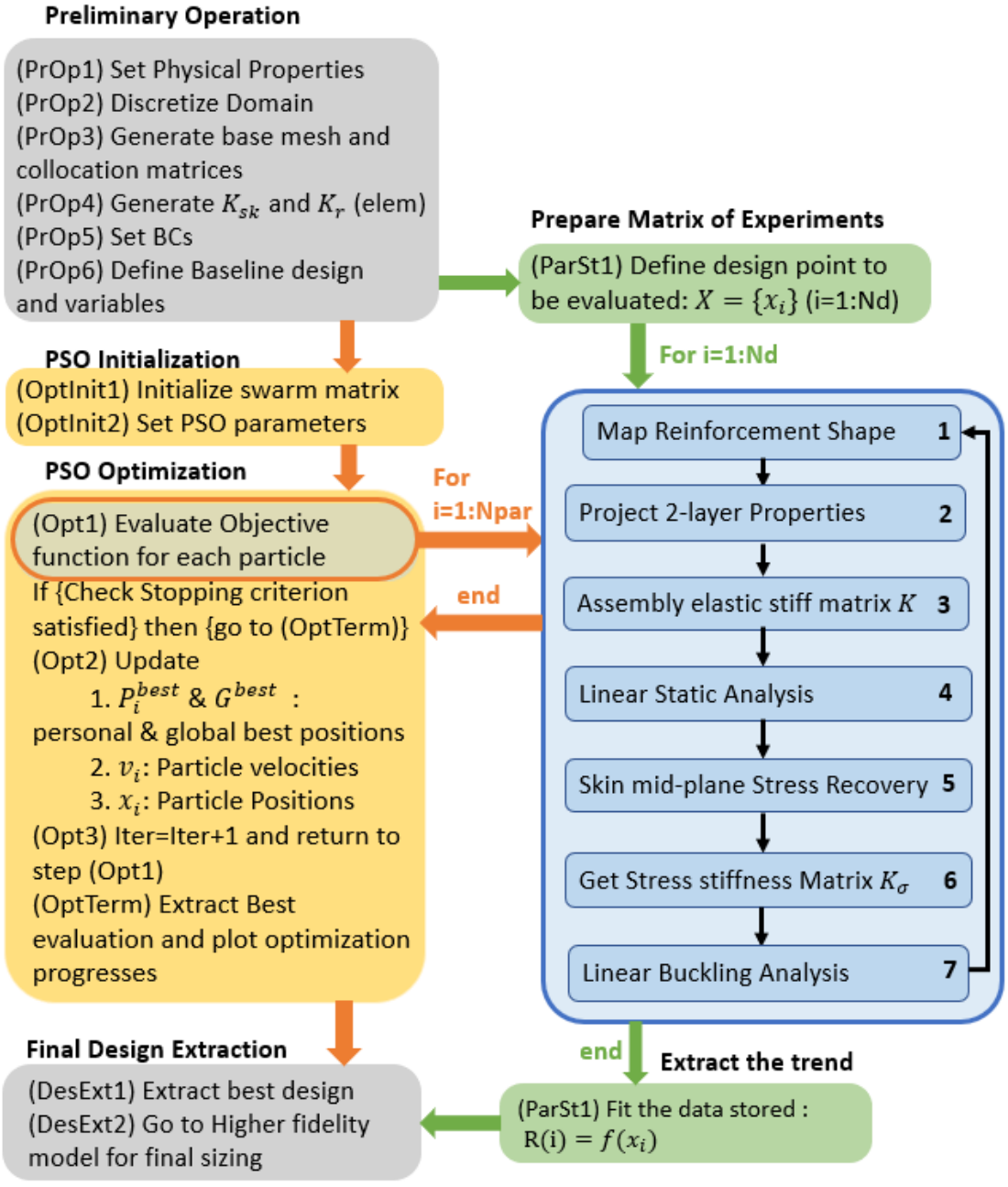

Figure 4.9 Flowchart of the code given in Appendix E for PSO-Optimization of stiffeners path parameters (yellow path), and the alternative one for Parametric Study (green path).

4.4 Results and Discussion

Firstly, the accuracy of the simplified model is estimated by performing some simple test cases. The comparison between the model (analysed in MATLAB) and a reference model (analysed in Optistruct) is reported in Appendix D.
The static solution has an estimated error below 4% for the displacement directly related to the load applied. Coupling between membrane and bending response is captured with an error below 11% on the displacement. The stress field is recovered only for the skin mid plane, as it is used for linearized buckling analysis. Relative error on the fundamental eigenvalue λ_1 is below 12% for the worst case tested. As the aim of the study is to capture the trend of structural responses in a simplified model, the obtained results are reasonable accurate.

4.4.1 Parametric Study 1: Panel under Uniform Compression - Stiffeners Spacing and Curvature Effects

In the first example a rectangular panel with two stiffeners with quadratic path (f^{II} of Tab.4.1) is considered. The dimensions of the panel and the cross-sectional size assumed for the 2-layer model are summarized in the Fig.4.10. Rotations and out-of-plane displacements are constrained on the four sides and an uniform load per unit length is applied. Since the load is unitary, the BLF represents the values of the critical load per unit length.

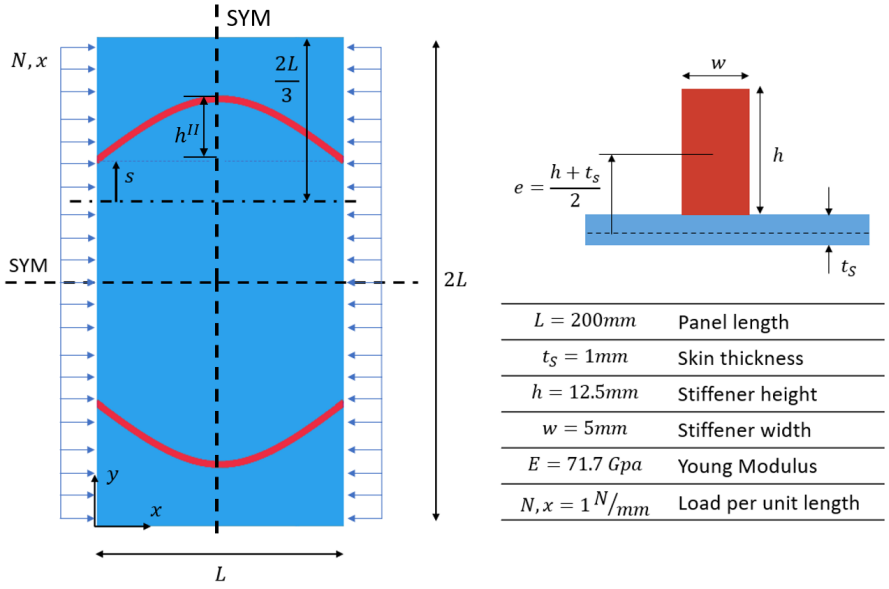

$L = 200mm$	Panel length
$t_S = 1mm$	Skin thickness
$h = 12.5mm$	Stiffener height
$w = 5mm$	Stiffener width
$E = 71.7\ Gpa$	Young Modulus
$N,x = 1\ ^N/_{mm}$	Load per unit length

Figure 4.10 Parametric Study 1: uniform compression panel - Geometry of the model used to investigate the effect of stiffeners curvature on the fundamental BLF

As sketched in the Fig.4.10, the geometry is maintained symmetric with respect to the axes $x = 100mm$ and $y = 200mm$, passing through the centre of the panel.

The effect of the two independent parameters $\{\boldsymbol{D}_x\} = \{h^{II}, s\}$ on the fundamental BLF are then observed. The parameters represents respectively:

- s: the distance of stiffeners endpoints from the mid-line position of stiffeners in the evenly-spaced configuration.
- h^{II} : maximum y-deviation of the quadratic path.

The results of the study are reported in Fig. 4.11, where it is shown that the maximum critical load is achieved with the traditional evenly-spaced straight stiffeners configuration, obtained for $s = 0$ and $h^{II} = 0$.

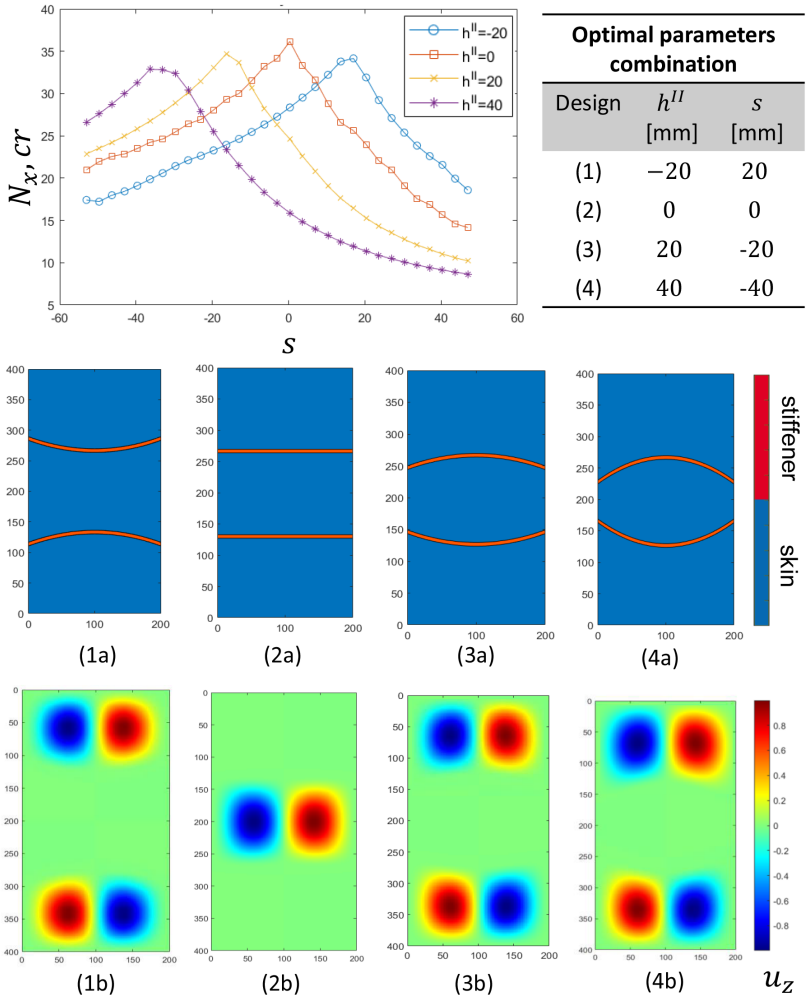

Optimal parameters combination

Design	h^{II} [mm]	s [mm]
(1)	−20	20
(2)	0	0
(3)	20	-20
(4)	40	-40

Figure 4.11 Results of Parametric Study 1 - Optimal spacing for fixed curvatures (ia) and skin buckling mode of the optimal configurations (ib)

However, it can be remarked that curvilinear stiffeners can performs better than straight ones if the stiffeners spacing is imposed to be different from the the evenly-spaced configuration. Another consideration is that the optimal set of parameters follows approximately the rule: $h^{II} + s = 0$.
This confirms the theoretical expectations. The curvilinear path induces the maximum compression state to be in the middle (for $h^{II} < 0$) or in the laterals bays (for $h^{II} > 0$). According to this, the spacing between the stiffeners changes to counteract this effect by minimizing the buckling free length (maximum width) of the critical skin portions.

4.4.2 Parametric Study 2: Panel under Linear Compression – Effect of the stiffeners y-position

On a panel with same stiffeners cross section and same total dimensions of the previous example, a second study has been performed to find the optimal disposition of straights stiffeners in case of uniaxial compression of variable magnitude.
The applied load per unit length varies linearly with the y-coordinate: $N_x = 1 + \frac{y}{2L}$.
In this case the vector of variable parameters is $\{\boldsymbol{D}_x\} = \{s, ds\}$, where s is the bottom stiffener y-position and ds is the positive increment given to the y-position of the upper stiffener. Fig.4.12.(a) introduces these parameters and reports the optimal stiffeners disposition.

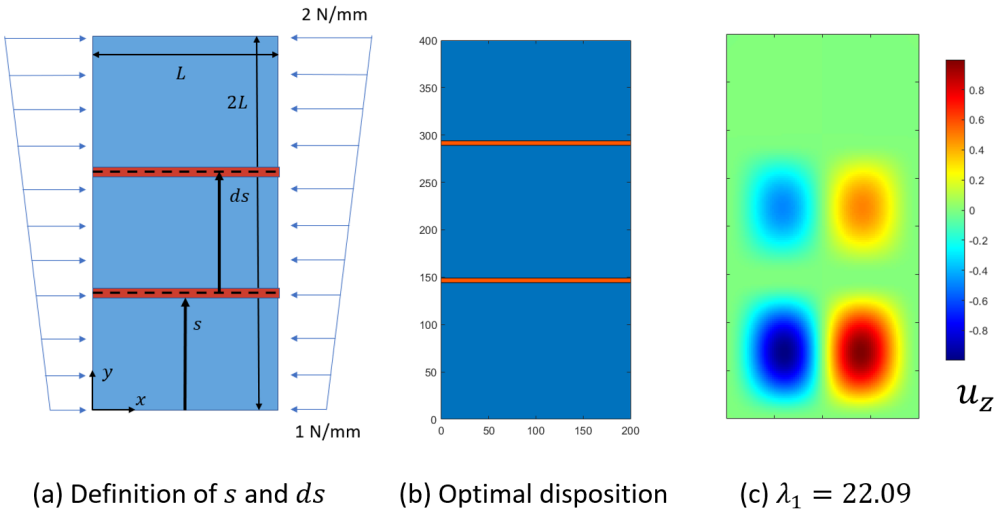

(a) Definition of s and ds (b) Optimal disposition (c) $\lambda_1 = 22.09$

Figure 4.12 Parametric Study 2: Parameters s and ds controlling stiffeners y-positions (a) Optimal disposition and corresponding buckling mode (b-c)

Among the parameter range of $s \in [0, 2L]$ and $ds \in [0, 2L - s]$, the optimal position for the stiffeners is $y_1 = 146.67mm$ and $y_2 = 291.43mm$. As expected, the reinforcements are slightly biased to the top of the panel, where compression is highest.

4.4.3 Parametric study 3: Panel under pure shear – stiffeners pitch and curvature effects

A third example illustrates the mechanical behavior of a squared pure shear panel. The cross sectional area of the blade stiffeners is the same as the previous example and the panel dimensions are 400x400 mm. The panel is subjected to unitary shear load per unit length. For the unstiffened panel, the principal stress directions are inclined $\pm 45°$ degrees with respect to global system axes. Therefore, the effect of spacing and curvature of two reinforcements aligned along this direction are studied and results are reported in Fig.4.13.

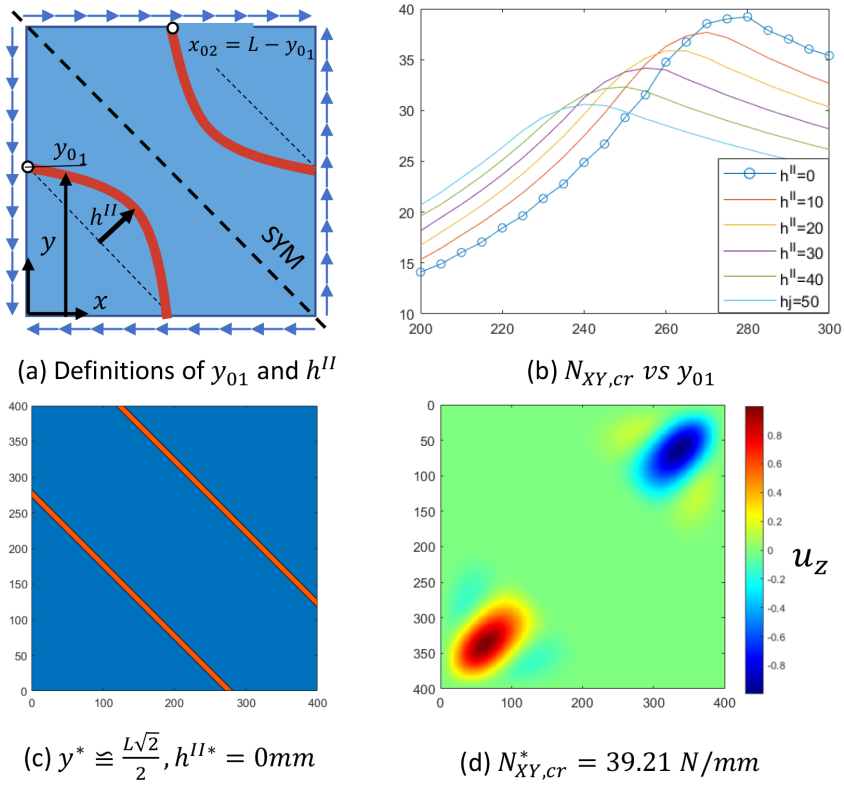

Figure 4.13 Parametric Study 3: Diagonal stiffeners spacing and curvatures (a) effect on the BLF of a pure shear panel (b); optimal configuration (c) and relative buckling mode (d)

The curvilinear path of the two stiffeners is obtained using the component design vectors as follows:

$$\begin{aligned} \boldsymbol{D}_1 &= \{0, y_{01}, -\tfrac{\pi}{4}, \tfrac{y_{01}}{\cos\frac{\pi}{4}}, h^{II}\} \\ \boldsymbol{D}_2 &= \{L - y_{01}, L, -\tfrac{\pi}{4}, \tfrac{y_{01}}{\cos\frac{\pi}{4}}, h^{II}\} \end{aligned} \tag{4.29}$$

As expected, straight components are more efficient and the optimal placement divides the diagonal into three equal segments.

4.4.4 PSO Problem 1: Panel with Run-Out Stiffener

A practical application for the optimization of curvilinear stiffeners path in the upper skin of an aircraft wing-box can be the case of panels with run-out stiffeners.
Due to the reduction in the wing cross-section, there may be portions of skin where one or more stiffeners are interrupted. Stiffeners can be interrupted at the ribs, but this may result in large portions of unstiffened skin that have low critical stress.
Extending the stiffeners into the next bay for a small stretch is cost-effective in terms of weight compared to the alternative of increasing the panel thickness.

A wing upper skin portion is modeled by a simplified rectangular flat panel with two stiffeners, one of which runs-out in the middle of the skin. Figure 4.14 presents the geometry and the boundary conditions of the test case. The connections of the skin to ribs and spars is modeled as simple supports. The long sides are also constrained in y-direction and x-rotation, to simulate the stiffness contribution of the adjacent components. A distributed load with total magnitude of 90KN is applied on one short side, while the other is restrained in the x-direction.

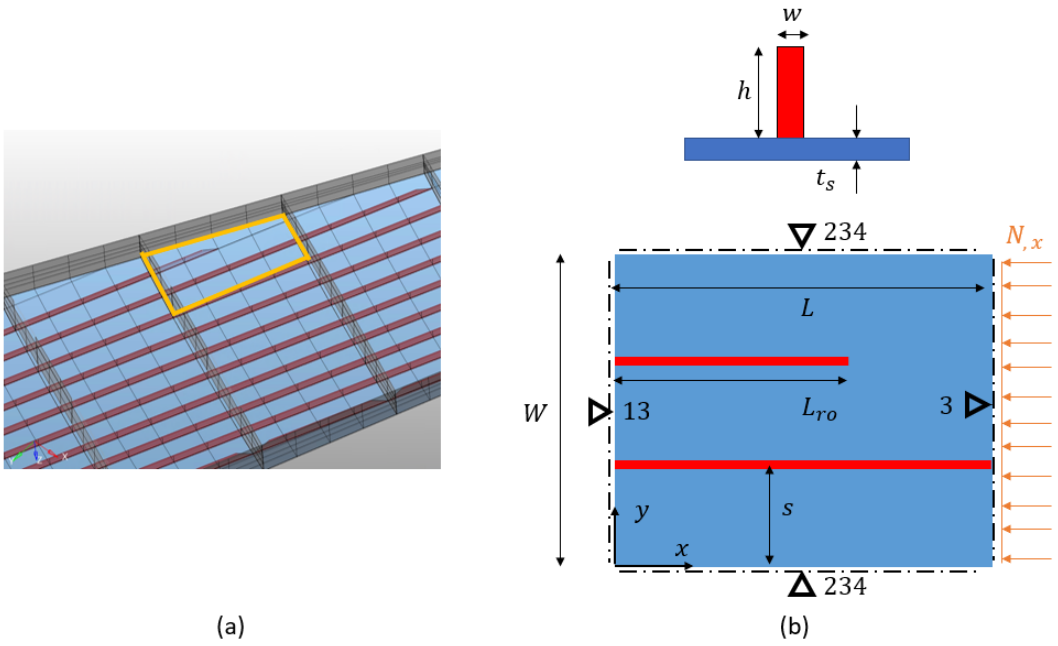

Figure 4.14 Upper skin panel with run-out stiffener - (a) example from a wingbox GFEM; (b) geometry and boundary conditions of the test case for PSO of the curvilinear paths

Starting from the baseline reported in Tab.4.2, the optimization problem of 4.28 is solved. The aim is determining if for the same volume of reinforcement curvilinear paths of the stiffeners lead to higher critical load. Using Hermite curves for the stiffeners paths, the design

component vectors are given as in Fig.4.15(a),where the parameters extracted to compose the layout optimization design variables are highlighted in red. The problem formulation and the initial positions assumed for the swarm particles are reported in Fig.4.15(b). The problem is solved using a swarm of three particles.

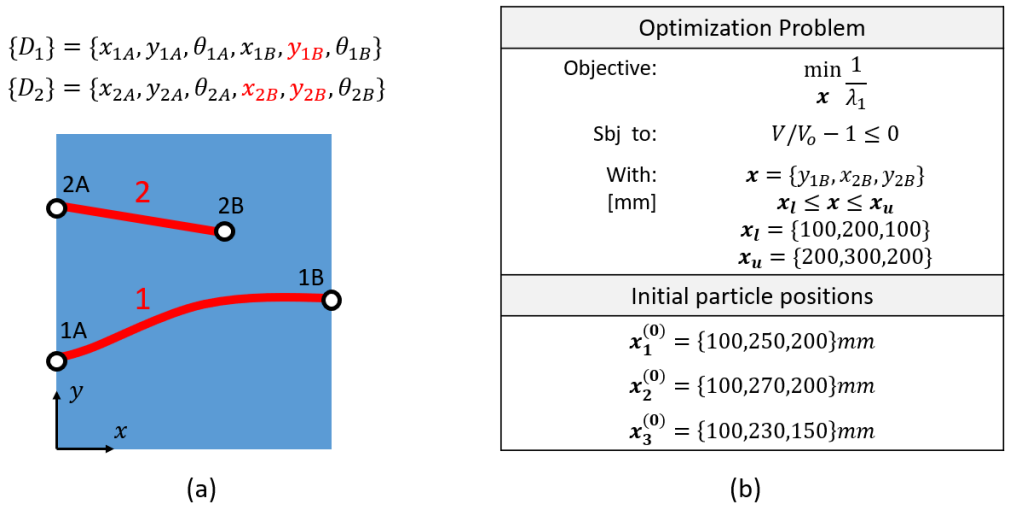

Figure 4.15 PSO problem formulation - (a) design variables (highlighted in red) from the component design vectors; (b) summary of the optimization and initial particles' positions

Table 4.2 Properties and sizes of the baseline panel with run-out stiffener

Parameter	Symbol	Value
Panel Length [mm]	L	400
Panel Width [mm]	W	300
Skin thickness [mm]	t_s	400
Stiffener Spacing [mm]	s	100
Stiffener width [mm]	w	5
Stiffener height [mm]	h_r	25
Run-out Stiffener Length [mm]	L_{ro}	250
Applied axial Load [KN]	P	90
Load per unit length [N/mm]	$N_{,x}$	300
Density (Al7075) $[Kg/mm^3]$	ρ	$2.81e-06$
Young Modulus (Al7075) [GPa]	E	71.7
Yielding Stress (Al7075) [MPa]	F_{cy}	503
Baseline Performance		
Mass [Kg]	m	1.24
Reinforcement volume $[mm^3]$	V_0	81250
BLF (2-Layer Model)	λ_1	0.93

The results of the optimization are summarized in Fig.4.16, where the history of the current global best position is plotted and the final optimal layout is reported. The optimized layout presents a curvilinear shape for the long stiffener, whose end point have been displaced towards the unstiffened panel portion to augment the critical load. The length of the run-out stiffener has decreased, since the curvilinear stiffener has increased its volume.

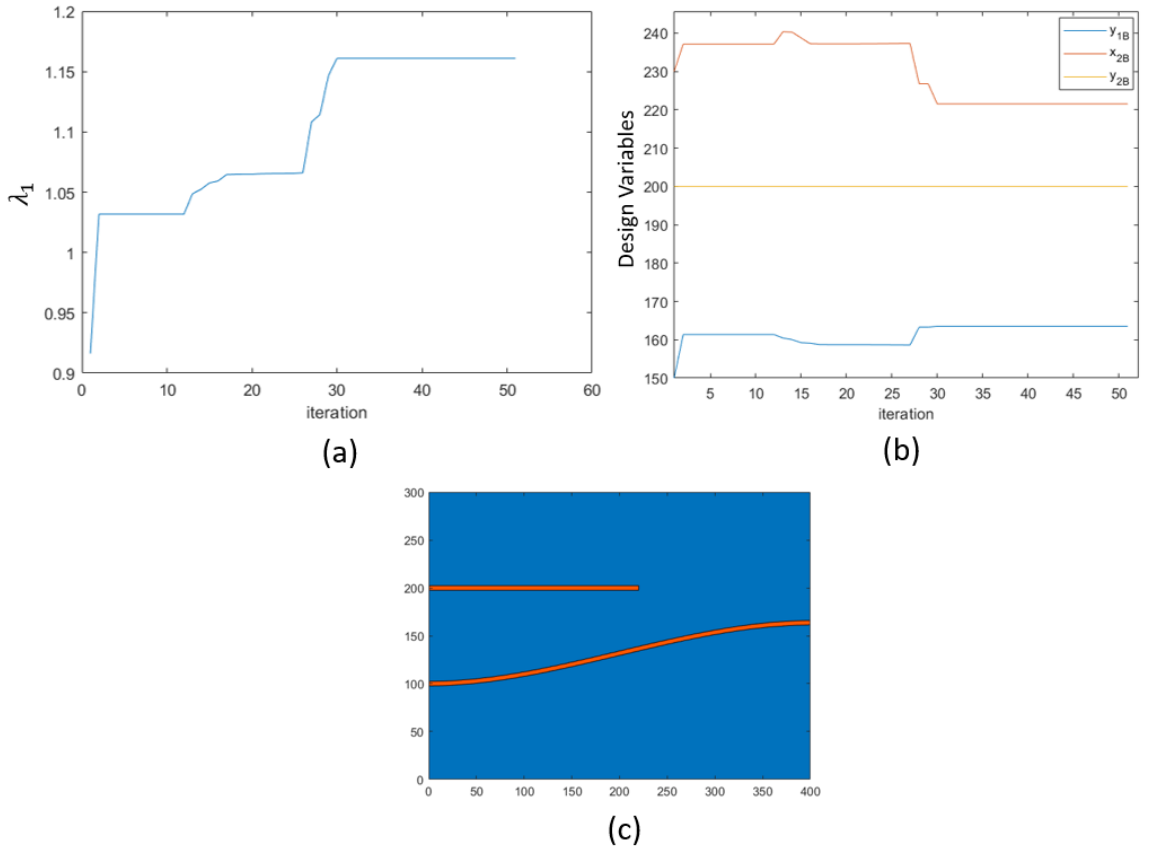

Figure 4.16 Results of the layout optimization. History of the best BLF (a) and of the current best position among the swarm (b); best curvilinear reinforcement layout found in the optimization (c)

Once the layout is fixed, a size optimization which consider the whole set of design constraints can complete the preliminary design procedure. This second phase is carried out in Optistruct on a model where the complete geometry of the panel is reconstructed.

The size optimization problem is performed for both the configurations (straight and curvilinear). The design variables, defined as in Fig.4.17, are now the cross sectional dimensions of the stiffeners, whose layout is now fixed. The design for minimum mass is searched, with bounds on the maximum Von Mises stress and the minimum fundamental buckling load factor. Here the upper bound for the stress is taken as the 60% of material yield limit. Side

constraints and initial values for the design variables are summarized in Tab.4.3.

The size optimization problem is stated in Eq.4.30:

$$\begin{aligned} find \quad & \{\boldsymbol{x}\} = \{t_{sk}, t_{str1}, t_{str2}, h_1, h_2, d_t\} \\ \min_x \quad & mass \\ \text{s.t.} \quad & g_{01} : \sigma_{max}^{VM} \leq 300Mpa \\ & g_{02} : \lambda_1 \geq 1 \\ & \underline{\boldsymbol{x}} \leq \boldsymbol{x} \leq \overline{\boldsymbol{x}} \end{aligned} \tag{4.30}$$

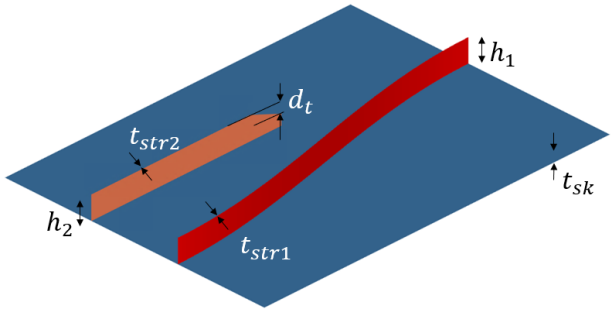

Design variables	
Skin thickness	t_{sk}
Stiffener-1 thickness	t_{str1}
Stiffener-2 thickness	t_{str2}
Stiffener-1 height	h_1
Stiffener-2 height	h_2
Taper depth	d_t

$\{\boldsymbol{x}\} = \{t_{sk}, t_{str1}, t_{str2}, h_1, h_2, \mathrm{d_t}\}$

Figure 4.17 Panel with Run-Out - Design Variable for the size optimization

Table 4.3 Size optimization side constraints considering manufacturing limitations

$\boldsymbol{x}$	$\underline{\boldsymbol{x}}$	$\boldsymbol{x}_0$	$\overline{\boldsymbol{x}}$
$t_{sk}[mm]$	1.5	3	5
$t_{str1}[mm]$	2.5	5	8
$t_{str2}[mm]$	2.5	5	8
$h_1[mm]$	15	25	35
$h_2[mm]$	15	2	35
$d_t[mm]$	0	0	10

The results of the optimization are summarized in Tab.4.4. They can show a further decrease in total mass of the panel brought by the curvilinear configuration (-11.02%). The final designs are driven by the buckling constraint, while the stress constraint is not active in none of them.

Table 4.4 Optimum designs - Panel with run out

Configuration	Optimum Design $\boldsymbol{x}^*$ [mm]	Panel mass [Kg]
Straight	$\{3.16, 2.50, 2.50, 23.47, 22.17, -4.315\}$	1.18
Curvilinear	$\{2.69, 2.50, 2.50, 29.19, 15.01, -0.33\}$	1.05

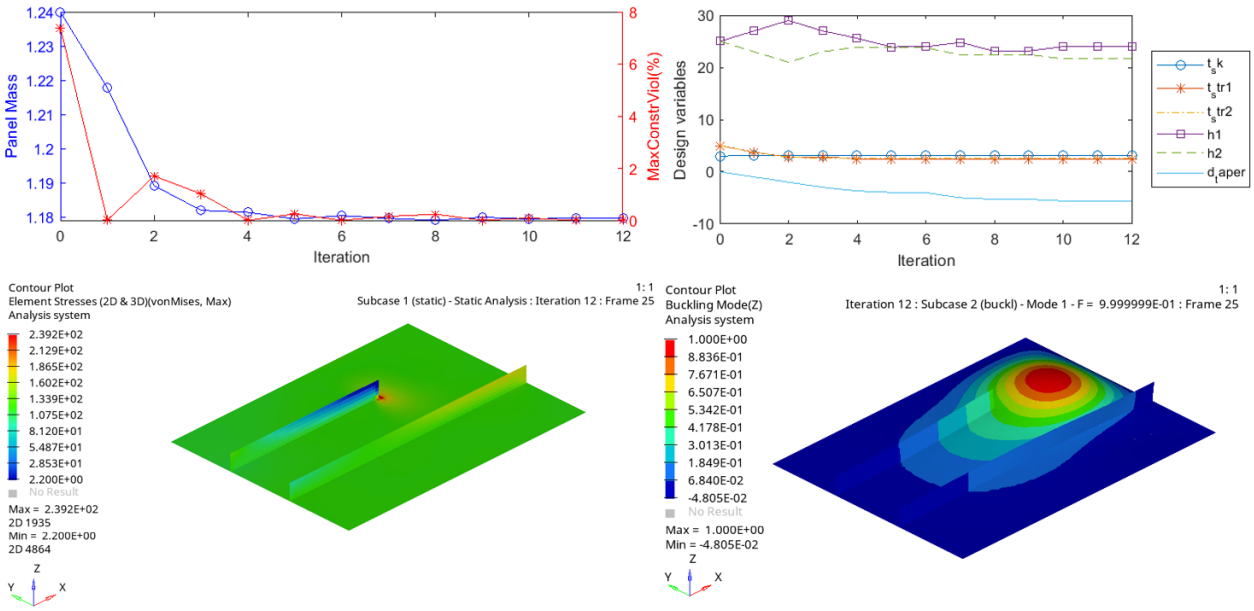

Figure 4.18 Panel with Run-Out - Size optimization of the rectilinear configuration. Optimization history and analysis of the final configuration

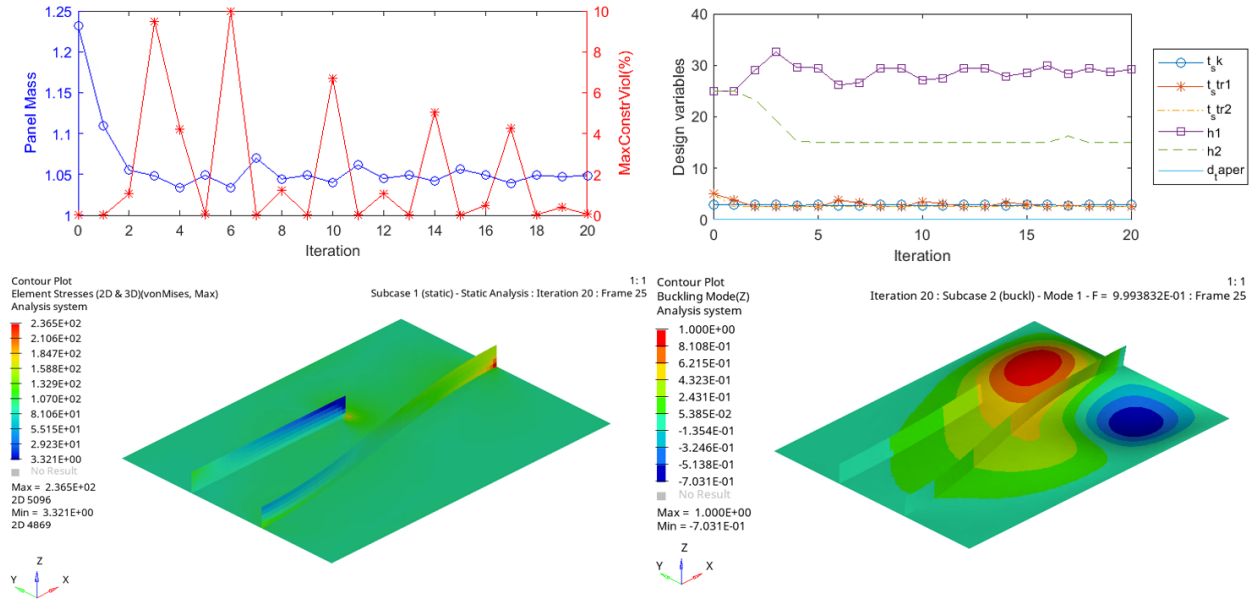

Figure 4.19 Panel with Run-Out - Size optimization of the curvilinear configuration. Optimization history and analysis of the final configuration

4.4.5 PSO Problem 2: Panel with variable compression and superimposed shear

This second example considers as baseline a representative panel portion of the upper skin of an aircraft wingbox with four straight equispaced stiffeners. The panel dimensions are 400x600mm, the stiffeners pitch is 120mm, and the skin is 2mm thick. The stiffeners cross sectional height and width are respectively $h = 26mm$ and $w = 6mm$. The material properties of a generic Al7075 alloy are taken as reported in Tab.4.2 of the previous examples.

The baseline geometry is sketched in Fig.4.20(a) which also summarizes the choice of the boundary conditions. They ideally recreate a portion of the skin which is attached on the ribs along the y-sides and to the spar caps along the x-sides. Four loading conditions are considered: linearly variable compression and constant shear loads per unit length are superimposed as summarized in Fig.4.20(b), according to the coefficients defined in Eq.4.31:

$$r_c = \frac{N^F_{xx}}{N^R_{xx}} \quad r_s = \frac{N_{xy}}{N^{av}_{xx}} \tag{4.31}$$

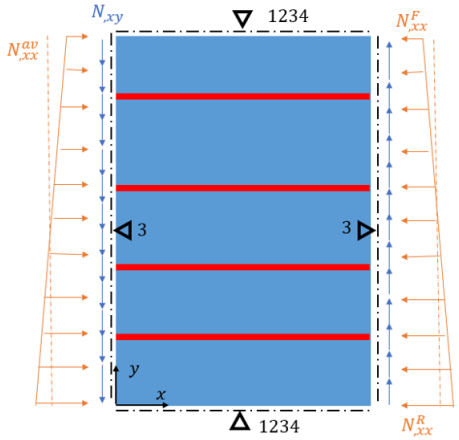

(a)

$$N^{av}_{xx} = 200\frac{N}{mm}$$

LOAD CASE	r_c	r_s	Description
A	1	0	Uniform compression without shear
B	1	0.5	Uniform compression with positive shear
C	1	-0.5	Uniform compression with negative shear
D	0.5	0.5	Linear compression and positive shear

(b)

Figure 4.20 Panel with variable compression and superimposed shear

The average compression N^{av}_{xx} is maintained constant in the four test cases.
The layout optimization problem of Eq.4.28 is solved for each load case independently. The design variables are defined as the perturbations from the baseline of the curvature and endpoint y-coordinates, as illustrated in Fig.4.21(a). Two variables for each stiffener are considered, and their effects on the i-th stiffeners design vector are remarked in Fig.4.21(b), where their bounds are reported as well. Stiffeners paths are defined with the Hermite polynomial function of Tab.4.1, as in the previous example.

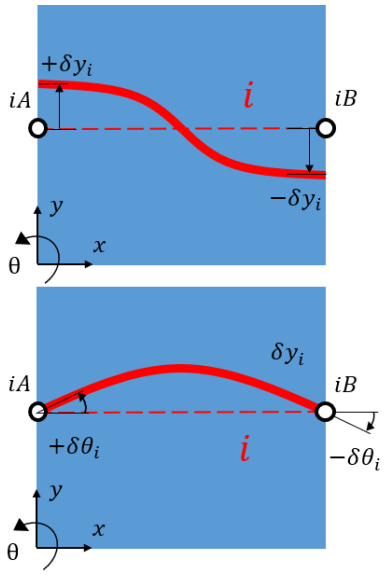

(a)

$$\{\boldsymbol{x}\} = \{\delta y_1, \delta\theta_1, \delta y_2, \delta\theta_2, \delta y_3, \delta\theta_3, \delta y_4, \delta\theta_4\}$$

$$\{D_i\} = \{x_{iA}, y_{iA} + \delta y_i, \theta_{iA} + \delta\theta_i, x_{iB}, y_{iB} - \delta y_i, \theta_{iB} - \delta\theta_i\}$$

Baseline volume : $V_0 = 2.496e05mm^3$

Max volume : $V_{max} = 1.05V_0$

x_i	$\underline{x_i}$	$\overline{x_i}$
$\delta y_1[mm]$	-20	20
$\delta\theta_1[°]$	-30	30
$\delta y_2[mm]$	-20	20
$\delta\theta_2[°]$	-30	30
$\delta y_3[mm]$	-20	20
$\delta\theta_3[°]$	-30	30
$\delta y_4[mm]$	-20	20
$\delta\theta_4[°]$	-30	30

(b)

Figure 4.21 Design variables definitions (a) and optimization constraints (b)

In all the optimizations a swarm of five particles is used, whose initial positions are given in Tab.4.5 and depicted in Fig.4.22. The first particle initial position coincides with the baseline design, while for the rest of the swarm initial positions represent configurations with different end-points or curvature perturbations.

Table 4.5 Initial particles positions for the layout optimizations

P1	$\boldsymbol{x}_1^{(0)} = \{0mm, 0°, 0mm, 0°, 0mm, 0°, 0mm, 0°\}$
P2	$\boldsymbol{x}_2^{(0)} = \{20mm, 0°, 20mm, 0°, 20mm, 0°, 20mm, 0°\}$
P3	$\boldsymbol{x}_3^{(0)} = \{-20mm, 0°, -20mm, 0°, -20mm, 0°, -20mm, 0°\}$
P4	$\boldsymbol{x}_4^{(0)} = \{0mm, 0°, 0mm, 10°, 0mm, 20°, 0mm, 30°\}$
P5	$\boldsymbol{x}_5^{(0)} = \{0mm, -30°, 0mm, -20°, 0mm, -10°, 0mm, 0°\}$

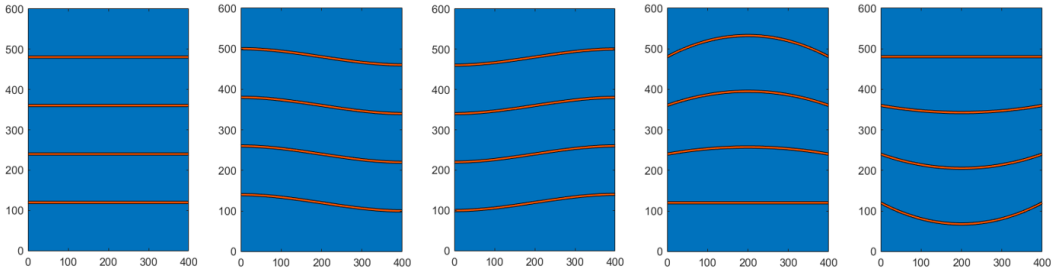

Figure 4.22 Initial Particles positions

The results of the four optimizations are summarized in Tab.4.6, and Figs.4.23 to 4.26 report the optimization history and the final design for each load case.

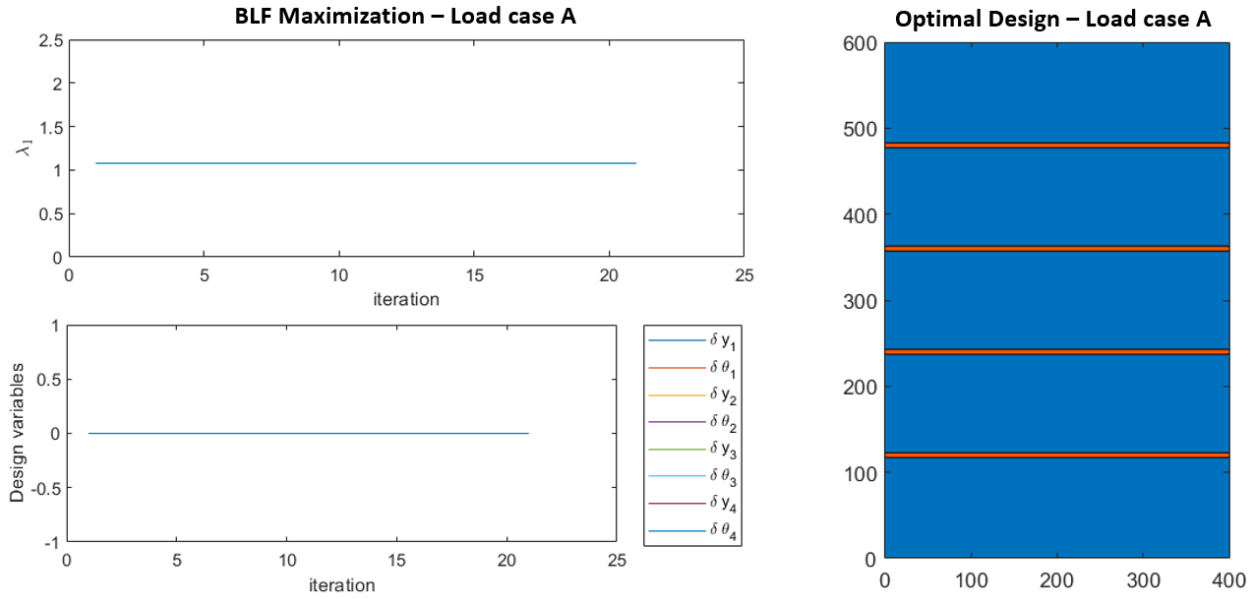

Figure 4.23 Layout optimization results for load case A

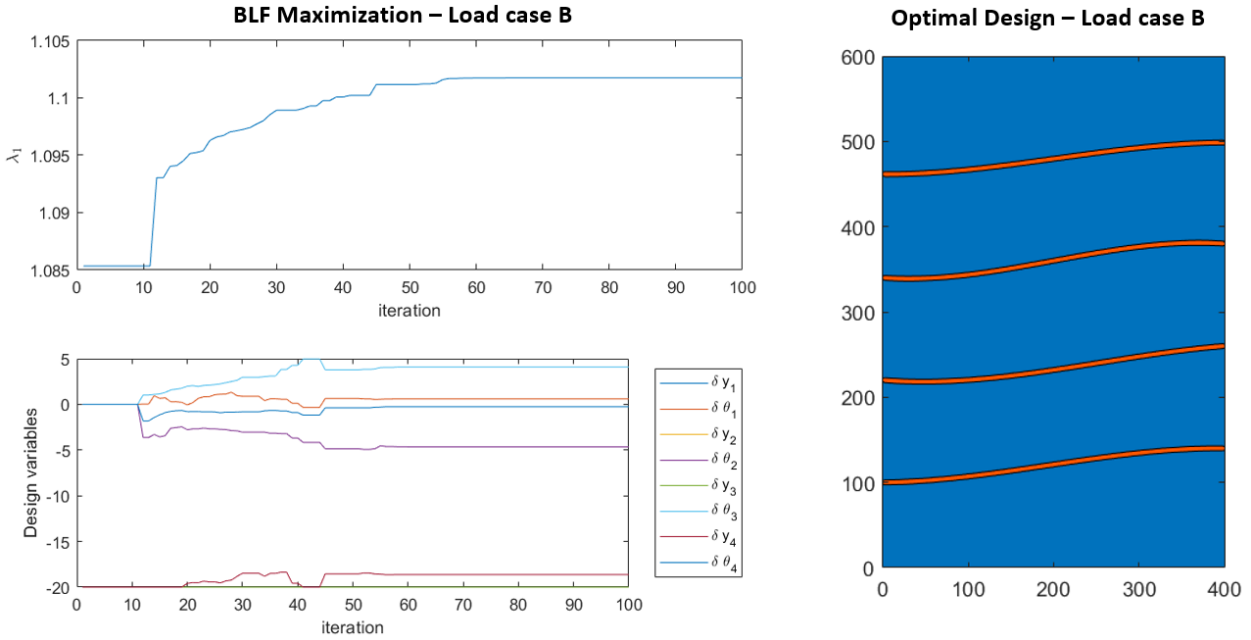

Figure 4.24 Layout optimization results for load case B

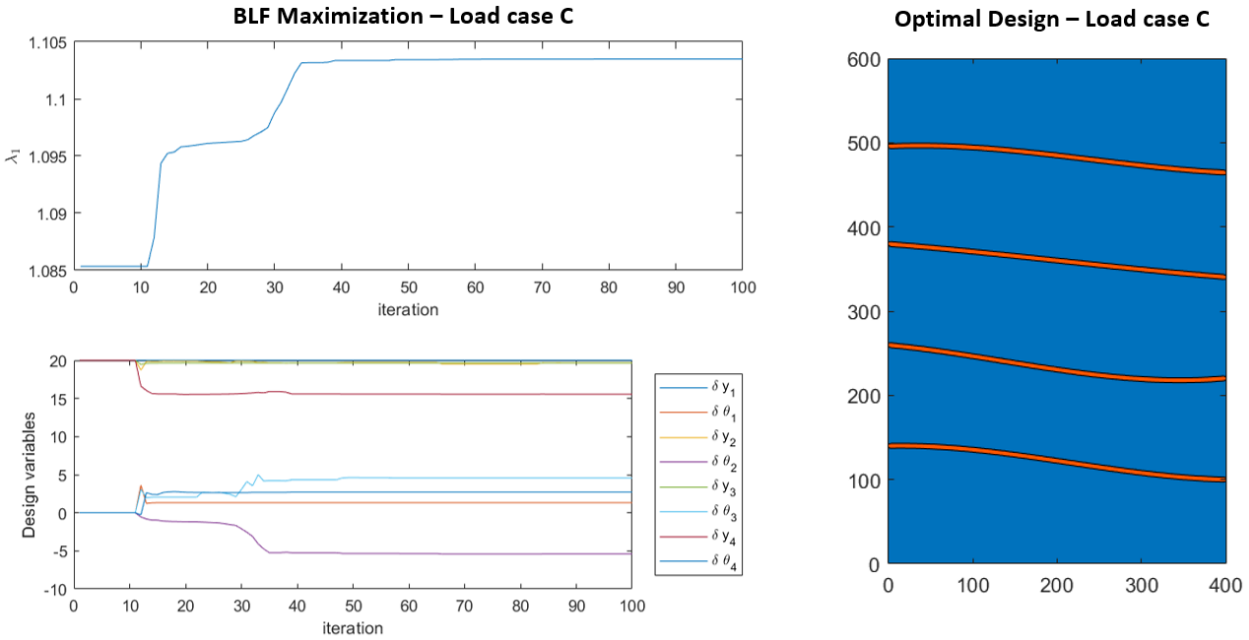

Figure 4.25 Layout optimization results for load case C

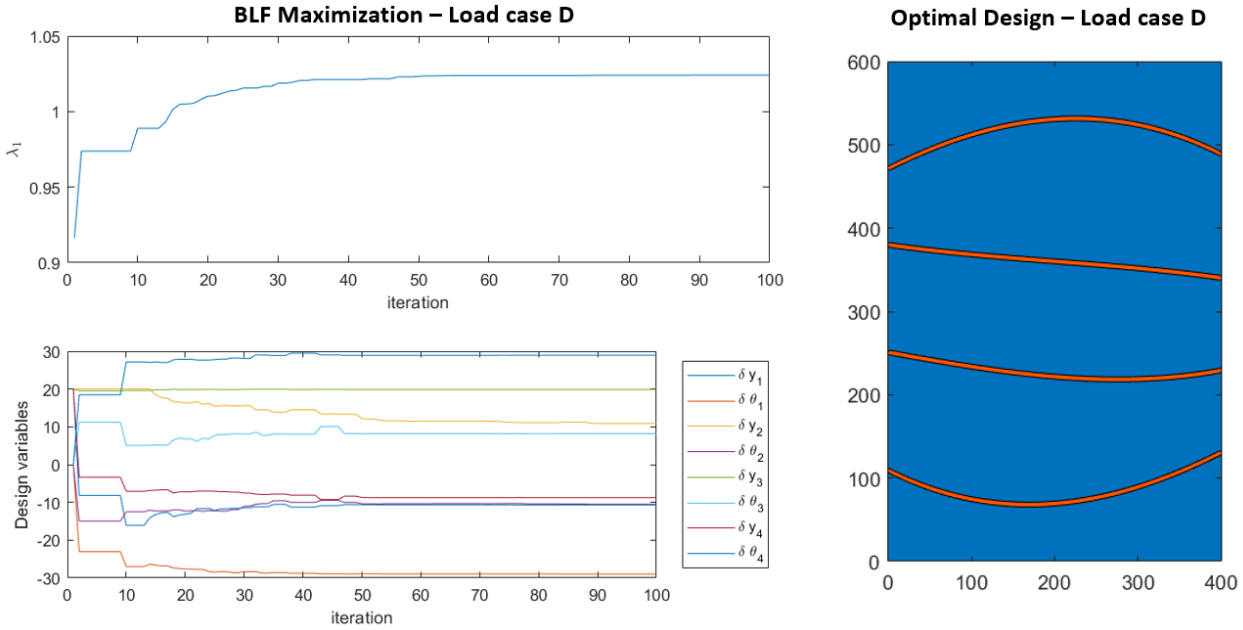

Figure 4.26 Layout optimization results for load case D

Table 4.6 Summary of the layout optimizations for the load cases A-D

Load CASE	BLF $[\lambda_1]$	Volume $[mm^3]$	Stopping condition
A	1.16	$2.496e+05$	21 stall iterations
B	1.10	$2.516e+05$	Max iter reached (100)
C	1.10	$2.520e+05$	Max iter reached (100)
D	1.03	$2.558e+05$	Max iter reached (100)

One can observe that in the case of uniform compression, the optimization stops after 21 stall iterations. The baseline design was among the initial swarm positions, and the solver found no better solutions.
In case B and C, shear loading is added with two different directions. The best initial positions are respectively the third and the second particles, which are slightly inclined along the principal tension directions of the shear loading. The trend of the endpoint variations changes sign accordingly to the shear direction.

However, in the design of a real aircraft component more than one load case should be considered, since the structure is subjected to multiple loading conditions during its life. Thus, the following sizing of one concept aims to only demonstrate the feasibility of the procedure, which needs to be extended to consider multiple loading conditions both in layout and size optimizations.

Focusing on LOAD CASE D, the optimal layout for this particular test case is reconstructed in a FEA software (here Altair Hypermesh). Starting from ten sample points along each curve, shown Fig.4.27(a), curvilinear paths are constructed with a smooth spline interpolation, and the panel is remodeled as showed in Fig.4.27(b).

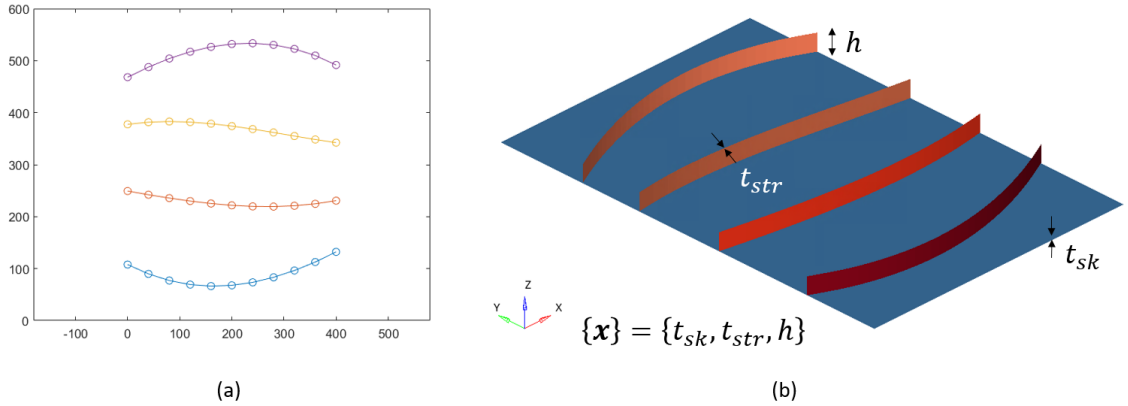

Figure 4.27 Panel with optimal curvilinear layout for LOAD CASE D : (a) Reconstruction stiffeners paths from a set of sample points (b) Variables for final sizing

Since the goal is to see if the beneficial effects on total panel weight are primarily due to curvilinear paths, the number of dimension variables considered for the final optimization is kept to a minimum: one uniform skin thickness , as well as identical thickness and height for all the stiffeners.
Thus, the baseline and the suggested layout are sized according to the following problem:

$$\begin{aligned} find \quad & \{\boldsymbol{x}\} = \{t_{sk}, t_{str}, h\} \\ \min_x \quad & mass \\ \text{s.t.} \quad & g_{01} : \sigma_{max}^{VM} \leq 300 Mpa \\ & g_{02} : \lambda_1 \geq 1 \\ & \underline{\boldsymbol{x}} \leq \boldsymbol{x} \leq \overline{\boldsymbol{x}} \end{aligned} \tag{4.32}$$

The same side constraints of Tab.4.3 are considered for the design variables.
The results of the optimization are reported in Fig.4.28 and Fig.4.29, for the configuration with straight stiffener and the configuration with curvilinear stiffener respectively.

As shown in Tab.4.7, a further decrease in total mass of the panel brought by the curvilinear configuration (-5.77%).

Table 4.7 Optimum designs - Panel with four stiffeners LOAD CASE D

Configuration	Optimum Design $\boldsymbol{x}^*$ [mm]	Panel mass [Kg]
Straight	$\{2.21, 4.05, 19.75\}$	1.852
Curvilinear	$\{2.24, 2.50, 20.16\}$	1.745

Also in this case, the final designs are driven by the buckling constraint, while the stress constraint is not active. By considering panels with smaller spacing between stiffeners the stress constraints may play an active role, as the buckling constraint is less stringent.
Most of the weight saving comes from the thinner stiffeners of the curvilinear configuration, which have reduced their mass of $0.128 Kg$ compared to the baseline stiffeners layout.

In conclusion this example demonstrated that for some load cases a curvilinear stiffener layouts may have beneficial effects on mass of a panel whose design is skin buckling driven. However in a real sizing case post-buckling behaviour has to be considered for failure assessment. Finally, the straight configuration is confirmed to be the best for load cases where compression is predominant. It is remarked, that load case D has investigated a loading condition where the shear was higher than the average compression load.

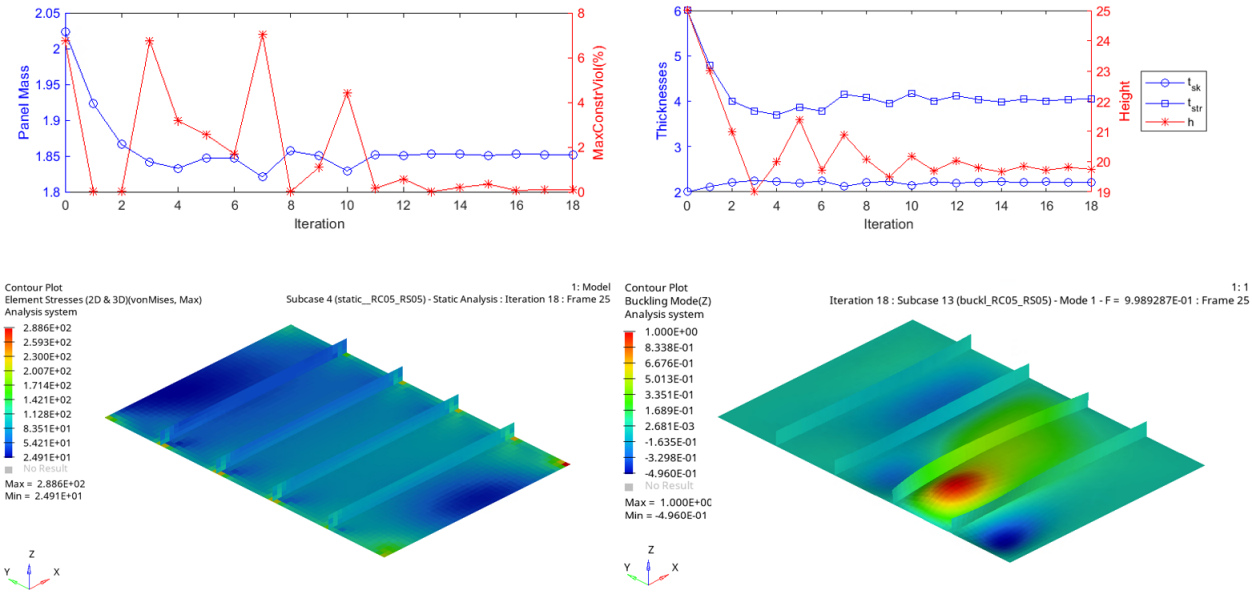

Figure 4.28 PSO: Panel with 4 stiffeners - Size optimization of the rectilinear configuration for load case D. Optimization history and analysis of the final configuration.

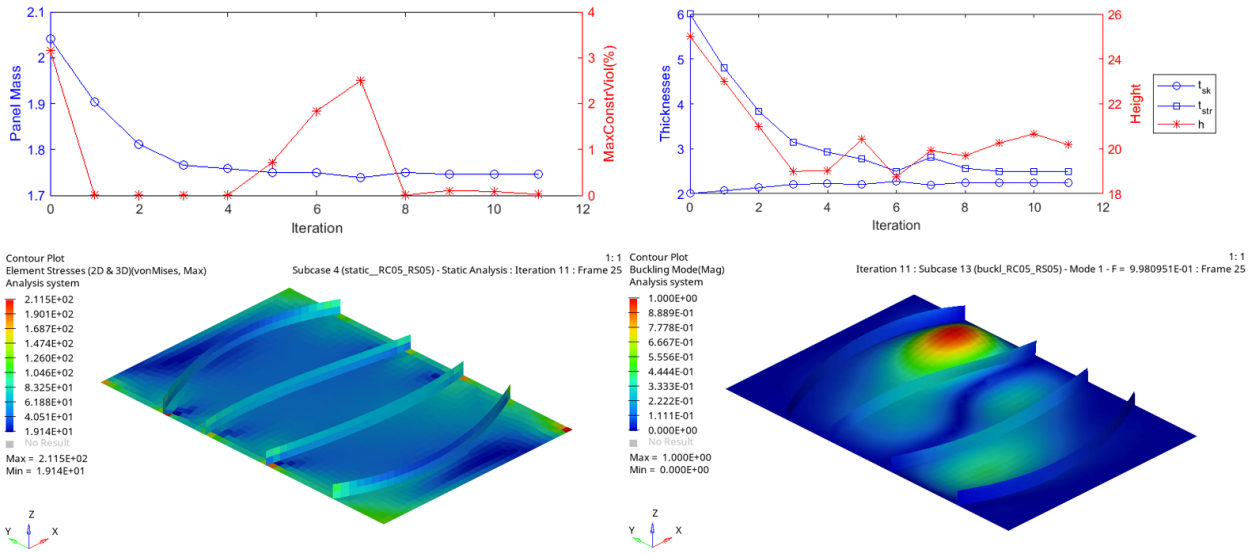

Figure 4.29 PSO: Panel with 4 stiffeners - Size optimization of the curvilinear configuration for load case D. Optimization history and analysis of the final configuration.

4.5 Conclusions on the MMC-based Stiffeners Layout Optimization

In this chapter, a new methodology based on the MMC approach has been developed for the design of stiffened panels subjected to buckling under compressive and shear loads.

The basic idea is to optimize the geometric parameters describing the path of the curvilinear blade stiffeners, by means of a simplified finite element model which reduce the computational cost of the optimization while maintaining a great flexibility in geometric representation.
The accuracy of structural responses is of minor importance during conceptual exploration. By lowering it, the layout optimisation is reduced to the problem of assigning two mechanical properties to a mesh of plates. Thanks to this simplification, the mesh is fixed and the to update the model it is only needed to re-evaluate the TDF used to map the regions where the reinforcement adds stiffness to the panel skin.

In thin-walled structures, stiffeners have both the task of carrying axial loads and providing support to the thin skin, which is prone to buckling for low stress levels. Therefore, integration of buckling in the layout optimization is obtained by adopting the criterion of maximum fundamental BLF with a constraint on the maximum available stiffeners volume.

Compared to the implicit methods (GSM and SIMP), this method offers two main advantages when used within a two-phase design procedure:
- the explicit description of components allows automatic transition to models used for size optimization and ensures satisfaction of any manufacturing constraints;
- the use of a minimal number of design variables allows the use of global optimization techniques to address problems with non-linear objective functions and constraints.

In the numerical examples addressed, it was confirmed that for panels loaded mainly in compression, the optimal configurations are those with parallel and evenly spaced stiffeners. However, it was also revealed that curvilinear configurations can lead to mass reduction in case of panels with local geometric discontinuities (run-outs) or under high shear loading. Even if topological changes (i.e. stiffeners intersection) are not advantageous for the cases studied, the increase of freedom in the stiffeners geometry can be used effectively to place, orient and curve the reinforcement in order to increase the maximum critical load of the panel.

To further develop the procedure it would be necessary to integrate the possibility to consider multiple load cases simultaneously when optimizing the layout. As well as, an extension of the method to 3D curved surfaces would open wide application perspectives for fuselage or wing box panels considered on a larger scale.

CHAPTER 5 DISCUSSION

The main objective **(MO)** of this research work was to develop a design procedure based on Topology Optimization (TO) applicable to the design of stiffened panels. In this procedure, TO is performed to obtain an optimal concept of the stiffener layout, which is interpreted and then sized to minimize mass considering the complete set of design requirements.
To achieve the main objective, two narrower sub-objectives have been identified that address also the following challenges:
- Formulate an explicit description of the stiffener layout to automate interpretation of the TO results **(S01)**;
- Integrate the stability criterion in the layout optimization to increase the skin buckling resistance **(S02)**;

Based on a review of the literature in the field of topology optimization and its applications to the design of stiffened panels, two methods were selected for further investigation and reformulation in order to meet the research objectives.

5.1 Summary of works

Generating Concepts for Optimal Stiffening Layout of Plates using Ground Structure Topology Optimization
The works reviewed in the literature proposed to interpret the stiffeners geometry from the density distribution of SIMP TO. This approach has been found unnecessarily computationally expensive because of the need of a rather fine mesh (hence a very high number of variables) to obtain stiffeners-like members using a continuous finite element mesh. Stiffeners can be easily represented with beam structural elements, as is commonly done in the preliminary design of wing structures. Hence, the idea of an extension of the Ground Structure Method (GSM) to mixed plate-beam models was derived.

The proposed formulation for the GSM applicable in the context of pressurized stiffened panel design constitutes an original extension of the classical method.
This formulation can be adopted in the two-phase design procedure, bringing the following advantages:
(1) The computational cost of the analysis model is reduced, since beams elements are used to represents the stiffeners.
(2) The effort in extracting the final layout is reduced. After removal of the vanishing

members, the resulting ground structure can explictly describe any piecewise linear layout because the coordinates of the endpoints for each beam are available.

The feasibility of the design procedure has been demonstrated through a practical study case, and the content of this chapter has been submitted and accepted for a short article and poster presentation at the ICTAM2021 Congress in Milano.

A Moving Morphable Component based Curvilinear Stiffeners Layout Optimization considering Buckling

With the extended GSM, a more explicit representation of the stiffener layout was obtained compared to the SIMP method. However, to perform more complete explorations of non-convex design spaces, it is essential to decrease the number of design variables and use global optimization techniques. This motivates shifting the attention on the MMC approach. In this explicit TO method, the geometry of the members is directly controlled by a vector of parameters, whose length is independent from the number of elements in the mesh.

By introducing a simplified panel model, the identification of the stiffeners layout was reduced to a problem of arranging two equivalent stiffness properties on a fixed plate mesh. The problem of maximizing the fundamental BLF with a constraint on maximum stiffeners' volume is then addressed using the Particle Swarm Optimization algorithm.

A few simple test cases were conducted to estimate the accuracy of the model, and some parametric studies verified that the theoretical expectations of the optimal layout were met for simple loads.

Finally, the layout optimization was applied in two practical examples: the designs of a panel with a run-out stiffener and the design of a panel under combined compression and shear loads. It was confirmed that parallel and equidistant stiffeners are optimal for panel mainly loaded in compression, but it was also shown that curvilinear configurations can lead to weight reduction in case of panels with run-out stiffeners or high shear loads.

Compared to the computational frameworks found in the literature to solve the optimization of curvilinear stiffeners layout, the one developed here brings the following advantages:

(1) The use of a fixed mesh, on which the stiffness properties are recursively re-mapped during the optimization, saves computational time and coding efforts.

(2) General stiffener layouts can be modeled by using a limited number of design variables, hence limiting the cost of global optimization algorithms.

(3) The control over components' geometry is made explicit, by imposing stiffeners' axis shape functions and proper bounds for the parameters to optimize.

5.2 General Discussion on the Achievement of Research Objectives

The reformulation of the GSM has been a first step toward understanding the main difficulties of addressing the stiffeners layout optimization.
To obtain clearly defined layouts, certain rules must be imposed on the final solution:
- each element of the design space must be considered either in or out of the final design;
- stiffeners' axis path must be interpreted without ambiguity;
- segments disconnected from both supports and other members must be disregarded;

When using an implicit TO method, there is no guarantee that all these rules are satisfied a priory. It is unlikely to violate them when considering simple problems, such as the minimum compliance design of a structure loaded and supported in concentrated points. But the problems considered here are not of this type. Indeed, in the specific case of aircraft structures, the loads applied to stiffened panels are usually modelled as forces distributed along their sides or surface pressure. Similarly, supports affect entire sides of a panel.

An MMC approach for optimizing stiffener layouts can meet the requirements of including only acceptable geometries in the possible solutions. In this way, performing conceptual design becomes more practical and the result of each optimization can be automatically interpreted in a stiffener layout.

It has been demonstrated that the methodology developed in Chapter 4 is a practical procedure for the design of stiffened panels, which fulfils the objectives of this research. The use of geometric parameters which describes explicitly the stiffeners layout **(S01)** as the design variables allows automatic interpretation of the optimization results and an easy control of the structural features. Essential conditions for manufacturability can be imposed by choosing appropriate shape functions for the axis of the stiffeners and the desired intervals for the design. The number of variables is reduced by at least two orders of magnitude compared to implicit methods, and this allows the use of global optimization techniques which are ideal when considering non-linear criteria such as buckling **(SO2)**. Global search allows a more complete exploration of the design space, which is essential in the conceptual design phase.

In conclusion, the contribution of this thesis to the field of topological optimization is twofold. First, the GSM method has been extended to the design for minimum compliance of pressurized stiffened panels through the use of a mixed plate-beam model. Second, an original formulation of the MMC approach is defined for buckling-driven design of stiffened panels subjected to compression-shear loads. The latter, embedded within a two-step procedure, has been shown to provide configurations that achieve the desired performance while reducing component weight, as compared to traditionally designed panels.

5.3 Recommendations on the Use of Various Topology Optimization Approaches

Based on the experience gained from the implementation and use of three different TO approaches, here some useful recommendations are provided regarding the proper selection of each of the methods depending on the particular type of problem and application.

The SIMP method is implemented in many FEM software due to the generality of its formulation and its applicability to any type of finite elements. Pre-processing and optimization solution are very easy to implement, while it is very limited in terms of post-processing.
The results, presented as a distribution of material "pixels" (or "voxels" in the 3D case), must be analyzed by means of additional interpretation tools to allow the continuation of the design process. Automating the interpretation can be difficult in the SIMP method, when the results present a certain level of geometrical complexity: e.g. a large number of elements of intermediate density or organic distributions presenting microstructures.
The computational cost of the SIMP method is the highest of the analyzed methods due to the large number of variables. It is recommended for use in small and medium-scale component designs that do not have special requirements in the manufacturing process.
The full potential of the SIMP method is expressed when there is maximum freedom in the shapes that can be adopted. Unfortunately, the design case of reinforced panels does not fall into this category. Panels are often assembled from precisely shaped individual components into large structures. Consequently, it is not advisable to address this design case with the SIMP method.

The GSM method is based on the use of beam elements to construct the design space.
Therefore, it is not applicable to all types of finite elements. However, due to the simplicity of the analysis model, it is the method with the lowest computational cost among those tested.
The construction of the design space and the initialization of the process are easy to implement. Automatic processes for building Ground Structure have been developed for 2D and 3D domains, based on polygonal and polyhedral meshes.
Its application is recommended for large structural assemblies, where it is convenient to use a model composed of beam elements. In addition to the well-known applications in civil engineering, e.g. frames of bridge and buildings, the potential in the context of pressurised stiffened panels has been demonstrated in this work. The method is also valuable for the easy extraction of the resulting layout. The extraction can be automated, and the available layout information is explicit and complete to reconstruct any layout composed with polygonal chains.
Its main limitation is that obtaining clear "a_{min} - a_{max} layouts" (recalling Fig.3.25), easy to interpret, is questioned when considering non-convex programming problems.

The MMC method is based on the use of geometric parameters as design variables.
This method needs a manual initialization by the user, since it is necessary to establish from the beginning some assumptions about the shape of the structural components: e.g., the number of basic components and their parameterization.
The definition of the design variables must also be done meticulously, to reasonably limit the design space. However, once shape requirements are imposed downstream of the optimization, it is possible to address problems that are more complex than the simple design for maximum stiffness. By limiting the complexity of the design space, in the examples addressed in this thesis, buckling driven optimizations have been addressed in practical computation time and with satisfactory results.
The use of global optimization algorithms makes it particularly suitable for application in the field of stiffened panels subject to buckling. Moreover, the explicit design variables makes the method particularly suitable for the design of structures that have shape or manufacturability requirements. These types of requirements are easily imposed a priori when formulating the optimization problem in the MMC approach.
Theoretically, the number of morphable components and free parameters can be raised as desired. However, it is suggested to limit the design space, so that the problem is tackled with global optimization algorithms. As a result of the experiments conducted when comparing the various methods, in Sect.3.3, we do not recommend the use of gradient-based algorithms for this method. The nonlinear nature of the Topology Description Function (TDF) makes each problem nonconvex, and consequently not suitable to be solved by local optimization techniques.

5.4 Limitations of Current Implementations

The two revisited TO methods has been implemented in MATLAB and they are only a proof of concept of proposed improvements. As a consequence, the first limitation of the current implementations is the lack of demonstrative examples where complex geometries and loads are used. In order to demonstrate their full potential, an optimization framework that can interface with commercial geometry modeling and finite element analysis packages should be built.
Then, some limitations related to each individual work are discussed in the following section:

GSM: The presented algorithm adopted Euler-Bernoulli beams and Discrete Kirchhoff quadrilateral elements because high accuracy on the displacements and complex geometries were out of the scope of a first implementation. To exploit the full potential of the method, a more complete finite element formulation has to be used.

As remarked in the study case, the stress constraint has to be added in the layout optimization phase. The compliance is a global indicator of the deformation which does not take into account stress concentrations. Stiffeners run-outs or relatively small junctions between them are likely to appear in the solution. These features need to be re-engineered in the following phases of the design.

When adding the buckling constraint, layouts with a lot of intermediate beams tend to appear as the result of the optimization. Beams with little cross section give a consistent stability contribution even if they add few stiffness. Thus, on one hand the use of a gradient based optimizer is needed because of the great number of design variables, but on the other, it is not likely that a lot of member are going to be removed from the starting ground structure. The solver gets stuck in local minima before the great portion of the ground structure vanishes. The results are 'feasible' because they satisfy the mechanical constraints but may be difficult to manufacture, and therefore not suitable for an automatic and practical design procedure.

MMC: To avoid time consumption and unsuccessful efforts, the optimization problem has to be formulated such that only clearly defined layouts (according to above mentioned rules) are included in the possible solutions. Then the numerical method will select the ones acceptable in terms of structural responses.

The parametric study approach is robust and allows the desired exploration to be performed easily. However, its drawback is that a large computational effort is required to evaluate a sufficient number of discrete design points as soon as the number of variables increases. A strategy based on global optimization techniques, like the Particle Swarm Optimization used here, is more suitable for practical problems with more design variables. The computational burden of such methods is greater than that of gradient-based optimization approaches, but in the current trend of growing computer powers this should be a minor concern.

The main limit of the current implementation is that it can only be applied to the layout optimization of flat panels. In order to open up new perspectives of use for fuselage panels or three-dimensional assemblies of wing-box panels, it would be necessary to extend the procedure to curved surfaces oriented generically in space. The use of shell elements can meet the first requirement, while for the second it is necessary to define a transformation between local and global coordinates that uses the normal vector of each surface to define the rotation matrix.

Finally it is worth noting that during the layout optimization phase the number of stiffeners is fixed. However, it is possible to repeat the layout optimization for several values of the number of stiffeners and select the configuration that leads to the lowest total weight.

5.5 Future Research

Overcoming the above discussed limits of the implementation is a first task for future development. In addition, some ideas for future research are noted as follows:

GSM: The method is based on the idea of using the cross sectional area of each beam as a topological variable. This implies that local stiffness matrices are recalculated at each iteration. An interpolation strategy (like in the SIMP) could be developed for the GSM to streamline this step.
The model adopted in this work used stiffeners with rectangular cross-sectional area and prescribed height-to-width ratio. As proposed by [63], a possible way to adopt cross-sections of common engineering practice in the GSM can be the use of polynomial interpolations to express the stiffness matrix coefficients as a function of the cross sectional area. This can be done by performing a regression analysis based on data provided by a design manual.
The construction of the starting ground structure is a major step in the process which determines the set of candidate reinforcements, hence the design space. In this work the automatic connection of each node to its neighbors, according to a certain level of connectivity, was adopted. However, making the GS construction smarter by exploiting information from the boundary conditions of the problem can effectively reduce the design space, by excluding candidates with less potential from the start.

MMC: A way to consider I or Z cross-sections in the equivalent stiffness method is proposed in [82]. One could easily define the expression for the reference frame along the parametric stiffener axis, but then the equivalent properties become design dependent, i.e. should be recalculated iteratively during the optimization.
A sensitivity analysis for the problem could be carried out to formulate a gradient-based approach, or to improve the global search by continuing the optimization with a local solver which operates after the global one stops. To do this, the topology description function gradients could be calculated analytically or by means of central finite differences [26].
It has been shown manually that the transition to the size optimization model requires a precise sequence of operations that can be automated for any curvilinear layout. Starting from the solution of the layout optimization problem, one has all the required information to retrace the curves of the stiffeners axes, and then construct the complete model of the panel by extruding the surfaces in the direction normal to the skin. This can be implemented in an automatic process within the software chosen to conduct the final sizing.

CHAPTER 6 CONCLUSION

In this research work, the main Topology Optimization (TO) approaches have been studied in order to develop a new design methodology for stiffened panels.

The difficulties of the standard TO method, i.e. the SIMP method, in the conceptual optimization of non-free-form structures, having components with special geometrical requirements, were highlighted. In addition, it was pointed out that the current literature lacks a thorough understanding of TO strengths and weaknesses when applied in the optimal reinforcement of panels subjected to buckling.

Among the implicit methods, which use the properties of the finite elements mesh as the optimization variables, the Ground Structure Method (GSM) was selected, since it is capable of using a design space composed of beam elements.
Mixed plates-beams models are commonly used for the preliminary sizing of large stiffened panels assemblies, e.g. wing-box structures, because of their low computational cost. Hence, the idea of an extension of the GSM to mixed plate-beam models was derived.
In this method, a network of beam elements is placed on the plate mesh and the cross sectional area distribution is optimized. By removing the beams with small area in the final design, the optimal layout of the stiffeners is then obtained. In the design for minimum compliance, the GSM has been shown to be capable of revealing the main path of the loads, and to outperform the SIMP method in terms of mesh with low computational cost and ease of interpretation of the resulting layout.
However, the inclusion of stress and buckling constraints remains the critical point of methods with implicit variables and large design spaces. For these methods, the high number of variables forces the use of gradient-based optimisation techniques, which have limited exploration capabilities when considering highly non-linear objective functions and constraints.

In order to obtain a direct control of the component geometry and to reduce the number of variables so that global optimization techniques can be used, the Moving Morphable Component (MMC) method was chosen to tackle the problem.
In this explicit method, a set of geometric parameters constitutes the vector of design variables, and this guarantees the imposition of any geometric requirements and manufacturing constraints.
A model with equivalent mechanical properties has been proposed to reduce the layout optimisation to the problem of arranging two different stiffness properties on a fixed plate mesh, which differentiate the zones with and without reinforcement.

By decreasing the complexity of the model, only the essential information for layout optimization is retained, i.e. the shape functions of the stiffeners' path. This is ideal in a two-stage design procedure, where first the stiffeners' layout information is obtained and then the various components are sized.

In the case of in-plane loaded panels, it has been shown that changes in topology, (i.e. stiffeners intersections) are not particularly advantageous. However, the augmented geometric freedom is exploited to achieve optimal layout with non-uniform positioning, general orientation and curvilinear axes of the stiffeners. In fact, when it is necessary to interrupt the stiffeners or when high shear loads are applied, curvilinear configurations can lead to a reduction in the total panel mass compared to the evenly spaced rectilinear stiffeners' layout. In the first design example, the mass of the panel with a run-out stiffener was reduced by 11% through the use of a curvilinear member. Similarly in the example, the optimum configuration suggested for the case with superimposed compression and shear loads resulted in a 6% reduction of the panel mass.

The layout optimisation through the MMC approach assumes a rather different aspect than a pure TO. The optimal layout is obtained by reshaping the chosen set of components, rather than trying to derive them from a blind starting guess.
Based on the experience gained in this work, we conclude that using TO without any initial assumptions is not practical for the design of complex assemblies, because the tool is ill-conditioned and still needs the validation of the designer's judgment and experience.
It is advantageous to set some rules about the possible layouts to evaluate and use knowledge of the problem to guide the exploration of new designs. The designer who formulates the optimization problem must be careful to include in the design space only those solutions with clearly identifiable stiffener paths, then the optimization software will deliver the designs with the best structural performance.

REFERENCES

[1] N. Aage *et al.*, "Giga-voxel computational morphogenesis for structural design," *Nature*, vol. 550, p. 84, Oct. 2017. [Online]. Available: https://doi.org/10.1038/nature23911

[2] Airbus, "Getting to grips with a320 family performance retention and fuel saving," Airbus, Tech. Rep. Issue 2, 2008. [Online]. Available: https://www.cockpitseeker.com/wp-content/uploads/goodies/ac/a320/pdf/data/GTGA320PerfoRetentionIssue2.pdf

[3] ICAO. New ICAO aircraft co2 standard one step closer to final adoption. [Online]. Available: https://www.icao.int/Newsroom/Pages/New-ICAO-Aircraft-CO2-Standard-One-Step-Closer-To-Final-Adoption.aspx

[4] E. Terrenoire *et al.*, "The contribution of carbon dioxide emissions from the aviation sector to future climate change," *Environmental research letters*, vol. 14, no. 8, p. 084019, 2019.

[5] A. Dugré, A. Vadean, and J. Chaussée, "Challenges of using topology optimization for the design of pressurized stiffened panels," *Structural and Multidisciplinary Optimization*, vol. 53, no. 2, pp. 303–320, Feb. 2016. [Online]. Available: http://link.springer.com/10.1007/s00158-015-1321-1

[6] J.-F. Gamache *et al.*, "Image-based truss recognition for density-based topology optimization approach," *Struct. Multidiscip. Optim.*, vol. 58, no. 6, p. 2697–2709, Dec. 2018. [Online]. Available: https://doi.org/10.1007/s00158-018-2028-x

[7] J. S. Arora, *Introduction to optimum design*. Elsevier, 2004.

[8] M. P. Bendsøe and O. Sigmund, *Topology optimization: theory, methods, and applications*. Berlin ; New York: Springer, 2003.

[9] M. P. Bendsøe and N. Kikuchi, "Generating optimal topologies in structural design using a homogenization method," *Computer Methods in Applied Mechanics and Engineering*, vol. 71, no. 2, pp. 197–224, Nov. 1988. [Online]. Available: https://linkinghub.elsevier.com/retrieve/pii/0045782588900862

[10] J.-H. Zhu, W.-H. Zhang, and L. Xia, "Topology optimization in aircraft and aerospace structures design," *Archives of Computational Methods in Engineering*, vol. 23, no. 4, pp. 595–622, Dec. 2016. [Online]. Available: http://link.springer.com/10.1007/s11831-015-9151-2

[11] L. Krog, A. Tucker, and G. Rollema, "Application of topology, sizing and shape optimization methods to optimal design of aircraft components," p. 12, 2011.

[12] M. C.-Y. Niu, *Airframe structural design: practical design information and data on aircraft structures*, 2nd ed. Hong Kong: Conmilit Press, 2002, oCLC: 248812908.

[13] T. H. G. Megson, *Aircraft structures for engineering students*, 6th ed., ser. Elsevier aerospace engineering series. Oxford ; Burlington, MA: Butterworth-Heinemann, 2017.

[14] F. Ferrari and O. Sigmund, "Revisiting topology optimization with buckling constraints," *Structural and Multidisciplinary Optimization*, vol. 59, no. 5, pp. 1401–1415, May 2019. [Online]. Available: http://link.springer.com/10.1007/s00158-019-02253-3

[15] R. D. Cook *et al.*, *Concepts and Applications of Finite Element Analysis*. John Wiley & Sons, 2007.

[16] B. H. Choi, J. J. Kim, and T.-H. Lee, "Bending stiffness requirement for closed-section longitudinal stiffeners of isotropic material plates under uniaxial compression," *Journal of Bridge Engineering*, vol. 20, no. 7, p. 04014092, 2015.

[17] X.-Y. Ni, G. Prusty, and A. Hellier, "Buckling and post-buckling of isotropic and composite stiffened panels: A review on analysis and experiment (2000-2012)," *Transactions of the Royal Institution of Naval Architects Part A1: International Journal of Maritime Engineering*, vol. 157, pp. A–9, 01 2015.

[18] G. Gerard, "The crippling strength of compression elements," *Journal of the Aerospace Sciences*, vol. 25, pp. 37–52, 1958.

[19] F. Ferrari and O. Sigmund, "Towards solving large-scale topology optimization problems with buckling constraints at the cost of linear analyses," *Computer Methods in Applied Mechanics and Engineering*, vol. 363, p. 112911, 2020.

[20] C.-Y. Lin and L.-S. Chao, "Automated image interpretation for integrated topology and shape optimization," *Structural and Multidisciplinary Optimization*, vol. 20, no. 2, pp. 125–137, Oct. 2000. [Online]. Available: http://link.springer.com/10.1007/s001580050144

[21] O. Sigmund and K. Maute, "Topology optimization approaches: A comparative review," *Structural and Multidisciplinary Optimization*, vol. 48, no. 6, pp. 1031–1055, Dec. 2013. [Online]. Available: http://link.springer.com/10.1007/s00158-013-0978-6

[22] W. Dorn, "Automatic design of optimal structures," *J. de Mecanique*, vol. 3, pp. 25–52, 1964.

[23] T. Zegard and G. Paulino, "Grand — ground structure based topology optimization for arbitrary 2d domains using matlab," *Structural and Multidisciplinary Optimization*, vol. 50, pp. 861–882, 2014.

[24] J.-F. Gamache *et al.*, "Topology Optimization for Stiffened Panels: A Ground Structure Method," in *IDETC-CIE2020*, Volume 11A: 46th Design Automation Conference (DAC), Aug. 2020, v11AT11A049. [Online]. Available: https://doi.org/10.1115/DETC2020-22103

[25] O. Sigmund and J. Petersson, "Numerical instabilities in topology optimization: A survey on procedures dealing with checkerboards, mesh-dependencies and local minima," *Structural Optimization*, vol. 16, pp. 68–75, 08 1998.

[26] X. Guo, W. Zhang, and W. Zhong, "Doing topology optimization explicitly and geometrically—a new moving morphable components based framework," *Journal of Applied Mechanics*, vol. 81, no. 8, p. 081009, Aug. 2014. [Online]. Available: https://asmedigitalcollection.asme.org/appliedmechanics/article/doi/10.1115/1.4027609/370419/Doing-Topology-Optimization-Explicitly-and

[27] K. Lee, *Principles of CAD/CAM/CAE Systems*. Addison-Wesley, 2000.

[28] W. Hare, J. Nutini, and S. Tesfamariam, "A survey of non-gradient optimization methods in structural engineering," *Advances in Engineering Software*, vol. 59, pp. 19–28, 2013. [Online]. Available: https://www.sciencedirect.com/science/article/pii/S0965997813000288

[29] K. Svanberg, "The Method of Moving Asymptotes—a new method for structural optimization," *International journal for numerical methods in engineering*, vol. 24, no. 2, pp. 359–373, 1987.

[30] ——, "MMA and GCMMA, versions September 2007," *Optimization and Systems Theory*, vol. 104, 2007.

[31] G. Kreisselmeier and R. Steinhauser, "Systematic control design by optimizing a vector performance index," in *Computer Aided Design of Control Systems*, M. CUENOD, Ed. Pergamon, 1980, pp. 113–117. [Online]. Available: https://www.sciencedirect.com/science/article/pii/B978008024488450022X

[32] P. Duysinx and O. Sigmund, "New developments in handling stress constraints in optimal material distribution," 09 1998.

[33] R. Byrd, M. E. Hribar, and J. Nocedal, "An interior point algorithm for large-scale nonlinear programming," *SIAM J. Optim.*, vol. 9, pp. 877–900, 1999.

[34] O. Sigmund, "On the usefulness of non-gradient approaches in topology optimization," *Structural and Multidisciplinary Optimization*, vol. 43, pp. 589–596, 05 2011.

[35] X. Guo *et al.*, "Explicit structural topology optimization based on moving morphable components (mmc) with curved skeletons," *Computer Methods in Applied*

Mechanics and Engineering, vol. 310, pp. 711–748, 2016. [Online]. Available: https://www.sciencedirect.com/science/article/pii/S0045782516307691

[36] J. Kennedy and R. Eberhart, "Particle swarm optimization," in *Proceedings of ICNN'95 - International Conference on Neural Networks*, vol. 4, 1995, pp. 1942–1948 vol.4.

[37] E. Mezura-Montes and C. A. Coello Coello, "Constraint-handling in nature-inspired numerical optimization: Past, present and future," *Swarm and Evolutionary Computation*, vol. 1, no. 4, pp. 173–194, 2011. [Online]. Available: https://www.sciencedirect.com/science/article/pii/S2210650211000538

[38] Y. Shi and B. Obaiahnahatti, "A modified particle swarm optimizer," vol. 6, 06 1998, pp. 69 – 73.

[39] P. Fourie and A. Groenwold, "The particle swarm optimization algorithm in size and shape optimization," *Structural and Multidisciplinary Optimization*, vol. 23, pp. 259–267, 05 2002.

[40] S. B. Mulani, W. C. Slemp, and R. K. Kapania, "Ebf3panelopt: An optimization framework for curvilinear blade-stiffened panels," *Thin-Walled Structures*, vol. 63, pp. 13–26, 2013. [Online]. Available: https://www.sciencedirect.com/science/article/pii/S0263823112002601

[41] M. E. H. Pedersen, "Good parameters for particle swarm optimization," 2010.

[42] S. Afonso, J. Sienz, and F. Belblidia, "Structural optimization strategies for simple and integrally stiffened plates shells," *Engineering Computations*, vol. 22, pp. 429–452, 06 2005.

[43] S. Liu *et al.*, "H-dgtp—a heaviside-function based directional growth topology parameterization for design optimization of stiffener layout and height of thin-walled structures," *Structural and Multidisciplinary Optimization*, vol. 52, pp. 1–11, 06 2015.

[44] J. Zhu, Y. LI, and W. Zhang, "Topology optimization with shape preserving design," 01 2014.

[45] A. HyperWorks, *OptiStruct-19.0 User's Guide*, Altair Engineering, Troy, MI, 2019.

[46] "HyperWorks," Detroit, USA, 2018.

[47] W. Zhang *et al.*, "A moving morphable component based topology optimization approach for rib-stiffened structures considering buckling constraints," *Journal of Mechanical Design*, vol. 140, no. 11, p. 111404, Nov. 2018. [Online]. Available: https://asmedigitalcollection.asme.org/mechanicaldesign/article/doi/10.1115/1.4041052/472606/A-Moving-Morphable-Component-Based-Topology

[48] Z. Sun *et al.*, "An optimization approach for stiffener layout of composite stiffened panels based on moving morphable components (mmcs)," *Acta Mechanica Solida Sinica*, pp. 1–13, 2020.

[49] X. Gao and H. Ma, "Topology optimization of continuum structures under buckling constraints," *Computers Structures*, vol. 157, pp. 142–152, 2015. [Online]. Available: https://www.sciencedirect.com/science/article/pii/S0045794915001662

[50] A. Seyranian, E. Lund, and N. Olhoff, "Multiple eigenvalues in structural optimization problems," *Structural Optimization*, vol. 8, pp. 207–227, 12 1994.

[51] M. Neves, H. C. Rodrigues, and J. Guedes, "Generalized topology design of structures with a buckling load criterion," *Structural optimization*, vol. 10, pp. 71–78, 1995.

[52] T. W. Chin and G. Kennedy, "Large-scale compliance-minimization and buckling topology optimization of the undeformed common research model wing," 2016.

[53] X. jun Gao *et al.*, "Improving the overall performance of continuum structures: A topology optimization model considering stiffness, strength and stability," *Computer Methods in Applied Mechanics and Engineering*, vol. 359, p. 112660, 2020.

[54] J. Gravesen, A. Evgrafov, and M. Nguyen, "On the sensitivities of multiple eigenvalues," *Structural and Multidisciplinary Optimization*, vol. 44, pp. 583–587, 10 2011.

[55] P. Khosravi and R. Sedaghati, "Local buckling and mode switching in the optimum design of stiffened panels," *AIAA Journal*, vol. 46, pp. 1542–1548, 2008.

[56] W. Achtziger, "Local stability of trusses in the context of topology optimization part i: Exact modelling," *Structural optimization*, vol. 17, pp. 235–246, 1999.

[57] ——, "Local stability of trusses in the context of topology optimization part ii: A numerical approach," *Structural optimization*, vol. 17, pp. 247–258, 1999.

[58] X. Guo, G. Cheng, and N. Olhoff, "Optimum design of truss topology under buckling constraints," *Structural and Multidisciplinary Optimization*, vol. 30, pp. 169–180, 2005.

[59] A. Tugilimana, R. F. Coelho, and A. P. Thrall, "Including global stability in truss layout optimization for the conceptual design of large-scale applications," *Structural and Multidisciplinary Optimization*, vol. 57, pp. 1213–1232, 2018.

[60] P. B. Poulsen, J. Olesen, and M. Baandrup, "Truss optimization applying finite element limit analysis including global and local stability," *Structural and Multidisciplinary Optimization*, vol. 62, pp. 41–54, 2020.

[61] N. L. Pedersen, "On topology optimization of plates with prestress," *International Journal for Numerical Methods in Engineering*, vol. 51, pp. 225–239, 2001.

[62] S. Townsend and H. A. Kim, "A level set topology optimization method for the buckling of shell structures," *Structural and Multidisciplinary Optimization*, vol. 60, pp. 1783–1800, 2019.

[63] N. Changizi and M. Jalalpour, "Stress-based topology optimization of steel-frame structures using members with standard cross sections: Gradient-based approach," *Journal of Structural Engineering (United States)*, vol. 143, 08 2017.

[64] E. F. Bruhn, *Analysis and Design of Flight Vehicle Structures.* Indianapolis: Jacobs Pub., 1973, oCLC: 928252817.

[65] P. D. T. O'connor, "Advanced strength and applied elasticity, a.c. ugural and s.k. fenster, second si edition, elsevier science publishing company inc., 1987. number of pages: 471. price: $35.00 (hardback only)," *Quality and Reliability Engineering International*, vol. 4, no. 3, pp. 297–298, 1988. [Online]. Available: https://onlinelibrary.wiley.com/doi/abs/10.1002/qre.4680040324

[66] A. Ferreira, *MATLAB codes for finite element analysis. Solids and structures. With CD-ROM*, 01 2008, vol. 157.

[67] MATLAB, *version 9.8.0 (R2020a).* Natick, Massachusetts: The MathWorks Inc., 2020.

[68] E. Andreassen *et al.*, "Efficient topology optimization in matlab using 88 lines of code," *Structural and Multidisciplinary Optimization*, vol. 43, pp. 1–16, 11 2011.

[69] T. Cui *et al.*, "Topology optimization of plate structures using plate element-based moving morphable component (MMC) approach," *Acta Mechanica Sinica*, vol. 36, no. 2, pp. 412–421, Apr. 2020. [Online]. Available: http://link.springer.com/10.1007/s10409-020-00944-5

[70] X. Guo, "A 188-line matlab code for moving morphable component (mmc) method for topology optimization," *Structural and Multidisciplinary Optimization*, 2015.

[71] O. Sigmund, "A 99 line topology optimization code written in Matlab," *Structural and Multidisciplinary Optimization*, vol. 21, no. 2, pp. 120–127, Apr. 2001. [Online]. Available: http://link.springer.com/10.1007/s001580050176

[72] Airbus. (consulted on 19/3/2021) Flight crew operating training manual - ch.21 air cond/press/vent. [Online]. Available: https://www.smartcockpit.com/docs/A320-Air_Conditioning_and_Pressurization.pdf

[73] X. Gao, L. Li, and H. Ma, "An adaptive continuation method for topology optimization of continuum structures considering buckling constraints," *International Journal of Applied Mechanics*, vol. 9, 12 2017.

[74] C. Mittelstedt, "Explicit analysis and design equations for buckling loads and minimum stiffener requirements of orthotropic and isotropic plates under compressive load braced by longitudinal stiffeners," *Thin-Walled Structures*, vol. 46, no. 12, pp. 1409–1429, 2008. [Online]. Available: https://www.sciencedirect.com/science/article/pii/S0263823108000864

[75] W. Thomas *et al.*, "Friction stir welding–process developments and variant techniques," *The SME Summit*, 01 2005.

[76] R. Hafley, "Electron beam freeform fabrication: A rapid metal deposition process," *Proceedings of the 3rd Annual Automotive Composites Conference*, 01 2003.

[77] R. Pettit, J. Wang, and C. Toh, "Validated feasibility study of integrally stiffened metallic fuselage panels for reducing manufacturing costs," 06 2000.

[78] R. Kapania, J. Li, and H. Kapoor, *Optimal Design of Unitized Panels with Curvilinear Stiffeners*. [Online]. Available: https://arc.aiaa.org/doi/abs/10.2514/6.2005-7482

[79] S. Kidane *et al.*, "Buckling load analysis of grid stiffened composite cylinders," *Composites Part B: Engineering*, vol. 34, no. 1, pp. 1–9, 2003. [Online]. Available: https://www.sciencedirect.com/science/article/pii/S1359836802000744

[80] B. Zhang *et al.*, "A load reconstruction model for advanced grid-stiffened composite plates," *Composite Structures*, vol. 82, no. 4, pp. 600–608, 2008. [Online]. Available: https://www.sciencedirect.com/science/article/pii/S0263822307000797

[81] S. Shi *et al.*, "Buckling resistance of grid-stiffened carbon-fiber thin-shell structures," *Composites Part B: Engineering*, vol. 45, no. 1, pp. 888–896, 2013. [Online]. Available: https://www.sciencedirect.com/science/article/pii/S1359836812006026

[82] X. Yu and Y. Wang, "Flutter analysis for wing structure using finite element modeling with equivalent stiffness," *Journal of Vibroengineering*, vol. 16, pp. 1483–1493, 01 2014.

[83] J.N.Reddy, *Mechanics of Laminated Composite Plates and Shells-Theory and Analysis*. 2nd Edition, CRC Press, USA., 2004.

[84] F. Ferrari, O. Sigmund, and J. Guest, "Topology optimization with linearized buckling criteria in 250 lines of matlab," 01 2021.

[85] J. R. Gilbert, C. Moler, and R. Schreiber, "Sparse matrices in matlab: Design and implementation," *SIAM J. Matrix Anal. Appl*, vol. 13, pp. 333–356, 1992.

APPENDIX A EXTENDED ABSTRACT FOR ICTAM 2021 CONGRESS

XXV ICTAM, 23-28 August 2020, Milano, Italy

A NOVEL USE OF THE GROUND STRUCTURE TOPOLOGY OPTIMIZATION FOR THE DESIGN OF PRESSURIZED STIFFENED PANELS

Mario Capo, JF Gamache, T. Rochefort-Beaudoin, Aurelian Vadean, Sofiane Achiche
Department of Mechanical Engineering, Polytechnique Montréal, Montréal QC, CANADA

Summary: The Ground Structure method is well-known in the literature for trusses and frames Topology Optimization, but its use in the design of stiffened panel has not been explored. In this work, an original reformulation of the method is proposed. Since beam elements are directly used as the set of candidate reinforcements, this approach ensures an explicit description of the final stiffener's geometry. This eliminates the need for interpreting the resultant material distribution or for imposing any geometric constraint to force the optimization towards manufacturability. The proposed reformulation has been implemented in MATLAB, tested on a benchmark problem and its potential as a design tool is demonstrated on the compliance-based topology optimization of the stiffeners layout of a simplified pressure bulkhead. The optimized design complies with those obtained by using SIMP and MMC methods.

INTRODUCTION

Stiffened panels are commonly used in aircraft structures for their high performance/weight ratio. The design process of such assemblies starts with an a priori choice on the reinforcement configuration (e.g. ortho-grid), mainly based on industrial experience. The use of Topology Optimization (TO) [1] can support this starting phase using a mathematical approach to enhance mechanical properties of stiffened panels from a global point of view.

Early research works proposed to roughly identify rib position optimizing thickness distribution of plates elements [2]. Methodologies based on the use of the SIMP method [3,4], propose to identify the stiffeners layout from the interpretation of high-density regions resulting from the TO. These approaches need the addition of geometric constraints to obtain manufacturable stiffener-like components, and post-processing procedures for the interpretation task [5]. To overcome these issues, new formulations based on the use of topological variables that explicitly control the geometry of the final structure rather than the mechanical properties of the starting mesh have been proposed. Belonging to this category, the MMC approach [6] has been recently applied to composite stiffened panels, where stiffeners are embedded in the plate model using equivalent stiffness method [7]. A major drawback of this method is the need of a very fine mesh to describe the stringers' features. The mesh size has to be at least smaller than the stringer's section width. This renders the use of such a model computationally expensive for large-scale applications.

The idea of a Ground Structure TO, which uses a mesh made of plates and beams comes from two basic considerations:
(1) This modelling strategy is computationally inexpensive and is commonly used in the industry for FEM analysis of large structures composed of stiffened plates, as well as for preliminary sizing of wingbox components. [8]
(2) The Ground Structure method is an easy-to-implement formulation which can deal with the structural members of interest in aircraft constructions. After the removal of vanishing members, the output of the TO contains explicit information on the final geometry without the need for interpretation.

METHODOLOGY

For the proposed formulation, a simple model made of Euler-Bernoulli beams coupled with discrete quadrilateral Kirchhoff plates with isotropic linear elastic material properties is used. In first approximation, one can consider that the two structural elements lie in the same plane and are connected to same nodal grid. Alternatively, to increase the accuracy of the analysis, the nodal points defining the beams must be offset and connected to the plate using rigid connections. Mechanical deformation of the stiffened panel under lateral loads is obtained from a linear static analysis.

An adaptation of the ground structure generation algorithm proposed by [9] is used to automatically superimpose a dense mesh of beam elements on a plate model, with an arbitrary level of connectivity. In the proposed method the topological design variables are the cross-sectional area of each beam elements composing the stiffeners, while the plates properties are kept constant.

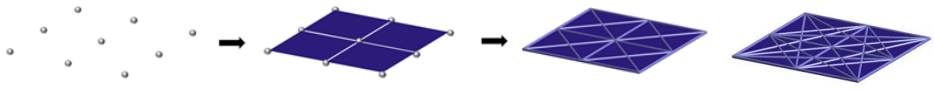

Figure 1. Ground Structure generation with arbitrary level of connectivity.

The formulation of the minimum compliance problem and the pseudo code of the algorithm are summarized in fig.2(a) and fig.2(b). The optimization problem is solved using the Interior Point Method implemented in the MATLAB Optimization Toolbox [10]. Load and nodal displacement vectors $\boldsymbol{f}, \boldsymbol{u}$ are expressed in the global reference system. Vector $\boldsymbol{l}$ contains all beam lengths and v_{max} is the maximum volume allowed for the reinforcement. A benchmark problem faced to test the algorithm is also shown in fig.2(c).

*Corresponding author. E-mail: **mario.capo@polymtl.ca**

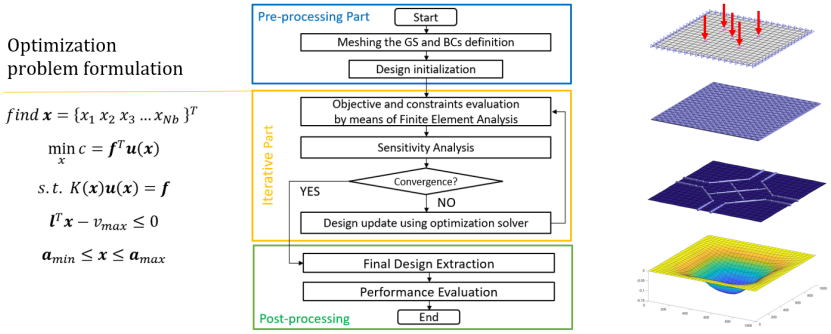

(a) (b) (c)

Figure 2. Overview of the method: (a) optimization formulation; (b) pseudo code implemented in MATLAB; (c) a benchmark problem test

A PRACTICAL ENGINEERING APPLICATION

A practical engineering problem is addressed to validate the procedure: the design of a flat pressure bulkhead subject to differential pressure ($0.1\ MPA$). Contour supports are located at equispaced points and simulate a riveting connection. The mechanical properties of Al2024-T4 are used, and geometric parameters are given as follows. A mesh of 40x24 rectangular element discretizes the design domain where $L = 2500\ mm$. This leads to an initial GS of 1984 members. The skin thickness is $1.25mm$, the interval for cross-sectional areas is $a_i \in [10^{-5}, 10^3]mm$, and v_{max} cannot exceed $5.625 \cdot 10^6\ mm^3$. The obtained optimized layout in fig.3 can be compared to those in [4,7].

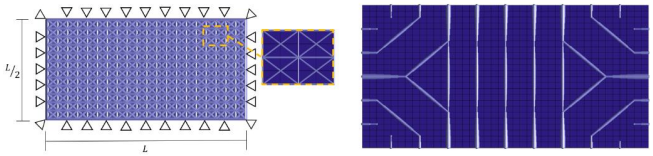

Figure 3. Starting GS and the optimized Stiffeners layout for a flat pressurized bulkhead.

CONCLUSIONS

In this work, a novel reformulation of the ground structure topology optimization is applied to the design of stiffeners layout for pressurized panels. The novelty of the method lies in the hybrid use of plates and beams elements to construct the ground structure, and in the context of application, never explored by the traditional method according to the authors' knowledge [11]. Numerical results indicate that the method can provide a clear stiffener layout for the compliance problem with volume constraints. The structure obtained is sound and one note the lesser involvement of designer during the post-processing procedure and particularly the TO interpretation. Inclusion of stress and buckling criteria, as well as a more complete finite element formulation are promising to be considered in future works.

References

[1] Bendsøe, Martin & Sigmund, Ole. (2004). Topology optimization. Theory, methods, and applications. 2nd ed., corrected printing. 10.1007/978-3-662-05086-6.
[2] Lam, Y.C. & Santhikumar, S.. (2003). Automated rib location and optimization for plate structures. Structural and Multidisciplinary Optimization. 25. 35-45. 10.1007/s00158-002-0270-7.
[3] Krog, L., A. Tucker, Airbus Uk and R. Boyd. "Topology Optimisation of Aircraft Wing Box Ribs." (2004).
[4] Dugré, Alexis & Vadean, Aurelian & Chaussee, Julien. (2016). Challenges of using topology optimization for the design of pressurized stiffened panels. Structural and Multidisciplinary Optimization. 53. 10.1007/s00158-015-1321-1.
[5] Gamache, Jean-François & Vadean, Aurelian & Noirot-Nérin, Emeric & Beaini, Dominique & Achiche, Sofiane. (2018). Image-based truss recognition for density-based topology optimization approach. Structural and Multidisciplinary Optimization.
[6] Zhang, W., Yuan, J., Zhang, J. et al. A new topology optimization approach based on Moving Morphable Components (MMC) and the ersatz material model. Struct Multidisc Optim 53, 1243–1260 (2016).
[7] Sun, Z., Cui, R., Cui, T. et al. An Optimization Approach for Stiffener Layout of Composite Stiffened Panels Based on Moving Morphable Components (MMCs). Acta Mech. Solida Sin. 33, 650–662 (2020).
[8] Megson, Thomas. (2013). Aircraft Structures for Engineering Students / T.H.G. Megson.. Aircraft Structures for Engineering Students
[9] Zegard, T., Paulino, G.H. GRAND — Ground structure based topology optimization for arbitrary 2D domains using MATLAB. Struct Multidisc Optim 50, 861–882 (2014). https://doi.org/10.1007/s00158-014-1085-z
[10] MATLAB and Statistics Toolbox Release 2016b, The MathWorks, Inc., Natick, Massachusetts, United States
[11] Gamache, Jean-François & Vadean, Aurelian & Dodane, Nicolas & Achiche, Sofiane. (2020). Topology Optimization for Stiffened Panels: A Ground Structure Method. 10.1115/DETC2020-22103.

*Corresponding author. E-mail: **mario.capo@polymtl.ca**

APPENDIX B GSM FOR STIFFENED PANELS - MATLAB CODE

This appendix reports the main code written for the work presented in Chapter 3. The full archive of the scripts can be found in the online repository `https://github.com/mariocapo/Thesis_TopOptStiffenedPanels_GSM` , where the nested functions are provided.

---------- PrOp1 - Set Physical Properties ----------

```
E = 71700;                                                          %Young Modulus [Mpa]
nu = 0.3;                                                           %Poisson
rho = 2.81e-06;                                                     %Material density [Kg
mm^-3]
t = 1.25;                                                           %Plate thickness [mm]
k_h_w = 3;                                                          %h/w ratio
Lx = 1000; Ly=1000;%example_square_plate                            %Plate Dimensions
[mm]
```

---------- PrOp2 - Discretize Domain ----------

```
Nx=10; Ny=Nx;%example_square_plate                                  %Mesh
[X,Y,Z] = meshgrid(linspace(0,Lx,Nx+1),linspace(0,Ly,Ny+1),0);      %Discretize space
NODE = [reshape(X,numel(X),1) reshape(Y,numel(Y),1) reshape(Z,numel(Z),1)]; %Panel Nodes
Coordinates
nodenrs = reshape(1:(1+Nx)*(1+Ny),1+Ny,1+Nx);                       %Nodes Matrix
Nn = (Nx+1)*(Ny+1); GDof = 3*Nn;                                    %No. of nodes & DOFs
Np = Nx*Ny;                                                         %No. of plates
elements
```

---------- PrOp3 - Generate base mesh(PLATEs GS) & K_GSP ----------

```
PLATES = zeros(Np,4); temp=0;
for i=1:Ny, for j=1:Nx
        temp = temp+1;
        n1 = (i-1)*(Ny+1)+j; n2 = i*(Ny+1)+j;
        PLATES(temp,:) = [n1 n2 n2+1 n1+1];                         %Plates Nodes Global
indices
end, end
xe = NODE(PLATES(1,:),[1:2]); % for regular mesh this can be used for all   %Elements extremes
k_P = get_KeP(E,nu,t,xe);                                           %Elem Kmatrix Plates
12x12
edofVec = reshape(3*nodenrs(1:end-1,1:end-1)+1,Nx*Ny,1);
edofMatP = repmat(edofVec,1,12)+...
           repmat([-3,-2,-1,3*Ny+[0,1,2,3,4,5],0,1,2],Nx*Ny,1);     %Global indices
Plates DOFs
iK_P = reshape(kron(edofMatP,ones(12,1))',144*Nx*Ny,1);
jK_P = reshape(kron(edofMatP,ones(1,12))',144*Nx*Ny,1);             %Indices for K_GSp
assembly
sK_P = reshape(k_P(:)*ones(Np,1)',144*Np,1) ;
K_GSP = sparse(iK_P,jK_P,sK_P); K_GSP = (K_GSP+K_GSP')/2;           %Assemble stiffness
matrix
clear iK_P jK_P sK_P X Y Z edofVec xe k_P
```

---------- PrOp4 - Generate BEAMs GS ----------

```
Lvl=1;                                                          %GS Level of
connectivity
[BEAMS] = GenerateGSBEAMS(NODE,PLATES,Lvl,0.999);               %Generate GS
(Zegard&Paulino,2014)
Nb = size(BEAMS,1);                                             %No. of beams
elements
l = sqrt(((NODE(BEAMS(:,2),1))-(NODE(BEAMS(:,1),1))).^2 + ...
    (NODE(BEAMS(:,2),2)-(NODE(BEAMS(:,1),2))).^2);              %vector of beams
lengths
```

---------- PrOp5 Set BCs ----------

```
fixedNode = [ 1 ; Ny+1 ; Nx*(Ny+1)+1;  (Nx+1)*(Ny+1) ];         % Index of clamped
nodes
fixedDof = unique([3*fixedNode-2; 3*fixedNode-1; 3*fixedNode]); % Constrained Dofs
freeDof = setdiff([1:GDof]',fixedDof);                          % Unknowns Dofs
loadedNode = round(Ny/2+1)+round(Nx/2)*(Ny+1); % central node in the ex.   % Index of loaded
nodes
F = sparse([],[],[],GDof,1,size(loadedNode,1));
F(3*loadedNode-2) = -1000;                                      % Load Vector
```

---------- Prop6 preparate K_GSB assembly ----------

```
edofMatB = [3*BEAMS(:,1)-2,3*BEAMS(:,1)-1,3*BEAMS(:,1),...
            3*BEAMS(:,2)-2,3*BEAMS(:,2)-1,3*BEAMS(:,2)];        %Global indices Beams
DOFs
T_i = zeros(6,6,Nb);
for i = 1:Nb
cost = (NODE(BEAMS(i,2),1)-NODE(BEAMS(i,1),1))/l(i);
sint = (NODE(BEAMS(i,2),2)-NODE(BEAMS(i,1),2))/l(i);
temp = [1 0 0; 0 sint -cost; 0 cost sint];
y = zeros(3);
T = [temp y;y temp];
T_i(:,:,i) = T;                                                 %
TransformationMatrix T_i
end
```

---------- PrOp7 Initialize design ----------

```
V0= Lx*Ly;                                                      %GSB starting Volume
lm = sum(l)/Nb;
x0 = V0/(Nb*lm)*ones(Nb,1);                                     %GSB starting areas
V=0.8Vmax
Cutoff = 0.01;                                                  %threshold A/Amax for
plot
%PlotGroundStructure(NODE(:,[1:2]),BEAMS,x0,Cutoff,1);
%PlotGS(Zegard&Paulino,2014)
```

------- PrOp8 Set constraints & Initialize Optimization----------

```
Vmax = 1.25*Lx*Ly;                                                    %Upper bound for GSB
volume
xmin = x0./x0 * 1e-03; xmax= x0./x0 *1e03;                            %Side constraints
x=x0;                                                                 %Design variables
maxit=300;                                                            %Maximum No. of
iterations
```

---------- Re-Design Loop by means of MATLAB fmincon ----------

```
objective=@(xx) Compliance(xx,l,T_i,E,nu,k_h_w,edofMatB,K_GSP,GDof,freeDof,F);
options = optimoptions(@fmincon,...
'Display','iter','Algorithm','interior-point',...
'SpecifyObjectiveGradient',true,'MaxIterations',maxit,...
'PlotFcn',{@optimplotx,...
    @optimplotfval,@optimplotfirstorderopt});
[xcompl,fvalcompl] = fmincon(objective,x,l',Vmax,[],[],xmin,xmax,[],options);
```

---------- FD1 Final Design Extraction ----------

```
Plot_stiffnedpanel3D(NODE,BEAMS,xcompl,PLATES,0.1,6)
%PlotGS(Zegard&Paulino,2014)
```

---------- FD2 Final Plots ----------

```
final_mass = rho*(Lx*Ly*t + xcompl'*l)                                %Final mass
[~,~,U]=Compliance(xcompl,l,T_i,E,nu,k_h_w,edofMatB,K_GSP,GDof,freeDof,F);  %Linear static
Analysis
figure; hold on; view(45,45); colormap(jet); set(gcf,'color','w');
title('Deformation'); colorbar;
for k = 1:Np
    patch(NODE(PLATES(k,:),1),...
    NODE(PLATES(k,:),2),...
    U(edofMatP(k,1:3:10),1),...
    U(edofMatP(k,1:3:10),1));
end                                                                   %Plot deformed Plate
```

Function called by fmincon

```
%%%%%%%%%%%%%%%%%%%%%%%%%%%%%%%%%%%%%%%%%%%%%%%%%%%%%%%%%%%%%%%%%%%%%%%%%%%%%%%%
%%%%%%%%%%%%%%%%%%%%%%%%%%%% (1) %%%%%%%%%%%%%%%%%%%%%%%%%%%%%%%%%%%%%%%%%%%%%
% This functions perform Static Analysys, and provides Sensitivity Analysis
% for MATLAB fmincon
function [C,dC,U]=Compliance(xx,l,T_i,E,nu,k_h_w,edofMatB,K_GSP,GDof,freeDof,F)
```

---------- RL1 Linear Analysis ----------

```
Nb=length(l);
K_eB_local= zeros(6,6,Nb); K_GSB = sparse(GDof,GDof); U = zeros(GDof,1);    %Initialization
for i = 1:Nb                                                                %ASSEMBLY GSB
    K_eB_local(:,:,i) = T_i(:,:,i)'*get_KeB(l(i),xx(i),E,nu,k_h_w)*T_i(:,:,i);
    K_GSB(edofMatB(i,:),edofMatB(i,:)) = K_GSB(edofMatB(i,:),edofMatB(i,:)) + K_eB_local(:,:,i);
end
K = K_GSP + K_GSB ; % Panel Stiffness Matrix = Plates + Beams
U(freeDof) = K(freeDof,freeDof)\F(freeDof);                                 %Static Displacements
```

---------- RL2 Obj f & SENSITIVITY ANALYSIS ----------

```
C = F(freeDof)'*U(freeDof);                                                 %Compliance
dC=zeros(Nb,1);
for i=1:Nb
U_loc = T_i(:,:,i)*U(edofMatB(i,:));
dC(i) = - U_loc'*get_dKeB_dx(l(i),xx(i),E,nu,k_h_w)*U_loc;                  %Compliance
sensitivities
end
end
```

APPENDIX C GSM EXTENSION TO DIFFERENT PROBLEMS

The proposed reformulation of the Ground Structure Method was developed in detail for models of reinforced panels subjected to out-of-plane loading. The FEM thus considered as DOFs the displacements normal to the panel plane and the two rotations with respect to the axes in the plane.
However, the formulation is easily extensible to the "in plane" problem, which considers two displacements in the plane and the rotation about the normal axis, or in general to the complete 3D formulation, which involves 6 DOFs for each node.

In the design of pressurized panels, the stiffeners layout has the main function of providing bending supports to the thin sheet. For this task the classical TO formulation for minimum compliance is ideal. In the design of panels loaded primarily in the plane, on the other hand, the reinforcement must perform the function of stabilising the thin sheet, in addition to helping carry the load. Since the same formulation of problem 3.1 is maintained in the this paragraph, the examples only aim at demonstrating that the GSM, like other topology optimisation methods, can effectively show the "main load path" by aligning the reinforcements accordingly. However, since buckling and stress are not included in the design criteria, they are only preliminary studies to demonstrate the flexibility of the method to generic geometries and loads.

C.0.1 Concepts Generation for a Rib Panel Reinforcement

The example considers a panel with the shape of the aerodynamic profile NACA 2412, taken as archetype of a generic aeronautical rib. This assembly transfers the aerodynamic forces from skin-stringers through clips and shear ties to the spars, and it is composed of a thin panel reinforced by stiffeners (namely rib chords,caps or uprights) [12].
Light rib's main function in the wing-box assembly is to maintain the shape of the profile "rigid" in its plane (within a certain limit of distortion). The rib also acts as a support for the stringers by limiting their effective length as a beam-column [12].
There are also heavier ribs particularly conceived to collect large concentrated loads coming from landing gear, engine pylons or control surfaces hinges [12].

The loads that a rib must resist are [13]:
- in-plane shear, applied from the shear ties connections with spars and skins;
- in plane compression, transferred by stringers clips from pressure applied on adjacent skin

portion and rib crushing generated by bending flexion of the wing.
- additionally, there can be span wise compression/tension due to the wing section Poisson effect, or lateral pressure if the rib has a secondary functions of composing a fuel tank.

The following illustrative model considers only in-plane effects. The GS finite elements are then plates, for which only membrane response is considered, and beams, with in-plane displacements and the rotation actives.
The hypotheses are made that forces are applied in concentrated point where connection with skin-stiffeners should be located and that the panel is clamped on the four corners, where is ideally attached to the spars.

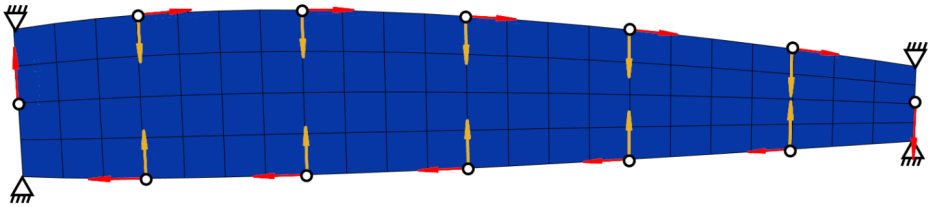

Figure C.1 Rib Panel with NACA2412 profile. Plates Mesh and BCs: in red concentrated shear forces and in yellow compression ones.

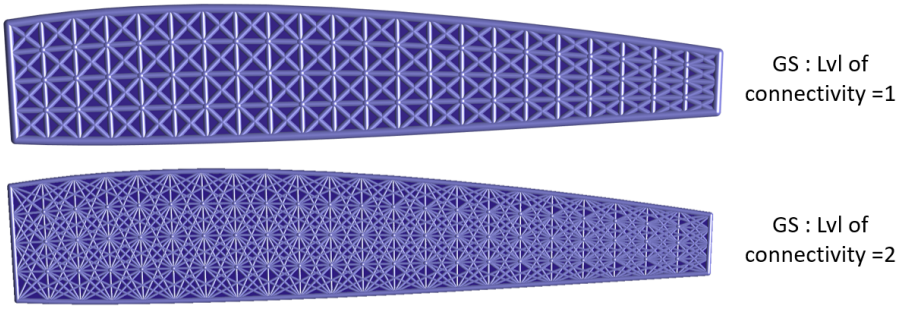

Figure C.2 Rib Panel with NACA2412 profiles. Different Beams Ground Structure: Lvl of connectivity 1 and 2.

Three ideal static load cases are considered:
- one with only compression loads applied (yellow arrows in Fig.C.1);
- one with only shear loads (red arrows in Fig.C.1);
- one with a compression/shear load ratio $(C)/(S) = 0.5$.

Load magnitude estimation is arbitrary, since a real dimensioning of the concepts is out the example's scope.

A summary of the numerical parameters used in the example is given in table C.1, then different conceptual layouts obtained for each load case and for different choices of the initial ground structure are reported.

Table C.1 Numerical example for the concept generation of Rib reinforcements

Chord length [mm]	3250	Material Properties	as Tab. 3.6
Panel mesh	$22x4$	Thickness	as Tab. 3.6
No. of Beam $LvL1$	378	No. of Beam $LvL2$	586
$V_{max}[mm^3]$	10^6	Range for $A[mm^2]$	$\in [10^{-3}; 10^{+3}]$

Load multiplier for each test case

Force magnitude	Compression(C)	Pure Shear(S)	Mixed (CS)
$1[KN]$	(C)=1 (S)=0	(C)=0 (S)=1	(C)=1 (S)=2

Beams on the boundary are set to not belong to design space. $A_{boundary} = 500mm^2$

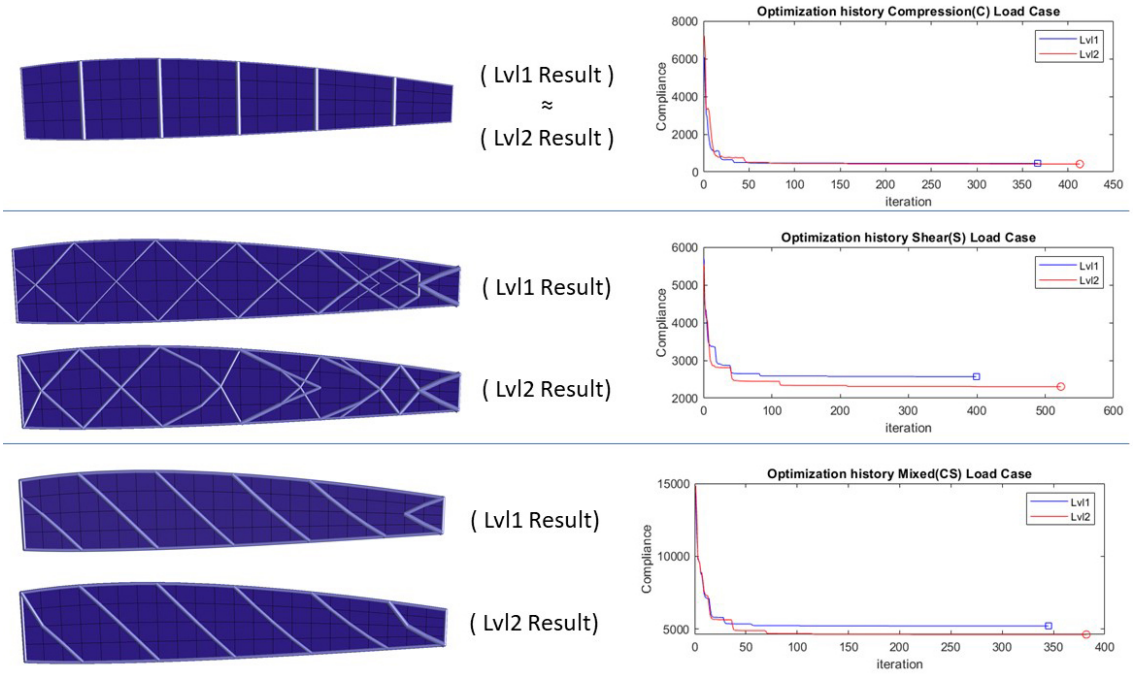

Figure C.3 Rib Panel with NACA 2412 profile. Conceptual layout exploration

By examining the results in Fig.C.3, it can be said that by using a denser ground structure (Lvl2) a better value of the objective function is generally obtained. This occurs due to the larger number of candidates, hence more freedom in revealing the final layout. However, this is associated with slower convergence due to the larger design space. The results plotted in Fig.C.3 cut out the vanishing beams with $A_i \leq 100mm^2$.

APPENDIX D NUMERICAL VALIDATION OF THE SIMPLIFIED MODEL WITH EQUIVALENT STIFFNESS PROPERTIES

In the following the results obtained using the 2-Layer Model are compared against the one obtained by using the commercial solver Optistruct [46] for some test cases.
The analyses conducted in the software are referred as "reference": in these models the stiffeners geometry is modelled with shell elements oriented perpendicular to the skin midplane. QUAD4 e TRIA3 linear PSHELL elements compose the mesh of the skin.

For a square panel with one curvilinear stiffener, whose features are presented in fig.D.1, two static load cases have been tested to conduct the comparison: the out-of-plane response is tested by loading the model with uniform normal pressure, while for the in-plane response a uniform uniaxial compression line load is applied in the skin midplane, as detailed in Fig.D.2.

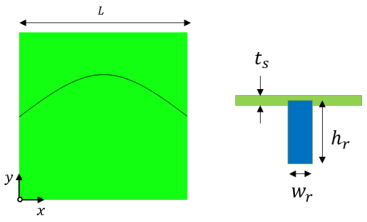

L	Panel length				200 m	
t_s	Skin thickness				1 mm	
h_r	Stiffener height				10 mm	
w_r	Stiffener thickness				5 mm	
$D1$	x_{01} = 0 [mm]	y_{01} = 100 [mm]	θ_1 = 0 [rad]	L_1 = 100 [mm]	h^{II} = 50 [mm]	

Figure D.1 Square Panel with one curvilinear stiffener for numerical validation

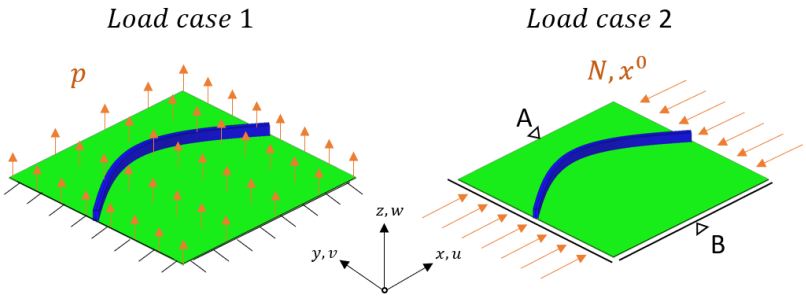

	Load Case 1	Load Case 2
Load	$p = 0.01\ MPa$	$N_{,x}{}^0 = 1\ N/mm$
Fixed DOFs	12345 (4 *sides*)	3 (4 *sides*) 1 (*at nodes A and B*)

Figure D.2 Two Load Cases for Numerical Validation - Boundary conditions and global displacements notation

For a proper representation of the stringers, the mesh of the equivalent model has to be refined to have at least 2-3 elements in the stiffeners width. The same mesh size of $2mm$ is adopted on both the models. The properties of a generic aluminium alloy are used: $E = 71.7GPa$ for the young modulus, $\nu = 0.33$ for the Poisson coefficient.

Bending Analysis For the load case 1, the plate is clamped and subjected to uniform upward pressure. The transverse displacement field are plotted in Fig.D.3, where it can be noticed that the relative error on the maximum displacement is 3.55%. Moreover, the accordance between the membrane stresses fields (plotted in Fig.D.4) proves that the mechanical behaviour of the panel under bending load is well approximated.

Uniform x-compression case For the load case 2, the plate is simply-supported and subjected to uniform load per unit length along the x global axis. The error on the maximum x-displacement is below the 1%, while error on the out of plane maximum displacement is about $4,2\%$.
For a panel with a curvilinear and eccentric stiffener the in-plane forces are coupled with the bending deformation as can be seen in Fig.D.5 where the out-of-plane displacement w is of the same order of magnitude of the in plane displacements. The membrane stresses fields are plotted in Fig.D.6: far from the stiffeners the stresses in the skin are very accurate. Regarding the reinforced zone it is underlined that the model taken as reference has elements in the xy plane for the skin, and elements orthogonal to the plane for the stiffeners. In the equivalent model the stiffeners is integrated in the skin elements. For this reason in this region the stress values assume an intermediate value between those of skin and stiffeners in the reference model.

Linear Buckling Analysis: Uniform x-compression The accuracy of the simplified model for the estimation of the fundamental buckling load factor by means of the linear buckling analysis is also estimated for this baseline panel. An unitary x-compression load per unit length is applied on the panel clamped (DOFs 2345) along all the side. This means that the numerical value of the eigenvalue coincides with the critical load per unit length. The analysis is performed for two different parameter of h^{II}, which adjusts the curvature of the stiffener as shown in figure 4.2. For the curvilinear stiffener configuration ($h^{II} = 50mm$) and for a rectilinear one ($h^{II} = 0mm$), figures D.7 and D.8 respectively show the comparison with models of same geometry analysed in Optistruct (reference). From the comparisons, the estimation for the fundamental buckling load factor results to be in the order of 11% at worst.

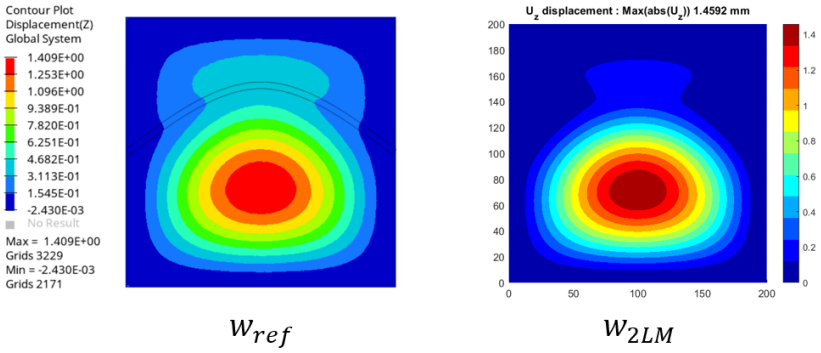

Figure D.3 Bending Analysis : deformation plots. "w_{ref}" refers to the model analysed in Optistruct, while w_{2LM} refers to the 2-layer model

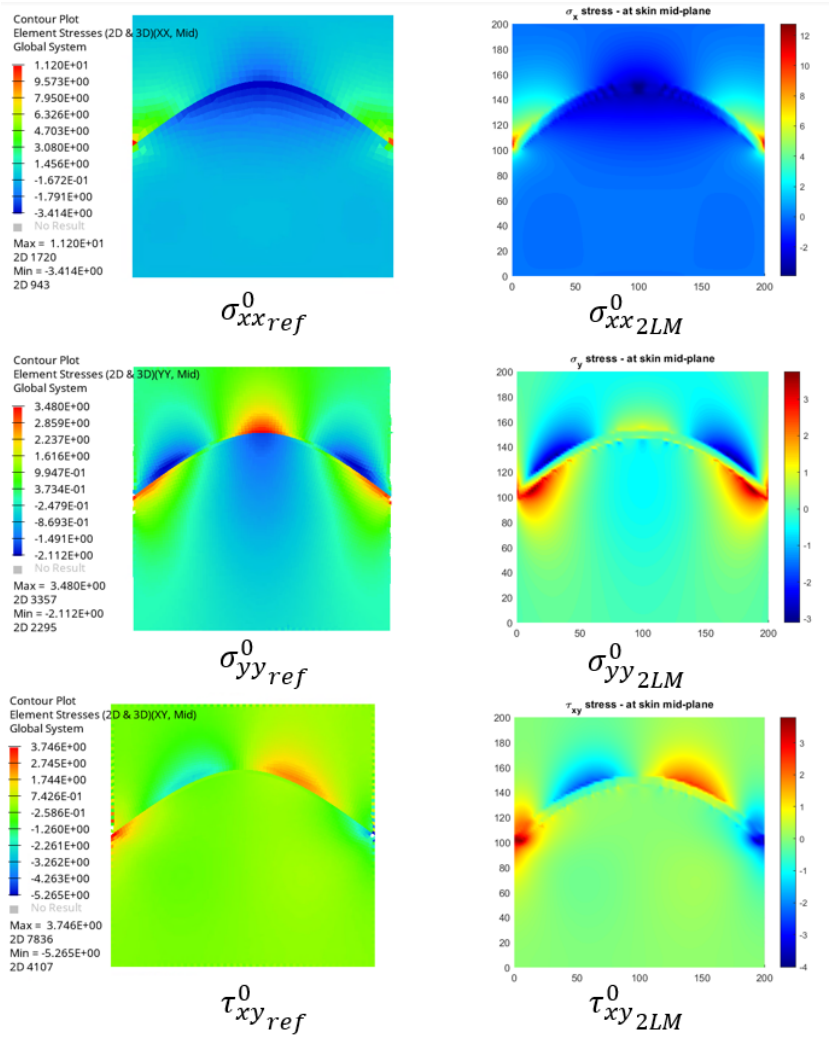

Figure D.4 Bending Analysis: Membrane stresses Plots.

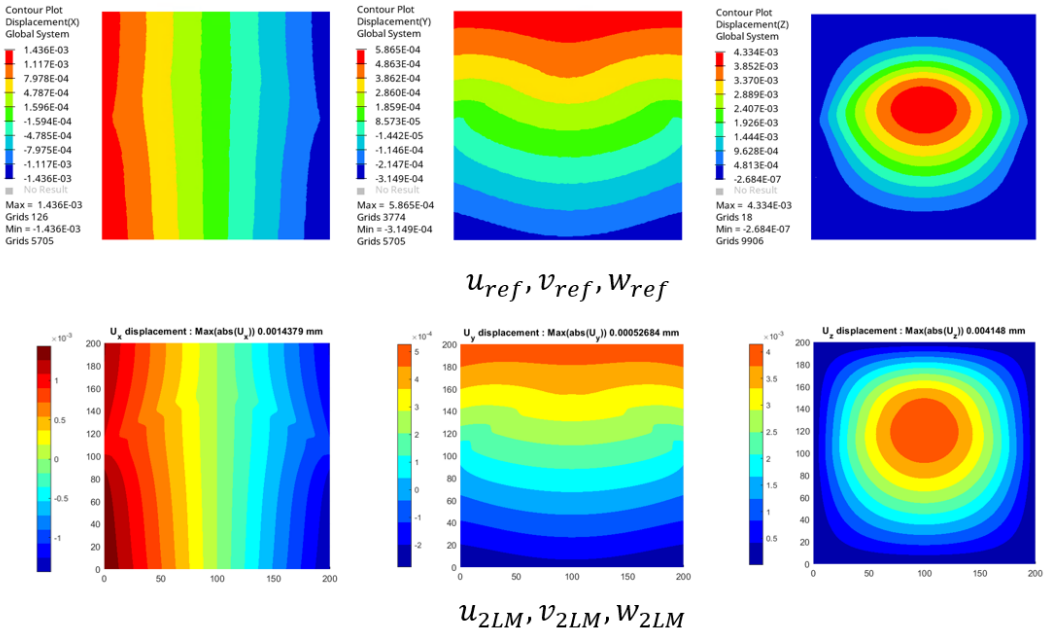

Figure D.5 Compression loading Analysis: deformation plots. "w_{ref}" refers to the model analysed in Optistruct, while w_{2LM} refers to the 2-layer model

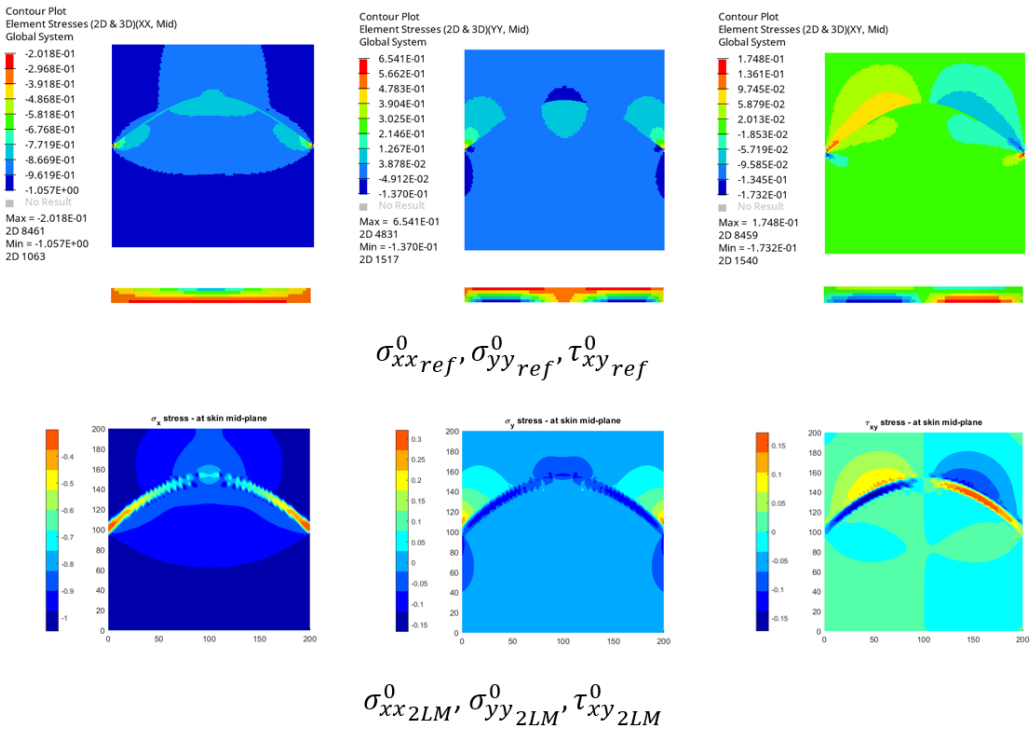

Figure D.6 Compression loading Analysis: Membrane stresses Plots. "ref"(model in Optistruct),"$2LM$"(the 2-layer model)

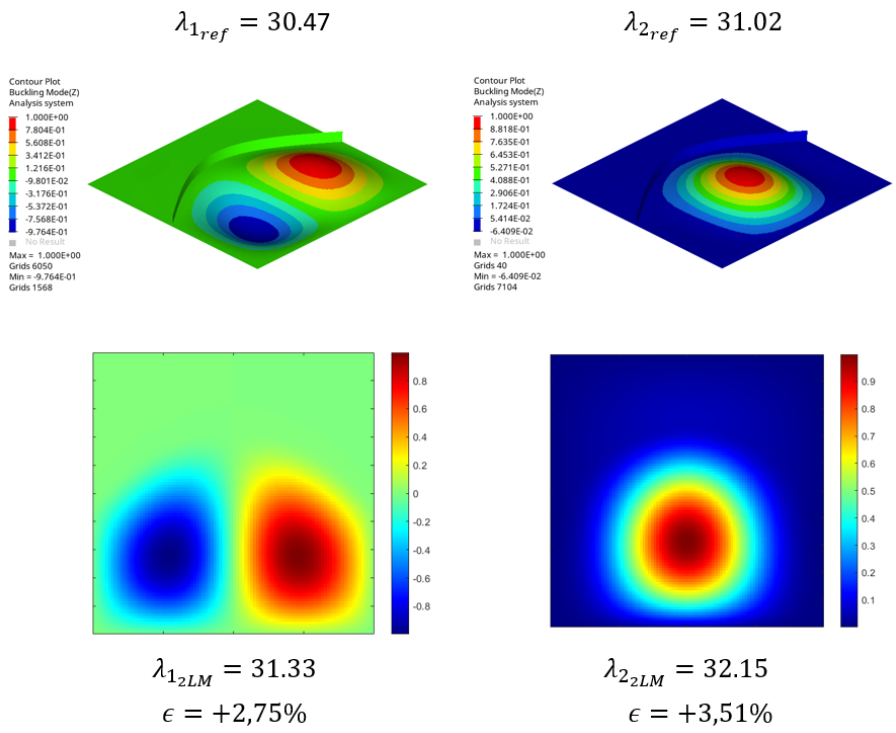

Figure D.7 Linear Buckling Analysis comparison: Buckling load factor and first two eigenmodes for a panel with curvilinear stiffener under uniform compression. "ref" refers to the model analysed in Optistruct, while $2LM$ refers to the 2-layer model

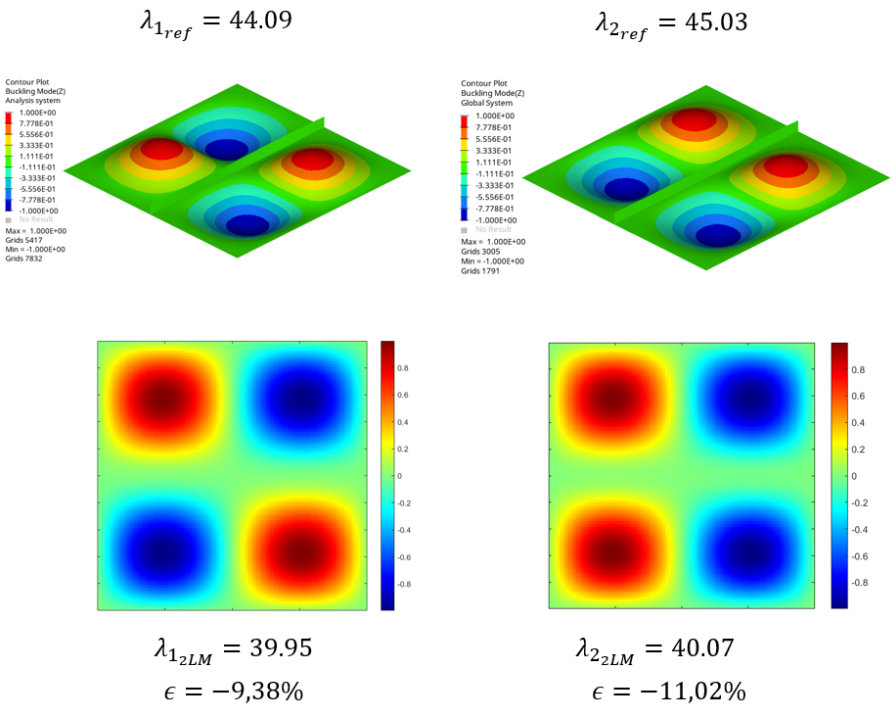

Figure D.8 Linear Buckling Analysis comparison: Buckling load factor and first two eigenmodes for a panel with rectilinear stiffener stiffener under uniform compression. "ref" refers to the model analysed in Optistruct, while $2LM$ refers to the 2-layer model

APPENDIX E MMC FOR STIFFENERS LAYOUT OPTIMIZATION - MATLAB CODE

This appendix reports the main code written for the stiffeners Layout Optimization of Sect.4.4.5. The full archive of the scripts can be found in the online repository `https://github.com/mariocapo/Thesis_TopOptStiffenedPanels_MMC` , where the nested functions are provided.

PrOp(1) Set Physical Properties

```
E = 71700; nu=0.33;                                                    % Material Properties
ts=2;                                                                  % Plate Thickness
hr=26; w0=6; e=hr/2+ts/2; %height,width,eccentricity                   % Reinforcement
section sizes
Lx = 400 ; Ly =600;                                                    % Panel Dimension
rho = 2.81e-06;                                                        % Material Density
```

PrOp(2) Discretize Domain

```
nelx = 200; nely=300;
M=[nely+1,nelx+1]; nEl = nelx*nely ;                                   % number of elements
Ex=Lx/nelx;                                                            % element x-length
Ey=Ly/nely;                                                            % element y-length
elNrs = reshape(1:nEl,nely,nelx);                                      % element numbering
[X,Y] = meshgrid(Ex*[0:nelx],Ey*[0:nely]);                             % nodal points grid
```

PrOp (3) Generate base mesh and collocation matrices

```
NODE = [reshape(X,numel(X),1) reshape(Y,numel(Y),1)];                  % nodal coordinates
PLATES = zeros(nEl,4);                                                 % Plates Nodes Global
indices
temp=0;
for i=1:nelx, for j=1:nely
        temp = temp+1;
        n1 = (i-1)*(nely+1)+j; n2 = i*(nely+1)+j;
        nn = [n1 n2 n2+1 n1+1];
        PLATES(temp,:) = nn ;
end, end
nodeNrs = int32(reshape(1:(1+nely)*(1+nelx),1+nely,1+nelx));           % node numbering
cMat = reshape(5*nodeNrs(1:end-1,1:end-1)+1,nEl,1)+...
int32([-5,-4,-3,-2,-1,5*nely+[0,1,2,3,4,5,6,7,8,9],0,1,2,3,4]);%
nDof = (1+nely)*(1+nelx)*5;                                            % total number of
DOFs
[sI,sII]=deal([]);
for j = 1:20 % build assembly indices for the lower symmetric part of K
sI = cat(2,sI,j:20) ;
```

```
sII = cat(2,sII,repmat(j,1,20-j+1));
end
[iK,jK] = deal(cMat(:,sI)',cMat(:,sII)');
Iar=sort([iK(:),jK(:)],2,'descend');                                    % indices for K
assembly
```

PrOp (4) Generate elemental Ke_sk and Ke_r

```
[AMat_sk,BMat_sk,DMat_sk,SMat_sk,AMat_r,BMat_r,DMat_r,SMat_r,Q_mat] =
LoadDefRelations(E,nu,e,ts,hr);
xe=[-Ex/2,-Ey/2;Ex/2,-Ey/2;Ex/2,Ey/2;-Ex/2,Ey/2];                        % dimensions of the
elements
[Ke_sk0] = BasicKe_lamina(AMat_sk,BMat_sk,DMat_sk,SMat_sk,xe);          % Skin contrib to
Stiff Matrix
mask = tril(true(size(Ke_sk0)));
Ke_sk = Ke_sk0(mask);                                                   % lower tringular
part
[Ke_r0] = BasicKe_lamina(AMat_r,BMat_r,DMat_r,SMat_r,xe);               % Skin contrib to
Stiff Matrix
mask = tril(true(size(Ke_r0)));
Ke_r = Ke_r0(mask);                                                     % lower tringular
part
```

PrOp (5) Set BCs

```
[fixed,~]=BCs(nodeNrs,nelx,nely,'Panel_4str');                          % Essential BCs
free = setdiff(1:nDof,fixed);
[F] = ForceVector_generic(nDof,nEl,nely,nelx,Ey,Ly,xe,cMat,'D');        % Natural BCs
```

PrOp (6) Define Baseline Design

```
Nmc=4;                                                                  % No. of components
xA = [0 0 0 0]';                                                        % start-point coord x
yA = 120*[1 2 3 4]';                                                    % start-point coord y
thA = [0 0 0 0]';                                                       % start-point
inclination
xB = [Lx Lx Lx Lx]';                                                    % end-point coord x
yB = yA;                                                                % end-point coord y
thB = [0 0 0 0]';                                                       % end-point
inclination
ww = [w0/2 w0/2 w0/2 w0/2]';                                            % component half
width
d_base = [xA,yA,thA,xB,yB,thB,ww];                                      % Baseline design [
Nmc x Nd_per_mc]
Np_per_mc = size(d_base,2);
```

OptInit(1) Initialize Swarm initial Matrix

```
npars = 5 ;                                                             %No of particles in
the initial swarm
```

```
% d_base = [xA,yA,thA,xB,yB,thB,ww]
VarIndices = [2,3,5,6]';                                                    % parameters selected
for D_x
nvars = Nmc*length(VarIndices)/2;                                           % total length of D_x
% Determine initial position of Particle Pi i=1:npars
d=zeros(length(d_base),Nmc,npars);
%P1
d(:,:,1) = d_base' ;
%P2
d(:,:,2) = d_base' ;
temp = [20*[1 1 1 1];zeros(1,4);-20*[1 1 1 1];zeros(1,4)];
d(VarIndices,:,2) = d_base(:,VarIndices)'+temp ;
%P3
d(:,:,3) = d_base' ;
temp =  [-20*[1 1 1 1];zeros(1,4);20*[1 1 1 1];zeros(1,4)];
d(VarIndices,:,3) = d_base(:,VarIndices)'+temp ;
%P4
d(:,:,4) = d_base' ;
temp =  [zeros(1,4);10*pi/180*[0 1 2 3];zeros(1,4);-10*pi/180*[0 1 2 3]];
d(VarIndices,:,4)= d_base(:,VarIndices)'+temp ;
%P5
d(:,:,5) = d_base' ;
temp =  [zeros(1,4);-10*pi/180*[3 2 1 0];zeros(1,4);10*pi/180*[3 2 1 0]];
d(VarIndices,:,5)= d_base(:,VarIndices)'+temp ;
% 'InitialSwarmMatrix' = size npars x nvar , where each row represents one particle
VarIndices = VarIndices(1:2);
xy0 = reshape(d(VarIndices,:,:),nvars,npars,1)';
xy0_base = d_base(:,VarIndices)'; xy0_base = xy0_base(:)';
xy0 = xy0 - repmat(xy0_base,npars,1);                                       %
'InitialSwarmMatrix'
```

See initial particles initial position x0_pi

```
Phi=cell(Nmc,1);
v0 = zeros(Nmc,1);
v0tot = zeros(npars,1);
for j=1:npars;
    for i=1:Nmc
    Phi{i}=tPhi(d(:,i,j)',X(:),Y(:),'Hermite');
    v0(i) = stiffener_volume(hr,d(:,i,j)',X(:),Y(:),'Hermite');
    end
%Union of components
    tempPhi_max=Phi{1};
    for i=2:size(d,2)
        tempPhi_max=max(tempPhi_max,Phi{i});
    end
v0tot(j) = sum(v0);
subplot(1,npars,j);
Phi_max=reshape(tempPhi_max,nely+1,nelx+1);
contourf(reshape(X,M), reshape(Y,M), Phi_max,[0,0]);
set(gca,'Color',[0 0.4470 0.7410]); colormap(hot);set(gcf,'Color','w');
```

```
axis equal;axis([0 Lx 0 Ly]);pause(1e-6);
end
```

OptInit(2) PSO Parameters and Inputs

```
%[dx0;dy0;dth0;dxend;dyend;dthend]
v_max=2.75e05;
delta_angle = 30*pi/180; delta_y = 20;
deltalow = repmat([-delta_y;-delta_angle],1,Nmc);
deltaup = repmat([delta_y;delta_angle],1,Nmc);
lb = reshape(+deltalow,nvars,1); %lower side constraint
ub = reshape(+deltaup,nvars,1); %upper side constraint
maxIt= 100; %max iteration for the PSO
fun=@(xy) CurvStiffMMC_Buckl_volconstr(xy,d_base,VarIndices,Nmc,X,Y,M,Ex,...
PLATES,Ke_sk,Ke_r,Iar,nDof,free,F,cMat,E,ts,iK,jK,xe,'Hermite',hr,v_max);   %objective function
subcall
```

PSO Optimization

```
[xsol,fval,historybestx,historybestfval] = runPSO(xy0,fun,maxIt,npars,nvars,lb,ub);
```

Final Design Extraction

```
d_best = d_base;delta = [xsol(1:2:end)',xsol(2:2:end)'];                    % Reconstruction
d_best(:,VarIndices)=d_best(:,VarIndices)+delta;                            % of D_i from the
d_best(:,VarIndices+3)=d_best(:,VarIndices+3)-delta;                        % PSO solution
```

Plot final configuration

```
Phi=cell(Nmc,1);
v0_best = zeros(Nmc,1);
    for i=1:Nmc
    Phi{i}=tPhi(d_best(i,:),X(:),Y(:),'Hermite');
    v0_best(i) = stiffener_volume(hr,d_best(i,:),X(:),Y(:),'Hermite');
    end
%Union of components
    tempPhi_max=Phi{1};
    for i=2:size(d_best,1)
        tempPhi_max=max(tempPhi_max,Phi{i});
    end
Phi_max=reshape(tempPhi_max,nely+1,nelx+1);
contourf(reshape(X,M), reshape(Y,M), Phi_max,[0,0]);
set(gca,'Color',[0 0.4470 0.7410]); colormap(hot);set(gcf,'Color','w');
axis equal;axis([0 Lx 0 Ly]);pause(1e-6);
% Final mass
v_besttot = sum(v0_best);
mass_best_reinforcement = v_besttot*rho;
mass_best = rho*(ts*Lx*Ly + mass_best_reinforcement);
```

Published with MATLAB® R2020a

APPENDIX F VECTORIZED SET-UP OF THE STRESS STIFFNESS MATRIX FOR MINDLIN PLATES

Large sparse and symmetric matrices can be assembled in a computational efficient way by using the algorithm of [85], implemented in the MATLAB built-in function "sparse" [67]. The coefficients of each elemental stress stiffness matrix, ordered column-wise, are collocated in a global vector according to their indices in the global system.
Three vectors are needed to carry out the assembly operation: the vector $\{vK_\sigma^{low}\}$ containing the unique coefficients of the (lower) symmetric part of the stress stiffness matrix, and two vectors containing the indices for positioning each coefficient $\{iK_\sigma^{low}\}$ and $\{jK_\sigma^{low}\}$ in the global matrix. The "sparse" function call to obtain the elastic stiffness matrix reads:

$$\boldsymbol{K_\sigma^{(low)}} = sparse(\{iK_\sigma^{low}\}, \{jK_\sigma^{low}\}, \{vK_\sigma^{low}\})$$
$$\boldsymbol{K}_\sigma = \boldsymbol{K_\sigma^{(low)}} + \boldsymbol{K_\sigma^{(low)}}^T - diag[\boldsymbol{K_\sigma^{(low)}}]$$

where the second line recovers the full symmetric matrix from the lower triangular.

Based on the work of Ferrari and Sigmund [84], a vectorized set-up of the stress stiffness matrix for iso-parametric Mindlin plate elements is developed here to speed up the LBA. The integrand of Eq.4.24 can be expanded, presenting the following structure:

$$[\mathbf{G}]^T[\mathbf{S}^0][\mathbf{G}] = \begin{bmatrix} z_{11}[\mathbf{Tz}] & & & sym \\ z_{21}[\mathbf{Tz}] & z_{22}[\mathbf{Tz}] & & \\ z_{31}[\mathbf{Tz}] & z_{32}[\mathbf{Tz}] & z_{33}[\mathbf{Tz}] & \\ z_{41}[\mathbf{Tz}] & z_{41}[\mathbf{Tz}] & z_{43}[\mathbf{Tz}] & z_{44}[\mathbf{Tz}] \end{bmatrix} \tag{F.1}$$

where the ten coefficients z_{ik} $(i, k = 1...4)$ depend on the membrane stresses components and the products between the shape functions gradient components [84] as follows:

$$z_{ik} = \sigma^0_{xx} N_{i/x} N_{k/x} + \sigma^0_{yy} N_{i/y} N_{k/y} + \tau^0_{xy}(N_{i/y} N_{k/x} + N_{i/x} N_{k/y}) \tag{F.2}$$

while the coefficients resulting from the integration in the thickness direction, are organized in the diagonal matrix $\boldsymbol{Tz}$. Along the diagonal of this matrix, only the first $(tz^{(a)})$ and the third coefficients $(tz^{(b)})$ are independent, as highlighted in the following expression of $\boldsymbol{Tz}$:

$$[\mathbf{Tz}] = \begin{bmatrix} t_s & 0 & 0 & 0 & 0 \\ 0 & t_s & 0 & 0 & 0 \\ 0 & 0 & t_s & 0 & 0 \\ 0 & 0 & 0 & \frac{t_s^3}{12} & 0 \\ 0 & 0 & 0 & 0 & \frac{t_s^3}{12} \end{bmatrix} = \begin{bmatrix} tz^{(a)} & 0 & 0 & 0 & 0 \\ 0 & tz^{(a1)} & 0 & 0 & 0 \\ 0 & 0 & tz^{(a2)} & 0 & 0 \\ 0 & 0 & 0 & tz^{(b)} & 0 \\ 0 & 0 & 0 & 0 & tz^{(b1)} \end{bmatrix} \tag{F.3}$$

Consequently, in the matrix product of Eq.F.1 only 20 coefficients are independent out of 210 ones. If the coefficient of $\boldsymbol{z}$ are ordered in a vector, by taking their position colomun-wise from F.1, a vector $\boldsymbol{z} = \{z_{11}, z_{21}, z_{31}, ..., z_{44}\}$ of size 1x10 is obtained.
These coefficient are multiplied either by $tz^{(a)}$ or $tz^{(b)}$ in the integrand of Eq.F.1. Then for each element we can obtain the vectorized form of the lower triangular elemental stress stiffness, namely $\{v\boldsymbol{K}^{(e)}_{\sigma_{low}}\}$, by listing $\{tz^{(a)}\boldsymbol{z}\}$ and $\{tz^{(b)}\boldsymbol{z}\}$ in the right order.

Table F.1 expresses the indices to map the coefficients $z_{ik}tz^{(a)}$ in the elemental stress stiffness matrix $\boldsymbol{K}^{(e)}_{\sigma}$, and in its lower triangular part reorganized in a vector, namely $\{v\boldsymbol{K}^{(e)}_{\sigma_{low}}\}$.

Table F.1 Position of the $z_{ik}tz^{(a)}$ coefficients in the elemental stress stiffness matrix and in its vectorized form

Array	position of $z_{ik}tz^{(a)}$
$\boldsymbol{K}^{(e)}_{\sigma}$	$\{(1,1);(6,1);(11,1);(16,1);(6,6);(6,11);(6,16);(11,11);(11,16);(16,16)\}$
$\{v\boldsymbol{K}^{(e)}_{\sigma_{low}}\}$	$\{(1);(6);(11);(16);(91);(96);(101);(156);(161);(196)\}$

Once the position of $z_{ik}tz^{(a)}$ are identified, the other elements are positioned by sliding down along the diagonal of sub-matrices $z_{ik}[\mathbf{Tz}]$. That is, two copies of $z_{ik}tz^{(a)}$ are positioned by sliding 1 and 2 positions. Then $z_{ik}tz^{(b)}$ is positioned by sliding 3 position, and 4 for its copy. This indexing is reported in Table F.2.

Table F.2 Position of the $z_{ik}[\mathbf{tz}]$ components in the elemental stress stiffness matrix and in its vectorized form

coefficient $z_{ik}[\mathbf{tz}]$	position in $\boldsymbol{K}^{(e)}_{\sigma}$	position in $\{v\boldsymbol{K}^{(e)}_{\sigma_{low}}\}$
$\mathrm{z}_{ik}tz^{(a)}$	$(\mathrm{i,j})_{z_{ik}tz^{(a)}}$	$(iv)_{z_{ik}tz^{(a)}}$
$\mathrm{z}_{ik}tz^{(a1)}$	$(\mathrm{i,j})_{z_{ik}tz^{(a1)}} = (i,j)_{z_{ik}tz^{(a)}} + (1,1)$	$(iv)_{z_{ik}tz^{(a1)}} = (\mathrm{iv})_{z_{ik}tz^{(a)}} + 21 - j_{z_{ik}tz^{(a1)}} + 1$
$\mathrm{z}_{ik}tz^{(a2)}$	$(\mathrm{i,j})_{z_{ik}tz^{(a2)}} = (i,j)_{z_{ik}tz^{(a)}]} + (2,2)$	$(iv)_{z_{ik}tz^{(a2)}} = (\mathrm{iv})_{z_{ik}tz^{(a1)}} + 21 - j_{z_{ik}tz^{(a2)}} + 1$
$\mathrm{z}_{ik}tz^{(b)}$	$(\mathrm{i,j})_{z_{ik}tz^{(b)}} = (i,j)_{z_{ik}tz^{(a)}]} + (3,3)$	$(iv)_{z_{ik}tz^{(b)}} = (\mathrm{iv})_{z_{ik}tz^{(a2)}} + 21 - j_{z_{ik}tz^{(b)}} + 1$
$\mathrm{z}_{ik}tz^{(b1)}$	$(\mathrm{i,j})_{z_{ik}tz^{(b1)}} = (i,j)_{z_{ik}tz^{(a)}]} + (4,4)$	$(iv)_{z_{ik}tz^{(b1)}} = (\mathrm{iv})_{z_{ik}tz^{(b)}} + 21 - j_{z_{ik}tz^{(b1)}} + 1$